Analysis and Design of Algorithms for the Improvement of Non-coherent Massive MIMO based on DMPSK for beyond 5G systems

Manuel José López Morales

in partial fulfillment of the requirements for the degree of Doctor of Philosofy in

Multimedia and Communications Interuniversity PhD Program

Universidad Carlos III de Madrid

Advisor/Tutor:
Prof. Ana García Armada

March 7, 2023

“The expert in anything was once a beginner.” — Anonymous

“Develop a passion for learning. If you do, you will never cease to grow.” — Anthony J. D’Angelo

“The greatest teacher, failure is.” — Yoda

“You do not really understand something unless you can explain it to your grandmother.” — Albert Einstein

“I am still learning.” — Michelangelo (age 87)

Abstract

Nowadays, it is nearly impossible to think of a service that does not rely on wireless communications. By the end of 2022, mobile internet represented a 60% of the total global online traffic. There is an increasing trend both in the number of subscribers and in the traffic handled by each subscriber. Larger data rates, smaller extreme-to-extreme (E2E) delays and greater number of devices are current interests for the development of mobile communications. Furthermore, it is foreseen that these demands should also be fulfilled in scenarios with stringent conditions, such as very fast varying wireless communications channels (either in time or frequency) or scenarios with power constraints, mainly found when the equipment is battery powered.

Since most of the wireless communications techniques and standards rely on the fact that the wireless channel is somehow characterized or estimated to be pre or post-compensated in transmission (TX) or reception (RX), there is a clear problem when the channels vary rapidly or the available power is constrained. To estimate the wireless channel and obtain the so-called channel state information (CSI), some of the available resources (either in time, frequency or any other dimension), are utilized by including known signals in the TX and RX typically known as pilots, thus avoiding their use for data transmission. If the channels vary rapidly, they must be estimated many times, which results in a very low data efficiency of the communications link. Also, in case the power is limited or the wireless link distance is large, the resulting signal-to-interference-plus-noise ratio (SINR) will be low, which is a parameter that is directly related to the quality of the channel estimation and the performance of the data reception. This problem is aggravated in massive multiple-input multiple-output (massive MIMO), which is a promising technique for future wireless communications since it can increase the data rates, increase the reliability and cope with a larger number of simultaneous devices. In massive MIMO, the base station (BS) is typically equipped with a large number of antennas that are coordinated. In these scenarios, the channels must be estimated for each antenna (or at least for each user), and thus, the aforementioned problem of channel estimation aggravates. In this context, algorithms and techniques for massive MIMO without CSI are of interest.

This thesis main topic is non-coherent massive multiple-input multiple-output (NC-mMIMO) which relies on the use of differential M-ary phase shift keying (DMPSK) and the spatial diversity of the antenna arrays to be able to detect the useful transmitted data without CSI

knowledge. On the one hand, hybrid schemes that combine the coherent and non-coherent schemes allowing to get the best of both worlds are proposed. These schemes are based on distributing the resources between non-coherent (NC) and coherent data, utilizing the NC data to estimate the channel without using pilots and use the estimated channel for the coherent data. On the other hand, new constellations and user allocation strategies for the multi-user scenario of NC-mMIMO are proposed. The new constellations are better than the ones in the literature and obtained using artificial intelligence techniques, more concretely evolutionary computation.

Acknowledgements

People usually say personal advancement comes from a right mixture of intelligence and effort, but for me, the most important factor is the people you surround yourself of, everyone you meet changes you in a way or another and makes you who you are.

First of all, I would like to thank my father, who has always supported me and still does and is a very important role model; my mother, who showed me the importance of effort and perseverance to achieve personal success; and my closest family members. All of you have accompanied me most of my life and in some way or another, you have contributed to helping me be the best I can. I want to specially thank Marta, my life partner, and her family, which have been very supportive during these PhD years and this thesis would probably have not been possible without them.

I want to acknowledge the trust, guidance and support of my thesis advisor, Prof. Ana García Armada. I sincerely thank her for selecting me as a PhD student in the TeamUp5G project. It has been an amazing experience to work with her, both personally and professionally. I also want to thank my colleagues from the GCOM research group, both professors and students. Noted thanks to Kun and Alejandro, both of them have been great colleagues with whom to collaborate and have been key to the development of this PhD thesis. I also want to thank the TeamUp5G students, supervisors and partners, for their support and guidance, and for their diligence. You have all made the MSCA experience much more rewarding.

Lastly, I cannot forget all the friends I have made in the different stages of my life, from my youth in Murcia, my college studies in Madrid, my stays in Tokyo, Italy and France, and my Erasmus in Lund. All of them, one way or the other, contributed to making this PhD thesis possible.

Thanks to all the people I have met in my life, I am who I am because of you, and I do not regret any of it.

Grant Information

This work has received funding from the European Union Horizon 2020 research and innovation programme under the Marie Skłodowska-Curie ETN TeamUp5G, grant agreement No. 813391. The PhD student was the Early Stage Researcher (ESR) number 2 of the project.

This work has also received funding from the Spanish National Project IRENE-EARTH (PID2020-115323RB-C33) (MINECO/AEI/FEDER, UE), which funded the work of some co-authors.

Any opinions, findings and conclusions or recommendations expressed in this material are those of the author(s) and do not necessarily reflect the views of the European Union or of the Spanish funding agency.

Published and submitted content

All of the information from all of the sources used in this thesis is highlighted using typographic and explicit references. The following articles from journals and conferences are included in this thesis:

Journal articles

1. M. J. Lopez-Morales, K. Chen-Hu, A. Alvarez-Polegre and A. Garcia-Armada, "Non-coherent Cell-free Large SIMO using DMPSK," under revision in IEEE Transactions on Vehicular Technology at the time of thesis submission.
   This work is wholly included in Chapter 4.
   The material from this source included in this thesis is not singled out with typographic means and references.

2. M. J. Lopez-Morales and A. Garcia-Armada, "Channel Estimation and Prediction in a Pilot-Less Massive MIMO TDD Using Non-Coherent DMPSK," in IEEE Access, vol. 10, pp. 112327-112341, 2022, doi: 10.1109/ACCESS.2022.3216834.
   The journal was ranked Q2 in the moment of acceptance for publication. This work is partially included in Chapter 5.
   The material from this source included in this thesis is not singled out with typographic means and references.

3. M. J. Lopez-Morales, K. Chen-Hu and A. Garcia-Armada, "Differential Data-Aided Channel Estimation for Up-Link Massive SIMO-OFDM," in IEEE Open Journal of the Communications Society, vol. 1, pp. 976-989, 2020, doi: 10.1109/OJ-COMS.2020.3008634.
   The journal was not ranked in the moment of acceptance for publication. This work is wholly included in Chapter 5.
   The material from this source included in this thesis is not singled out with typographic means and references.

4. M. J. Lopez-Morales, K. Chen-Hu, A. Garcia-Armada and O. A. Dobre, "Constellation Design for Multiuser Non-Coherent Massive SIMO based on DMPSK Modulation," in

IEEE Transactions on Communications, 2022, doi: 10.1109/TCOMM.2022.3217575.
The journal was ranked Q1 in the moment of acceptance for publication. This work is wholly included in Chapter 6.
The material from this source included in this thesis is not singled out with typographic means and references.

Conferences articles

5. M. J. L. Morales, K. Chen-Hu and A. G. Armada, "Effect of Spatial Correlation on the Performance of Non-coherent Massive MIMO based on DMPSK," 2021 IEEE Global Communications Conference (GLOBECOM), 2021, pp. 1-6, doi: 10.1109/GLOBECOM46510.2021.9685812.
   This work is wholly included in Chapter 4.
   The material from this source included in this thesis is not singled out with typographic means and references.

6. M. J. L. Morales, K. Chen-Hu and A. G. Armada, "Pilot-less Massive MIMO TDD System with Blind Channel Estimation using Non-coherent DMPSK," GLOBECOM 2022 - 2022 IEEE Global Communications Conference, Rio de Janeiro, Brazil, 2022, pp. 693-698, doi: 10.1109/GLOBECOM48099.2022.10000841.
   This work is wholly included in Chapter 5.
   The material from this source included in this thesis is not singled out with typographic means and references.

Other research merits

The following works have also been produced during the PhD studies and have a partial relation with the thesis but are not directly included as part of this report:

1. CONFERENCE: L. M. Campos et al., "Reference Scenarios and Key Performance Indicators for 5G Ultra-dense Networks," 2020 12th Intern. Sym. on Comm. Systems, Networks and Digital Signal Proc. (CSNDSP), 2020, pp. 1-5, doi: 10.1109/CSNDSP49049.2020.9249513.

2. CONFERENCE: M. J. López-Morales, K. Chen-Hu and A. G. Armada, "A Survey about Deep Learning for Constellation Design in Communications," 2020 12th International Symposium on Communication Systems, Networks and Digital Signal Processing (CSNDSP), 2020, pp. 1-5, doi: 10.1109/CSNDSP49049.2020.9249528.

3. CONFERENCE: Diego González Morín, Manuel J. López Morales, Pablo Pérez, and Alvaro Villegas. 2022. TCP-Based Distributed Offloading Architecture for the Future of Untethered Immersive Experiences in Wireless Networks. In ACM International Conference on Interactive Media Experiences (IMX '22). Association for Computing Machinery, New York, NY, USA, 121–132. https://doi.org/10.1145/3505284.3529963

4. CONFERENCE: M. J. L. Morales, K. Chen-Hu and A. G. Armada, "Optimum Constellation for Symbol-Error-Rate to PAPR Ratio Minimization in SWIPT," 2022 IEEE 95th Vehicular Technology Conference: (VTC2022-Spring), 2022, pp. 1-5, doi: 10.1109/VTC2022-Spring54318.2022.9860473.

5. CONFERENCE: M. J. Lopez-Morales et al., "MOOC on "Ultra-dense Networks for 5G and its Evolution": Challenges and Lessons Learned," 2022 31st Annual Conference of the European Association for Education in Electrical and Information Engineering (EAEEIE), 2022, pp. 1-6, doi: 10.1109/EAEEIE54893.2022.9819989.

6. BOOK CHAPTER: V. P. Gil-Jimenez et al., "MOOC as a Way of Dissemination, Training and Learning of Telecommunication Engineering," in Massive Open Online Courses-Current Practice and Future Trends, IntechOpen, published: January 4th, 2023, doi: 10.5772/intechopen.1000574

7. CONFERENCE: M. J. L. Morales, R. Dinis and A. G. Armada, "Near-Optimal Detection of CE-OFDM Signals with High Power Efficiency via GAMP-based Receivers," 2022 IEEE Globecom Workshops (GC Wkshps), Rio de Janeiro, Brazil, 2022, pp. 7-12, doi: 10.1109/GCWkshps56602.2022.10008696.

8. BOOK: M. Morales-Cespedes et al., "Ultra-dense networks for 5G communications and beyond," in IEEE Books. Under revision at the time of thesis submission.

9. JOURNAL: Diego Gonzalez Morin, Manuel J. Lopez-Morales, Pablo Pérez, Ana García Armada, Alvaro Villegas, "FikoRE: 5G and Beyond RAN Emulator for Application Level Experimentation and Prototyping," under revision in IEEE Network Magazine at the time of thesis submission.

10. AWARD: Student Competition 2022 (FIRST PRIZE) "The Owl: An Accessible Immersive Telepresence System for the Future of Human Communication" `https://www.comsoc.org/membership/ieee-comsoc-student-competition/winners#:~:text=Manuel%20J.%20L%C3%B3pez%20Morales`

Contents

List of figures

List of tables

Acronyms and abbreviations

2G	2nd generation
3G	3rd generation
3GPP	3rd Generation Partnership Project
4G	4th generation
5G	5th generation
b5G	beyond 5th generation
6G	6th generation
AMPS	Advanced Mobile Phone System
AoA	angle of arrival
AP	access point
ASK	amplitude shift keying
AWGN	additive white Gaussian noise
BER	bit error rate
BS	base station
CB	conjugate beamforming
CF	cell-free
CF-M-MIMO	Cell-free massive SIMO
CP	cyclic prefix
CSI	channel state information
CSIR	CSI at receiver
CPU	central processing unit
CoMP	coordinated multi-point
DL	downlink
DMPSK	differential M-ary phase shift keying
DFT	discrete Fourier transform
DSSS	Direct Sequence Spread Spectrum
DUSTM	Differential Unitary Space-Time Modulation
E2E	extreme-to-extreme
EC	evolutionary computation

EDGE	Enhanced Data rates for GSM Evolution
eMBB	enhanced mobile broadband
FCC	Federal Communications Commission
FDD	frequency-division duplex
FDMA	frequency-division multiple access
FFT	fast Fourier transform
FSK	frequency shift keying
GAO	Gaussian-approximated optimization
GPRS	General Packet Radio Service
GSM	Global System for Mobile Communications
HDS	hybrid demodulation scheme
HetNet	heterogeneous network
IC	individual constellation
IDFT	inverse discrete Fourier transform
IoT	Internet of things
IR-UWB	Impulse Radio-Ultra Wide Band
ISI	inter-symbol interference
IUI	inter-user interference
JC	joint constellation
JCM	joint constellation and mapping
LOS	line-of-sight
LS	least-squares
LTE	Long-Term Evolution
LTE-A	LTE Advanced
MCO	Monte-Carlo based optimization
MF	matched filter
MIMO	multiple-input multiple-output
mMIMO	massive multiple-input multiple-output
mMIMO-OFDM	massive MIMO with OFDM
MMSE	minimum mean-squared error
mMTC	massive Machine Type Communications
mmWave	millimeter-wave
MR(T/C)	maximum ratio (transmission/combining)
MS	mobile station

MSDD	Multiple-Symbol Differential Detection
MSE	mean squared error
MU	multi-user
MU-MIMO	multi-user MIMO
MU-SIMO	multi-user SIMO
NC	non-coherent
NC-mMIMO	non-coherent massive multiple-input multiple-output
NC-M-MIMO	non-coherent massive SIMO
NC-CF	non-coherent cell-free
NC-CF-mMIMO	NC-CF massive SIMO
NCM	number of complex multiplications
NLOS	non-line-of-sight
NR	New Radio
OFDM	orthogonal frequency-division multiplexing
OOK	on-off-keying
P2P	point-to-point
PAPR	peak-to-average power ratio
PDF	probability density function
PSAM	pilot-symbol assisted modulation
QAM	quadrature amplitude modulation
QPSK	quadrature phase-shift keying
RF	radiofrequency
RX	reception
SC	small-cell
SCS	subcarrier spacing
SE	spectral efficiency
SER	symbol error rate
SNR	signal-to-noise ratio
SINR	signal-to-interference-plus-noise ratio
SISO	single-input single-output
SIMO	single-input multiple-output
SMS	short message service
ST	superimposed training
SU	single-user

TDD	time-division duplex
TDMA	time-division multiple access
TX	transmission
UC	user-centric
UE	user equipment
UL	uplink
ULA	uniform linear array
UMTS	Universal Mobile Telecommunications System
URLLC	Ultra-Reliable Low-Latency Communications
VG	variance Gamma
ZF	zero-forcing

Notation

$a, \boldsymbol{a}, \boldsymbol{A}$	scalar, vector and matrix
$[\boldsymbol{a}]_n$	n-th element of $\boldsymbol{a}$
$[\boldsymbol{A}]_{m,n}$	m-th row and n-th column of $\boldsymbol{A}$
$\boldsymbol{A}^T, \boldsymbol{A}^*, \boldsymbol{A}^H$	transpose, conjugate and conjugate transpose (Hermitian) of $\boldsymbol{A}$
$\boldsymbol{A}^{-1}$	inverse of $\boldsymbol{A}$
$\mathrm{tr}(\boldsymbol{A})$	trace of $\boldsymbol{A}$
$\mathrm{diag}(\boldsymbol{a})$	diagonal matrix with the element of $\boldsymbol{a}$ on its main diagonal
$\mathrm{diag}(\boldsymbol{A})$	column vector of diagonal elements of $\boldsymbol{A}$
$\mathrm{diag}(\boldsymbol{A}_1, \ldots, \boldsymbol{A}_n)$	block-diagonal matrix with square matrices $\boldsymbol{A}_1, \ldots, \boldsymbol{A}_n$ on its main diagonal
$\boldsymbol{I}_N$	identity matrix of size $N \times N$
$\mathbf{0}_N$	zero vector of size N
$\mathbf{1}_N$	one vector of size N
$\odot$	element-wise product
$\mathbb{E}\{\cdot\}$	expectation operator
$\mathbb{C}$	set of complex numbers
$\mathrm{Var}\{\cdot\}$	variance operator
$\Re, \Im$	real and imaginary part
$\lvert\cdot\rvert$	absolute value
$\lVert\cdot\rVert_2$	Euclidean norm of order 2
$\Gamma(\cdot)$	gamma function
$\mathcal{N}(\mu, \sigma^2)$	circularly-symmetric normal distribution with mean μ and variance σ^2
$\mathcal{CN}(\mu, \sigma^2)$	circularly-symmetric complex normal distribution with mean μ and variance σ^2
$\asymp$	asymptotic equality
$Q(\cdot)$	Q-function
$\Gamma(k, \xi)$	Gamma distribution, shape parameter k and scale parameter ξ
$f(a\|b)$	conditional PDF of a to b for continuous random variables
$P(a\|b)$	conditional PDF of a to b for discrete random variables
$U(a, b)$	uniform distribution between a and b
$\angle(x)$	angle of x for $x \in \mathbb{C}$

Chapter 1
Introduction

Mobile communications have their earliest roots in 1947, when the Bell System business offered an early prototype of the current broadband mobile networks. Using very low-power transmitters [4], it was intended to deliver radio services across a wide area. Unfortunately, the Federal Communications Commission (FCC) refused to permit the use of the desired spectrum band. More than 30 years would pass before the first mobile communications system would be commercially available. The Bell Laboratories created the analog frequency-division multiple access (FDMA)-based Advanced Mobile Phone System (AMPS) during the 1980s, which was one of those pioneering technologies. The Global System for Mobile communications (GSM) standard, the most popular 2nd generation (2G) technology, was introduced later, in 1991 [5]. The analog voice service based on FDMA was replaced by the new digital service when digital time-division multiple access (TDMA) emerged. With the launch of the General Packet Radio Service (GPRS) and Enhanced Data rates for GSM Evolution (EDGE) protocols [6], more functionality like short message service (SMS) and other improvements were added over time. Nonetheless, the introduction of Universal Mobile Telecommunications System (UMTS) technology [7], or the 3G of mobile communications, marked the beginning of the multimedia revolution. There was a clear need to deliver more reliable and flexible communications while meeting significant data traffic needs, despite the fact that continuous advancements were made with the new mobile communications technology. In this context, Long-Term Evolution (LTE) technology (almost-4G) began to be adopted quickly after it became standardized in the late 2000s [8]. Orthogonal frequency-division multiplexing (OFDM) and multiple-input multiple-output (MIMO) are key technologies in LTE and its successive improvements carried in the second decade of the 21st century, which was gradually introducing new improvements until LTE Advanced (LTE-A) was obtained (true-4th generation (4G)). Since then, the technology continued evolving up until these days, in which the 5th generation (5G) New Radio (NR) standard [9] was defined and started its deployment. A summary of the evolution of mobile communication technologies is found in Fig. 1.1.

Wireless communications have gained more and more importance in our lives during the last 40 years. Nowadays, it is nearly impossible to think of a service that does not rely on them.

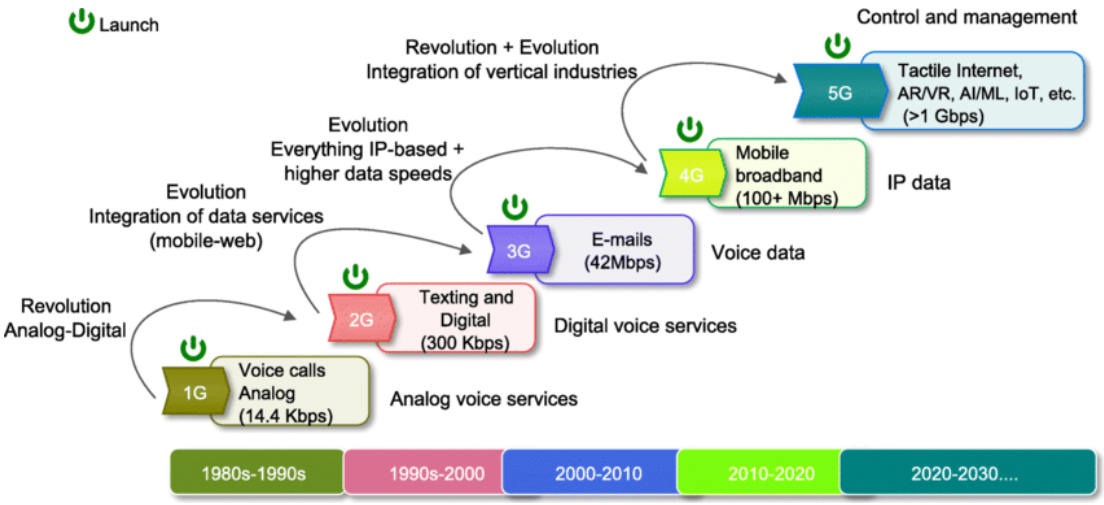

Figure 1.1: *Evolution of mobile communication technologies from 1G to 5G.*

Nowadays, the mobile networks are used by the majority of the society, and this is supported by the fact that by the end of 2021, about 4.3 billion people (more than half of the total population) actively use mobile internet. In fact, the mobile internet traffic represents about a 57% of the total global online traffic. Last but not least, there is an increasing trend both in the number of subscribers and in the traffic handled by each subscriber, caused by the fact that new services and applications emerge day after day and more and more people use them. It is clear that the technology will keep evolving to allow for better and more demanding services and applications, which will motivate the development of even more capable technologies. The next foreseen mobile technology is beyond 5G (b5G) currently under development with respect to the date of publication of this PhD thesis, followed by the 6^{th} generation (6G), which is expected to start its development around 2025. Mobile networks, along with numerous other telecommunications innovations, have connected every region of the planet. *The world is one*, as Arthur C. Clarke would remark [10].

1.1 Motivation

A clear demand for larger data rates, smaller E2E delays and greater number of devices is a current issue for the development of mobile communications. Furthermore, it is foreseen that these demands should also be fulfilled in scenarios with stringent conditions, such as very fast varying wireless communications channels (either in time or frequency) [11] or scenarios with power constraints [12], mainly found when the wireless equipment is battery powered.

Since most of the wireless communications techniques and standards rely on the fact that the wireless channel is somehow characterized or estimated to be pre/post-compensated in TX/RX [13], there is a clear problem when the channels vary rapidly or the available power is constrained. To estimate the wireless channel and obtain the so-called CSI, some of the available resources (either in time, frequency or any other dimension), are utilized by including known reference signals in the TX and RX, typically called pilots, thus avoiding the use of these resources for data transmission [14]. Another issue that limits the performance of the channel estimation is the pilot contamination problem, which consists on the fact that neighbouring cells utilize the same resources to estimate the channel, interfering between them in the process.

If the channels vary rapidly, they must be estimated many times, which results in a very low data efficiency of the communications link. Also, in case the power is limited, the wireless link distance is large or we have the problem of pilot contamination, the resulting SINR will be low, which is a parameter that is directly related to the quality of the channel estimation and the performance of the data reception [15–17]. An illustrative image of the previous concepts is shown in Fig. 1.2.

This problem is aggravated in massive multiple-input-multiple-output (MIMO), which is a promising technique for future wireless communications since it can increase the data rates, increase the reliability and cope with a larger number of simultaneous devices. In massive MIMO, the base-station (BS) is typically equipped with a large number of antennas that are coordinated. In these scenarios, the channels must be estimated for each antenna (which in TDD is simplified to at least each user due to channel reciprocity), and thus, the aforementioned problem of channel estimation aggravates [17]. In this context, algorithms and techniques that can make the massive MIMO work without the use of CSI are of interest.

The proposed algorithms and techniques are based on the NC-mMIMO, which allows to receive the data sent by a TX without the need to acquire the CSI. In this thesis, the NC will be based on the use of DMPSK, by means of a differential detection of the received signals

1.2 Research contributions

This thesis is focused on analyzing several properties of NC-mMIMO and designing and implementing new algorithms to improve the performance of single-user (SU) and multi-user (MU)

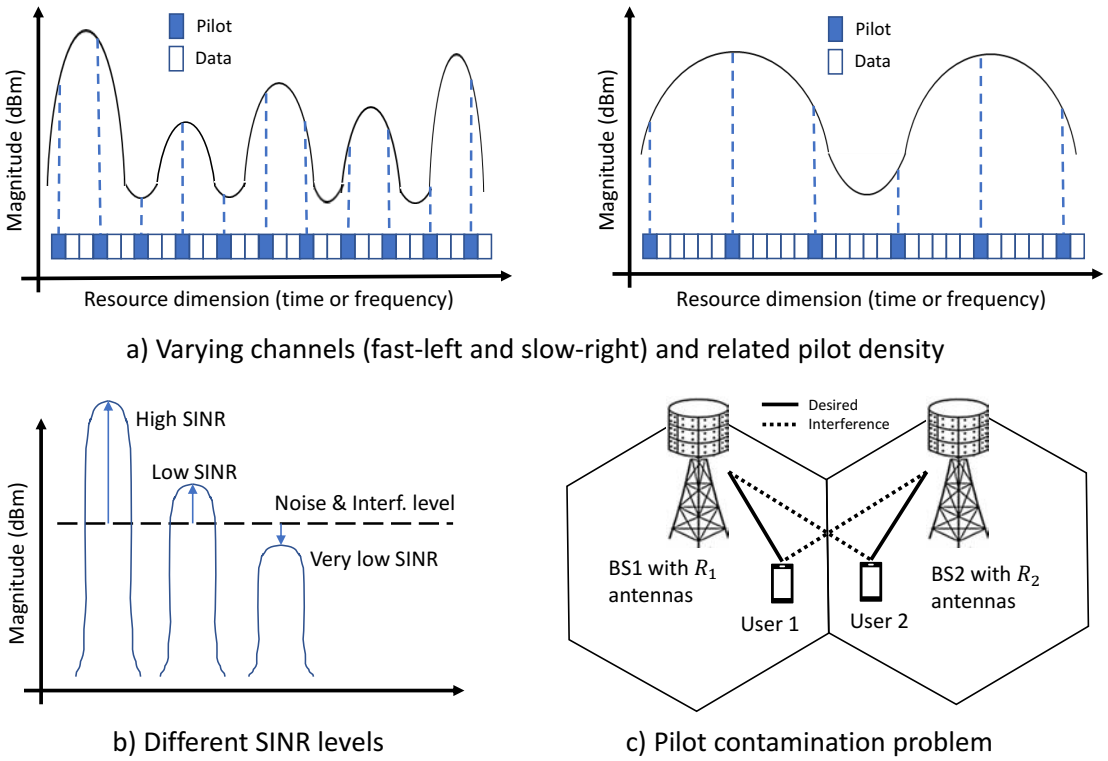

Figure 1.2: *Conceptual images of a) varying channels (fast-left and slow-right), b) different SINR levels and c) pilot contamination problem.*

NC-mMIMO. All contributions can be summarized as follows:

- A cell-free (CF) approach is proposed for the SU NC-mMIMO. The main idea is to make use of the access to several uncorrelated APs in order to increase the performance of the NC-mMIMO. First, a detailed analysis of the effect of Rician spatially correlated channels on the performance of NC-mMIMO is provided. Second, a set of techniques for AP selection in the proposed CF NC-mMIMO are provided. Third, a comparison between coherent and NC CF massive MIMO is done to demonstrate that the NC approach is better in scenarios with stringent conditions.

- A blind channel estimation technique based on reconstructing the NC data in RX to extract the channel information from the received signal is proposed. With this idea, first, an UL hybrid scheme combining the NC with the coherent scheme is proposed. In a classical pilot-symbol assisted modulation (PSAM), the pilots are substituted by NC data which will serve for both data trasmission and channel estimation, thus increasing the efficiency of the UL. Second, a pilot-less time-division duplex (TDD) massive MIMO

is proposed, in which the UL is only composed of NC data with which the channel is estimated for precoding the downlink (DL).

- Two constellation design techniques are proposed for MU NC-mMIMO based on solving numerical optimization problems due to the intractability when trying to apply classical constellation design techniques. The first technique approximates the joint constellation (JC) to a regular QAM shape and later conducts a bit mapping optimization over the individual constellations (ICs), while the second technique performs a Monte Carlo simulation of the performance allowing a joint constellation and mapping (JCM) design that does not make assumptions and is potentially optimal. A set of constellations is proposed with different number of users (up to 5), different constellation sizes (even between the users and up to 16-PSK) and different average received power.

1.3 Thesis outline

The remainder of this thesis is organized as follows:

- Chapter 2 addresses the background this thesis is built on. The coherent massive MIMO and OFDM are presented and their unsuitability for propagation channels with stringent conditions (fast time and frequency variations and low pilot SINR) is explained. The NC-mMIMO is presented as an alternative suitable for the aforementioned scenarios and a thorough explanation of its state-of-the-art is given.

- Chapter 3 explains the system model that this entire thesis relies on. Firstly, the channel model is presented, which consists of a Rician spatially correlated and time varying channel. Secondly, the coherent massive MIMO-OFDM is explained, which will be used for comparison purposes with the NC-mMIMO, which is lastly explained in this chapter.

- The contributions for the SU NC-mMIMO are included in Chapter 4 and Chapter 5. Two main contributions are included, the first one being the CF approach to be used in the NC-mMIMO scheme and the second one being the blind channel estimation technique conducted with detected NC-mMIMO data. This blind channel estimation is used on the one hand to increase the efficiency of the UL of a OFDM-MIMO system and on the other hand, to propose a pilot-less TDD massive MIMO system.

- Chapter 6 addresses the problem of constellation design in MU NC-mMIMO and proposes the two design methods previously indicated in Sec. 1.2 and indicates the constellations proposed for MU NC-mMIMO.

- Finally, Chapter 7 concludes by summarizing the work presented and the main contributions. Additionally, future research indications are outlined.

1.4 Mathematical Preliminaries

In this section we summarize some mathematical properties that will be useful along the mathematical derivations found in this thesis:

- The product of two zero mean uncorrelated normal random variables X and Y with standard deviation σ_X and σ_Y respectively, follows a variance-gamma distribution with parameters $VG(1, 0, \sigma_X\sigma_Y, 0)$.

- The sum of R variables distributed according to $VG(k, 0, \sigma_i, 0)$ is distributed according to $VG\left(kR, 0, \sqrt{\frac{\sum_{i=1}^{R}\sigma_i^2}{R}}, 0\right)$.

- Scaling a $VG(1, 0, \sigma, 0)$ random variable by any parameter k results in a variable distributed as $VG(1, 0, k\sigma, 0)$.

- A distribution $VG(R, 0, \sigma, 0)$ with $R \to \infty$ can be regarded as a $\mathcal{N}(0, R\sigma^2)$.

- If a variable that follows a Gamma distribution $\Gamma(\delta, \beta)$ is scaled by a parameter k, the new variable is distributed as $\Gamma(\delta, k\beta)$.

The distribution of the sum of n independent Gamma variables $\Gamma(\delta_i, \beta_i)$ is approximated as a $\Gamma(\delta_m, \beta_m)$ with

$$\delta_m = \frac{\left(\sum_{i=0}^{n}\delta_i\beta_i\right)^2}{\sum_{i=0}^{n}\delta_i\beta_i^2}, \quad \text{and} \quad \beta_m = \frac{\sum_{i=0}^{n}\delta_i\beta_i^2}{\sum_{i=0}^{n}\delta_i\beta_i}, \tag{1.1}$$

and when $\delta_m >> \beta_m$ (true when there are several APs with small correlation), according to [18],

$$\Gamma(\delta_m, \beta_m) \approx \mathcal{N}\left(\delta_m\beta_m, \delta_m\beta_m^2\right) = \mathcal{N}\left(\sum_{i=0}^{n}\delta_i\beta_i, \sum_{i=0}^{n}\delta_i\beta_i^2\right). \tag{1.2}$$

Besides this, $\mathfrak{R}$ and $\mathfrak{I}$ are the real and imaginary parts of a random variable, and thus we can decompose the product of two complex variables as

$$(\mathfrak{R}_1 + j\mathfrak{I}_1)(\mathfrak{R}_2 + j\mathfrak{I}_2) = (\mathfrak{R}_1\mathfrak{R}_2 - \mathfrak{I}_1\mathfrak{I}_2) + j(\mathfrak{R}_1\mathfrak{I}_2 + \mathfrak{I}_1\mathfrak{R}_2), \tag{1.3}$$

composed of the sums and products of real normal variables, distributed according to

$$\mathfrak{R}_1\mathfrak{R}_2 - \mathfrak{I}_1\mathfrak{I}_2 \sim VG\left(2, 0, \sqrt{\frac{\sigma^2_{\mathfrak{R}_1}\sigma^2_{\mathfrak{R}_2} + \sigma^2_{\mathfrak{I}_1}\sigma^2_{\mathfrak{I}_2}}{2}}, 0\right), \tag{1.4}$$

$$\mathfrak{R}_1\mathfrak{I}_2 + \mathfrak{I}_1\mathfrak{R}_2 \sim VG\left(2, 0, \sqrt{\frac{\sigma^2_{\mathfrak{R}_1}\sigma^2_{\mathfrak{I}_2} + \sigma^2_{\mathfrak{I}_1}\sigma^2_{\mathfrak{R}_2}}{2}}, 0\right). \tag{1.5}$$

Chapter 2

Towards pilot-less massive MIMO for stringent scenarios

Making wireless communications feasible in scenarios with stringent conditions, i.e., fast time and/or frequency channel variations and/or low SINR, has been of interest since the beginning of mobile communications. We have observed how new scenarios have been anticipated with each successive 3rd Generation Partnership Project (3GPP) standard, either being those with a faster speed mobility, scenarios with more multipath presence or scenarios in which the available transmit power is smaller. Therefore, it is of interest for the research community to develop new technologies that can work in the aforementioned scenarios with stringent conditions. In this chapter, we talk about massive multiple-input multiple-output with orthogonal frequency-division multiplexing (massive MIMO-OFDM), a technology that is of interest for future 3GPP standards and we show the importance of its NC variant for the foreseen scenarios.

2.1 Coherent massive MIMO-OFDM

2.1.1 Massive MIMO

The proposal of a multi-antenna system to enhance the data rates dates back to the early 90s, in which a larger spectral efficiency was intended by means of combining signals that were spatially multiplexed. Multi-antenna communications were afterwards referred to as MIMO, in which both the transmitter and the receiver have several antennas to achieve either more robustness or a higher data rate in the wireless link [19]. In later 2000s, the concept evolved to an access point, e.g. a cellular BS, with several antennas and several users with very few antennas, comparatively, which was named multi-user MIMO (MU-MIMO) [20]. The computational complexity and the training resources required to get the CSI of MU-MIMO grows with the number of active users. Thus, massive MIMO, firstly introduced by Marzetta in [21], consists of a BS equipped with a very large number of antennas and a smaller set of users (as

a rule of thumb, it is considered that the number of BS antennas is ten times that of the number of active users). The work in [22] lists the three primary benefits of massive MIMO as great spectrum efficiency, high energy efficiency, and low complexity linear signal processing. The channel hardening and favorable propagation [23, 24] make massive MIMO a competitive technology, whose meaning are shown below mathematically. Assuming $\mathbf{h}_u$ is the channel impulse response represented as a vector between user u and the BS with R antennas that tend to infinity, and backed by the law of large numbers [25], we have that

$$\frac{\mathbf{h}_u^H \mathbf{h}_{u'}}{\sqrt{\mathrm{E}\{||\mathbf{h}_u||^2\}\mathrm{E}\{||\mathbf{h}_{u'}||^2\}}} = \begin{cases} 1, & u = u' \quad \text{and} \quad R \to \infty \\ 0, & u \neq u' \quad \text{and} \quad R \to \infty \end{cases} . \tag{2.1}$$

A figure showing the concept behind massive MIMO and a real world testbed from Lund's university can be found in above Fig. 2.1.

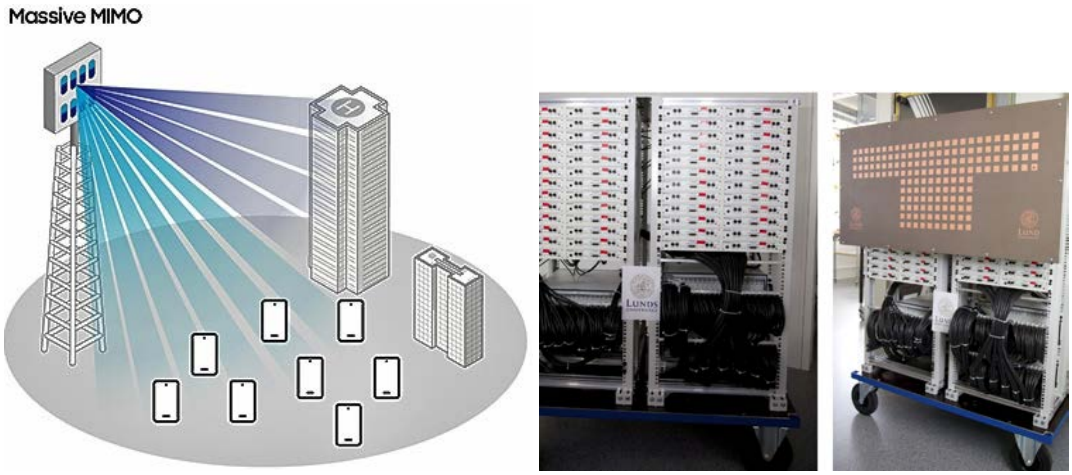

(a) *Massive MIMO concept.* **(b)** *Massive MIMO testbed from Lund.*

Figure 2.1: *Massive MIMO concept and testbed.*

From the two previous channel propagation properties induced by massive MIMO, the following consequences can be exploited:

- The excess number of antennas in the BSs allows for a reduction in transmission power that improves energy efficiency and allows for the utilization of additional degrees of freedom.
- The inter-user interference (IUI) vanishes as R grows, thus also resulting in the improvement of the energy and spectral efficiency.

- Linear processing becomes optimal when R is much larger than the number of users, and different linear pre/post-coders exist, them being maximum ratio combining (MRC) (which can be applied in each antenna independently), zero-forcing (ZF) (which can eliminate the IUI but must be processed in a centralized manner in the baseband and can create noise enhancement) and minimum mean-squared error (MMSE) (which is optimal in the SINR sense).

2.1.2 Orthogonal Frequency Division Multiplexing (OFDM)

OFDM is a multicarrier technique which was first proposed in 1985 in [26]. In the OFDM, the subcarriers are orthogonal between them, and has a series of advantages and disadvantages [27]. Robustness against multipath fading, ease of implementation and versatility to improve the transmission efficiency are some of its advantages. Some of its drawbacks include high peak-to-average power ratio (PAPR) and high side lobes in frequency domain, among others.

The baseband sampled version of the OFDM signal is the inverse discrete Fourier transform (IDFT) of the transmitted symbols and can be efficiently implemented with a fast Fourier transform (FFT). A guard interval or a cyclic prefix (CP) is very important to avoid inter-symbol interference (ISI) caused by the delay spread of the wireless channels. The receiver can be efficiently implemented with a discrete Fourier transform (DFT) or an FFT. A conceptual image of the time-frequency representation of the OFDM signal is shown in Fig. 2.2.

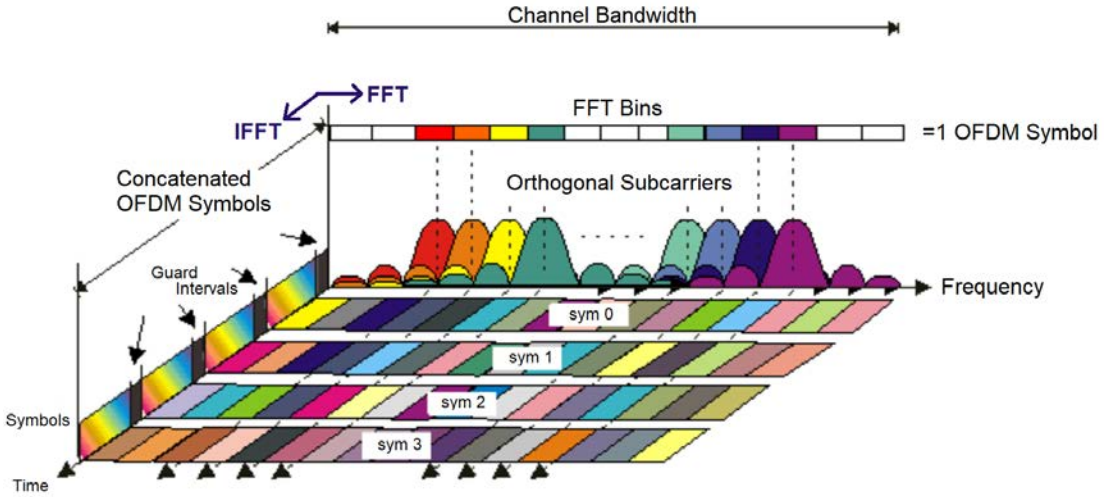

Figure 2.2: *Conceptual image of the time-frequency representation of the OFDM signal.*

2.1.3 Channel estimation for scenarios with stringent propagation conditions

In wireless communications, the physical properties of the propagation channels are critical to the performance of the communication link. Recalling the Shannon's capacity formula for a point-to-point (P2P) additive white Gaussian noise (AWGN) channel

$$C = W \cdot \log_2 \left(1 + \frac{P_T |h|^2}{N}\right), \tag{2.2}$$

where P_T is the transmitted power, N is the noise power in the receiver, W is the channel bandwidth and h is the instantaneous complex baseband channel response of the propagation channel. In this case, h is an scalar due to the fact that we are considering a P2P link for a certain frequency in a certain time instant. Beyond this, h can have several dimensions, caused by the fact that we may have:

- Several antennas in TX, RX or both.
- Several frequencies, mainly because of the use of multicarrier modulations.
- Several time instants.
- Several users.
- Any additional dimension.

Therefore, there are as many channels as the product of the sizes of each dimension.

In order to take advantage of the previously mentioned technologies (massive MIMO and OFDM), following a classical approach, it is necessary to estimate the channels between the TXs and the RXs. The family of techniques in which the channel estimation is required will be called coherent schemes. To estimate the channel, the TX must send reference known signals, typically known as pilots, to the RX [28]. In this manner, the RX can estimate the channel and can, in some cases, feed the so called CSI to the TX via a feedback link. In case the scenarios are static and there are not many multipath components, we only have to estimate the channels every once in a while for all the antennas combinations. On the contrary, when the channels vary very rapidly in time due to mobility and/or the existence of many multipath components between any pair of TX-RX antenna, the channels must be estimated much more frequently to keep track of channel variations [29]. Not only this, it is worth noting that in case the channel

estimated in the RX must be fed back to the TX, there is a certain delay in this process that results in a mismatch between the channel fed back by the RX and the actual channel that the TX sees. Apart from this, the channel estimation quality directly depends on the SINR of the received pilot signal, since the channel estimation is an estimation problem in the presence of interference and noise. This SINR is affected by the transmission power of the pilot signal, which is low in case the transmitter is battery powered, and by the interference to the pilot signal, which is mainly affected by the existence of other cells utilizing the same pilot signal, thus resulting in the so-called pilot contamination effect [16]. So, in case the channel must be estimated very often, many available resources (which are limited by definition) are used for channel estimation and not for data transmission, greatly affecting the data efficiency.

To summarize, these are the factors that affect the channel estimation quality and thus the performance of the communications link:

- Mobility: the mobility at a certain velocity between the TX and the RX creates a Doppler frequency spread that results in variations in the channel response in the time dimension.
- Reciprocity: it is directly related with the mobility and is caused by the fact that the channel reciprocity is true for a static channel. When the channel must be fed back from RX to TX, the channel is not the same.
- Multipath: the existence of several propagation paths between one antenna of the TX and one antenna of the RX. This causes a channel response that varies in frequency.
- SINR: the SINR affects the channel estimation quality since it is an estimation problem in the presence of interference and noise.

It is worth noting that some techniques have been proposed or foreseen to deal with the aforementioned problems, such as:

- Channel prediction: utilizing statistical time and frequency properties of the channel, the channel response can be predicted and less pilots would be needed. A classical example is the Kalman filter for channel prediction [30].
- TDD massive MIMO: the channel is estimated only in the BS and there is no neeed to feed it back to the users [17]. In this case, the number of required pilots is independent of the number of antennas in the BS.

- Pilot design to maximize the SINR: there are several techniques to increase the SINR of the pilot signals [31].

In any case, the capabilities of these techniques are limited and if the factors affecting the quality of the channel estimation are too severe, they will not succeed and the performance of the communication will be largely degraded, up to the point of making the communication unfeasible, as shown in [11].

2.2 Towards non-coherent massive MIMO communications

From the previous section, it can be concluded that, for propagation scenarios with stringent conditions of mobility, multipath and pilots' SINR, there is a need for techniques that can perform data transmission without the need of CSI. In this context, the concept of NC-mMIMO arises, which allows to receive the data transmitted by one or several TXs without the need to estimate any channel parameter, including the channel response h. Besides this, it is worth noting that the coherent schemes have a large complexity caused by the need to estimate the channel, compensate it and then perform data detection. Thus, there are two additional steps in the coherent scheme (estimation and compensation) that are not needed in the non-coherent schemes.

2.2.1 History of non-coherent MIMO

Since the 1960s, NC communications have been widely studied, with on-off-keying (OOK) and frequency shift keying (FSK) being the three predominant schemes, used only with binary signals. The technical features of all these schemes are described and compared to coherent schemes in [32]. The comparison is made in terms of spectral properties, complexity, performance and the effects provided by fading, delay distortion and interference. Even though initially it was FSK the preferred candidate, DMPSK was considered a better alternative than FSK around the 1990s [33, 34]. Generally, the structure of an NC receiver was based on a matched filter, an envelope detector, and a comparator, in that order. Successive developments of NC techniques resulted in contributions for radar systems [35], which later resulted in the development of Direct Sequence Spread Spectrum (DSSS) modulation schemes for the detection of NC [36].

2.2.2 State-of-the-art of non-coherent massive MIMO

All the previous work were focused on the single-input single-output (SISO) case, while the recent wireless technologies make use of MIMO, so it is interesting to explore NC techniques based on MIMO. In this context, Differential Unitary Space-Time Modulation (DUSTM) [37, 38] is the background of NC-mMIMO and is an extension of the standard DMPSK in a higher dimension to obtain NC communications using MIMO channels. In DUSTM, the channel is employed in R_T transmission blocks, where the number of transmit antennas is R_T, and the signals that are transmitted are part of a codebook composed of a set of $R_T \times R_T$ predefined unitary matrices. The main advantage of DUSTM is that it can be decoded using Multiple-Symbol Differential Detection (MSDD) in the receiver [39]. It is worth noting that DUSTM does not need to use CSI, but it needs the time coherence to occupy several intervals and high SNR. Other works for NC-mMIMO are based on codebooks of isotropically distributed unitary matrices on the compact Grassmannian manifold [40]. Since the codebooks take advantage of the MIMO channel features and take into account orthogonal subspaces that identify the transmitted symbols at the non-coherent receiver, these schemes are specifically made for block-fading. The main limitation of Grassmannian codes is that the proposed schemes are limited for high SINR and low number of antennas.

In the last years, the development of NC-mMIMO has gained a lot of interest. A DMPSK with $M = 4$ is proposed where the users can be geographically segregated using a special channel that mimics a Impulse Radio-Ultra Wide Band (IR-UWB) system, depending on their non-overlapping power-space characteristics. Nonetheless, it is not possible to exploit this channel model in general. Other NC-mMIMO studies are based on energy detection amplitude shift keying (ASK), which is simple in terms of complexity for the receiver, while the performance is not very good when compared with the DMPSK alternative. Several works from the research group of A. Goldsmith have been done in the topic of ASK for NC-mMIMO. The achievable rates scaling law were shown to be equivalent in [41] for coherent and NC schemes, assuming perfect CSI for the former. In [42], it was shown that NC schemes can outperform coherent schemes. Regarding the constellations design issue, [43] performed the constellation design for the ASK applied in the NC-mMIMO.

In contrast to energy-based designs, [44] proposes a number of constellations based on DMPSK that enable us to use differential detection and distinguish the received signals from various users simply by knowing their average power of the received signals while taking advantage

of the benefits of using a greater number of receive antennas. The users are multiplexed in the constellation domain, since, at the BS, a joint-symbol is received. This is a result of superposing all individual symbols transmitted by each UE with their different channel effects, in the same time-frequency resource. Another work [45] was based on the design of hexagonal uniquely factorable constellations for SU NC-mMIMO, which is of interest to be extended for the MU case. Suboptimal constellations for the multi-user scenario based on energy detection schemes were proposed in [46]. A small set of suboptimal constellations for the multi-user case were proposed in [2] and [3], for the NC based on DMPSK namely Type A, Type B, and equal error protection (EEP), with the first one based on designing the constellation to separate the users over sub-quadrants, the second one based on separating the elements via power control of the users and the third one based on placing the constellation elements of each user with a certain phase shift with respect to the others.

More recently, [47–49] have worked towards improving the development of NC-mMIMO schemes. Reference [47] proposes a differential space-time block coded spatial modulation (STBC-SM) that combines differential coding and STBC-SM to enhance the diversity benefits in the absence of CSI. Reference [48] develops a non-coherent index modulation (IM) system in which activation patterns are characterized by multi-level block codes. Last, [49] propose a simple constellation construction consisting in partitioning a single-user constellation, useful for joint constellation design for NC-mMIMO multiple-access. Furthermore, and due to the recent interest in machine learning techniques for wireless communications, some authors have utilized deep learning to improve the performance of non-coherent schemes [50].

We may say that the combination of differential schemes and massive MIMO gave birth to the NC-mMIMO concept that is dominant nowadays. There is much more literature on NC-mMIMO, but these are the main foundations upon which this work is built. Several other references are cited in this document to support claims, prove analytical statements, and/or justify assumptions.

Chapter 3
System Model for coherent and non-coherent massive MIMO systems

The baseline system model for NC-mMIMO, which forms the basis for the rest of the document, will be discussed throughout this chapter. First, the general channel model of a Rician channel with spatial, time and frequency correlation is presented. Second, the system model for coherent massive MIMO-OFDM is presented, including the UL training phase, the channel estimation and the UL filtering and DL precoding. Last, the multiuser NC-mMIMO system model is presented, with a detailed explanation of the DMPSK scheme followed by the application of spatial diversity in reception, which is the basis why NC-mMIMO works. It is worth noting that we present the multiuser system model since it can straightforwardly be simplified for the single user.

3.1 Propagation channel model

Unless otherwise stated in a specific section of this document, the works in this manuscript will follow a generic Rician channel model with spatial, time and frequency correlation, which we explain in this section. For this, we first describe the Rician channel and then, we describe the spatial, time and frequency correlation. We will make the description for a generic BS a with R_a antennas and a generic user u, for a generic discrete time instant n and a generic carrier frequency k. The channel of this thesis work follows a Rician distribution, which is a stochastic model for radio propagation caused when the signal arrives at the RX by several different paths where one of the paths (tipically the line-of-sight (LOS) component) is much stronger than the rest, which compose the non-line-of-sight (NLOS) component. The channel vector that links the user u with the BS a is

$$\mathbf{h}_{a,u}^{n,k} = \sqrt{\alpha_{a,u}^{n,k}} \left(\bar{\mathbf{h}}_{a,u}^{n,k} + \tilde{\mathbf{h}}_{a,u}^{n,k} \right), \tag{3.1}$$

where $\alpha_{a,u}^{n,k}$ is the channel gain accounting for pathloss and shadow fading (large-scale fading), $\bar{\mathbf{h}}_{a,u}^{n,k}$ is the LOS component and $\tilde{\mathbf{h}}_{a,u}^{n,k}$ the NLOS component, so $\mathbf{h}_{a,u}^{n,k} \sim$

$\mathcal{CN}(\sqrt{\alpha_{a,u}^{n,k}}\bar{\mathbf{h}}_{a,u}^{n,k}, \alpha_{a,u}^{n,k}\mathbf{R}_{a,u}^{n,k})$, where the undefined terms are defined below.

The pathloss will follow a simplistic version of the urban microcell 3GPP, which is described in [51], and was partially validated via measurements in the field [52]. It is expressed as $L_{a,u}^{n,k} = L_0 + 10p\log_{10}(d_{a,u}^{n,k}) + \chi_{a,u}^{n,k}$, where L_0 is the pathloss at a reference distance of 1 meter, p is pathloss exponent that depends on the environment, $d_{a,u}^{n,k}$ is the distance between the center of the array of the BS a and the user u and $\chi_{a,u}^{n,k}$ is the shadow fading component which is modeled as $\chi_{a,u}^{n,k} \sim \mathcal{N}(0, \sigma^2_{\chi_{a,u}^{n,k}})$. Thus, the channel gain is defined as $\alpha_{a,u}^{n,k} = 10^{-L_{a,u}^{n,k}/10}$.

Since each BS a is located in a different physical location, it happens that the channel responses of different BSs are totally uncorrelated, so $\mathbb{E}\left\{\left(\mathbf{h}_{a,u}^{n,k}\right)^H \mathbf{h}_{a',u}^{n,k}\right\} = 0$. Also, since the users are located in different physical locations, the channel responses of different users are totally uncorrelated, $\mathbb{E}\left\{\left(\mathbf{h}_{a,u}^{n,k}\right)^H \mathbf{h}_{a,u'}^{n,k}\right\} = 0$.

The LOS component $\bar{\mathbf{h}}_{a,u}^{n,k}$ is usually expressed as $\bar{\mathbf{h}}_{a,u}^{n,k} = |\bar{\mathbf{h}}_{a,u}^{n,k}|e^{j\mathbf{\Phi}_{a,u}^{n,k}}$, where $|\bar{\mathbf{h}}_{a,u}^{n,k}|$ denotes the vector of channel amplitudes and $\mathbf{\Phi}_{a,u}^{n,k}$ denotes the vector of channel phases. Besides, any element r_a (with $1 \leq r_a \leq R_a$) of the vector of channel amplitudes is defined as $\left[|\bar{\mathbf{h}}_{a,u}^{n,k}|\right]_{r_a} = \frac{\mathcal{K}_{a,u}^{n,k}}{\mathcal{K}_{a,u}^{n,k}+1}$, where $\mathcal{K}_{a,u}^{n,k}$ with $10\log_{10}\left(\mathcal{K}_{a,u}^{n,k}\right) \sim \mathcal{N}\left(\mu_{\mathcal{K}_{a,u}^{n,k}}, \sigma^2_{\mathcal{K}_{a,u}^{n,k}}\right)$ is the Ricean factor between BS a and user u.

The NLOS component $\tilde{\mathbf{h}}_{a,u}^{n,k}$ follows a $\mathcal{CN}(\mathbf{0}_{R_a}, \mathbf{R}_{a,u}^{n,k})$ distribution, where $\mathbf{R}_{a,u}^{n,k}$ represents the semi-definite spatial correlation matrix of the antenna array of BS a as seen from the user u. The spatial correlation is caused by three factors mainly: the antenna radiofrequency (RF) coupling in the antenna array, the antenna array geometry and the clustered channel propagation [53, 54]. Unless otherwise stated, the spatial correlation matrix will be defined as $\left[\mathbf{R}_{a,u}^{n,k}\right]_{r,r'} = (\delta_{a,u}^{n,k})^{|r-r'|}$, where r and r' are two antennas in the array and $\delta_{a,u}^{n,k}$ is the spatial correlation factor for user u and AP a between two consecutive antennas.

The time correlation between two time instants n and n' is modeled with the time variability as

$$\mathbb{E}\left\{\left|([\mathbf{h}_{a,u}^{n,k}]_{r_a})^*[\mathbf{h}_{a,u}^{n',k}]_{r_a}\right|\right\} = \left|J_0\left(2\pi f_D \frac{|n'-n|}{\Delta f}\left(1+\frac{L_{CP}}{K}\right)\right)\right| = \eta_{\vec{n}}, \tag{3.2}$$

where $J_0(\cdot)$ is the zero-th order Bessel function of the first kind, L_{CP} is the cyclic prefix (CP) length in samples (which is set sufficiently large in this thesis to avoid ISI), K is the number of subcarriers of the OFDM, Δf is the subcarrier spacing (SCS) and f_D is the maximum Doppler

frequency, with the last two measured in Hz. Furthermore, $f_D = f_c \frac{v}{c}$, where f_c is the carrier frequency, v is the moving velocity of the TX, c is the light speed and θ is the angle between the direction of propagation of the electromagnetic wave and the direction of the motion. The coherence time T_c of the channel is related in [121] to f_D as $T_c = \frac{1}{16\pi f_D}$. The symbol period of an OFDM symbol is $T_s = 1/\Delta f$. Along the text, we usually normalize the T_c to the T_s and refer to the coherence time in numbers of symbol periods as $N_c = \frac{T_c}{T_s} = \frac{3 \cdot 10^8 \cdot \Delta f}{16\pi f_c v}$.

We can define the frequency correlation [55] between subcarriers k and k' as

$$\mathbb{E}\left\{\left|([\mathbf{h}_{a,u}^{n,k}]_{r_a})^*[\mathbf{h}_{a,u}^{n,k'}]_{r_a}\right|\right\} = \sum_{l=0}^{L-1} d_l^2 \exp\left(j2\pi \frac{l|k-k'|}{K}\right) = \eta_{\vec{k}}, \tag{3.3}$$

where L is the number of paths of the multipath channel and d_l^2 is the variance of each path l. It is worth noting that $d_0^2 = \frac{\mathcal{K}_{a,u}^{n,k}}{\mathcal{K}_{a,u}^{n,k}+1}$ and $\sum_{l=1}^{L-1} d_l^2 = \frac{1}{\mathcal{K}_{a,u}^{n,k}+1}$, since the first (shortest path) is the LOS and the rest of the paths compose the so called NLOS.

There are some particularizations along this document to the channel model presented here, as:

- Should there only be one BS, the pathloss is normalized as $\alpha_{a,u}^{n,k} = 1$ and $A = 1$.
- If a Rayleigh (only NLOS) channel is considered, the Rician factor is $\mathcal{K}_{a,u}^{n,k} = 0$.
- In case there is no spatial correlation, then the spatial correlation matrix is the identity matrix of size $(R_a \times R_a)$ $\mathbf{R}_{a,u}^{n,k} = \mathbf{I}_{R_a}$.
- For no time variability, it is considered that the correlation is $\eta = 1$ and thus time block fading is considered.
- When no frequency correlation, or no OFDM is considered, and just a single carrier flat fading, then $\eta_k = 1$.

3.2 Coherent TDD massive MIMO-OFDM

In coherent massive MIMO-OFDM, the channel between the TX and the RX must be estimated and known at least at the RX side. For this, it is typical that some resources in the UL are occupied by reference signals, known in both sides of the communication link, and that are orthogonal for all the channels that want to be estimated. To minimize the number of reference

signals in massive MIMO, the best is to rely on the TDD alternative. In TDD, the steps of the communication process usually are:

- UL training phase: this step is in charge of estimating the channel, so both the pilot assignment and the channel estimation processes are considered and explained.

- DL precoding (data payload in the DL): in this step, with the estimated channel, the DL data is precoded to adapt it to the channel characteristics when transmitting from the BS to the user.

- UL filtering (data payload in the UL): similarly to the previous step, the UL data is filtered in the BS to remove the channel effects from the user to the BS.

3.2.1 UL training phase

The communication in a TDD massive MIMO system must start with the users sending training pilots (ideally orthogonal) to allow the RX side (the BSs) to estimate the channel. During the UL training phase, all U users simultaneously transmit pilot signals to the BSs. This approach is called PSAM. The received signal at the BS a from user u is given by

$$\mathbf{y}_{a,u} = \mathbf{h}_{a,u}\mathbf{p}_u + \sum_{\substack{u'=1 \\ u' \neq u}}^{U} \mathbf{h}_{a,u'}\mathbf{p}_{u'} + \boldsymbol{\nu}_a, \tag{3.4}$$

where $\mathbf{p}_u$ is the pilot of user u, $\boldsymbol{\nu}_a$ is the noise added by the BS a in reception and is distributed as $\mathcal{CN}(\mathbf{0}_{R_a}, \sigma^2_{\nu_a}\mathbf{1}_{R_a})$ unless otherwise stated. It is worth noting that the signal from user u is affected by IUI, which is the sum term. To reduce the interference from other users, the pilot signals between users are designed so that they are as orthogonal as possible. In an OFDM grid, it is common to place the pilots of different users in different resource elements, and thus the pilots will be orthogonal [56].

To estimate the channel, there are different approaches to process the received signal Eq. 3.4 that contains the pilot, including the least-squares (LS) or MMSE criteria. In this thesis, unless otherwise stated, when channel estimation is performed, it is done with the PSAM combined

with LS detection. The LS detection is performed such that

$$\hat{\mathbf{h}}_{a,u} = \mathbf{y}_{a,u}\mathbf{p}_u^\dagger = \mathbf{h}_{a,u}\mathbf{p}_u\mathbf{p}_u^\dagger + \sum_{\substack{u'=1 \\ u'\neq u}}^{U} \mathbf{h}_{a,u'}\mathbf{p}_{u'}\mathbf{p}_u^\dagger + \boldsymbol{\nu}_a\mathbf{p}_u^\dagger = \mathbf{h}_{a,u} + \hat{\boldsymbol{\nu}}_a, \tag{3.5}$$

where $\mathbf{p}_{u'}$ is the Moore-Penrose pseudoinverse of $\mathbf{p}_u$. The pilots are typically designed to minimize the IUI and avoid the noise enhancement, and thus $\mathbf{p}_u\mathbf{p}_u^\dagger = 1$ and $\mathbf{p}_{u'}\mathbf{p}_u^\dagger = 0$. The term $\hat{\boldsymbol{\nu}}_a$ is a varied noise term that has the same power, since $|\mathbf{p}_u^\dagger|^2 = 1$.

3.2.2 DL precoding and UL filtering

Once the channel is estimated, for the DL, a precoding vector is constructed for each BS a and for each user u, so that the data intended from the BSs to the user affects the least possible the other users. The DL data signal from BS a is given by

$$\mathbf{x}_{a,dl}^{n,k} = \sum_{u=0}^{U-1} \mathbf{b}_{a,u}^{n,k} s_{u,dl}^{n,k}, \tag{3.6}$$

where $\mathbf{b}_{a,u}^{nk}$ is the precoding vector of the data $s_{u,dl}^{n,k}$ (which satisfies $\mathbb{E}\{|s_{u,dl}^{n,k}|^2\} = 1$) in the DL and thus intended to user u from the BS a. At each user, the received signal will be

$$\mathbf{y}_{u,dl}^{n,k} = \sum_{a=0}^{A-1} (\mathbf{h}_{au}^{n,k})^H \mathbf{x}_{a,dl}^{n,k} + \boldsymbol{\nu}_u^{n,k}, \tag{3.7}$$

where $\boldsymbol{\nu}_u^{n,k}$ is the noise introduced by the receiver of user u and is distributed as $\mathcal{CN}(0, \sigma_{\nu_u}^2)$. A certain cooperation among BSs is possible and that is why there is a summation in the equation above. Some further processing may be needed such as compensation of power constraints, TRX chains imperfections or inequalities, and so on. This leads to the fact that additional processing may be needed over $\mathbf{y}_u^{n,k}$ to detect the desired data $\hat{s}_{u,dl}^{n,k}$ that most likely resembles $s_{u,dl}^{n,k}$, but these details are out of the scope of this part of the thesis and details will be given in each chapter in case it is necessary.

Firstly, we define the received signal in BS a as

$$\mathbf{y}_{a,ul}^{n,k} = \sum_{u=0}^{U-1} \mathbf{h}_{a,u}^{n,k} \mathbf{s}_{u,ul}^{n,k} + \boldsymbol{\nu}_a^{n,k}, \tag{3.8}$$

where $\boldsymbol{\nu}_a^{n,k}$ is the noise introduced by the receiver of the BS a and is distributed as $\mathcal{CN}(0, \sigma_{\nu_a}^2)$. Similarly to the DL, a filtering vector $\mathbf{g}_{a,u}^{n,k}$ is defined in each BS a for the uplink operation, which is used as

$$\mathbf{z}_{u,ul}^{n,k} = \sum_{a=0}^{A-1} \mathbf{g}_{a,u}^{n,k} \mathbf{y}_{a,ul}^{n,k} = \sum_{a=0}^{A-1} \mathbf{g}_{a,u}^{n,k} \left(\sum_{u=0}^{U-1} \mathbf{h}_{a,u}^{n,k} \mathbf{s}_{u,ul}^{n,k} + \boldsymbol{\nu}_a^{n,k} \right), \tag{3.9}$$

where a summation over the BSs is possible and can increase the performance over detecting only over a single BS. Once again, further processing is needed over $\mathbf{z}_{u,ul}^{n,k}$ to detect the desired data $\hat{s}_{u,ul}^{n,k}$ that most likely resembles $s_{u,ul}^{n,k}$.

Usually, both the precoding vector $\mathbf{b}_{a,u}^{n,k}$ and the filtering one $\mathbf{g}_{a,u}^{n,k}$ are functions of the estimated channel $\hat{\mathbf{h}}_{a,u}$, and thus any channel estimation error or problem will result in detection problems, getting to the case of making it unfeasible to estimate the channel.

3.2.3 Channel estimation imperfection

In this section, and for the sake of clarity, we are showing how the channel estimation errors stack onto each other given the channel time or frequency variations and the error in the channel estimation given the noise presence in the estimation process.

Following [57], we define an autoregressive model that approximates the correlation in time as

$$\mathbf{h}_{a,u}^{n',k} = \eta_{\vec{n}} \mathbf{h}_{a,u}^{n,k} + \sqrt{1 - \eta_{\vec{n}}^2} \vec{\mathbf{h}}_{a,u}^{n',k}, \tag{3.10}$$

where $\vec{\mathbf{h}}_{a,u}^{n',k}$ denotes what is called the independent innovation component. Therefore, the channel in time instant n' is related to the channel in time instant n by the time correlation $\eta_{\vec{n}}$ and the innovation component. The innovation component is composed of a Rician correlated channel that is uncorrelated with the channel $\mathbf{h}_{a,u}^{n,k}$ and is defined as $\vec{\mathbf{h}}_{a,u}^{n,k} \sim \mathcal{CN}(\sqrt{\alpha_{a,u}^{n,k}} \vec{\mathbf{h}}_{a,u}^{n,k}, \alpha_{a,u}^{n,k} \vec{\mathbf{R}}_{a,u}^{n,k})$.

The channel is estimated in time instant n as $\hat{\mathbf{h}}_{a,u}^{n,k} = \mathbf{h}_{a,u}^{n,k} + \hat{\boldsymbol{\nu}}_a^{n,k}$ and compensated in time instant n'. This compensation is usually done with either the MRC, the ZF or the MMSE precoding and filtering.

As an illustrative case, the MRC filter for the UL is defined as $\mathbf{g}_{a,u}^{n,k} = (\widehat{\mathbf{h}}_{a,u}^{n,k})^H$, so in case it is

applied to the received signal in Eq. 3.8. The filtered signal in all BS would be

$$\begin{aligned}\mathbf{z}_{u,ul}^{n',k} &= \sum_{a=0}^{A-1}(\hat{\mathbf{h}}_{a,u}^{n,k})^H \mathbf{y}_{a,ul}^{n',k} = \sum_{a=0}^{A-1}\left(\mathbf{h}_{a,u}^{n,k}+\hat{\boldsymbol{\nu}}_a^{n,k}\right)^H\left(\sum_{u=0}^{U-1}\mathbf{h}_{a,u}^{n',k}\mathbf{s}_{u,ul}^{n',k}+\boldsymbol{\nu}_a^{n',k}\right)\\ &= \sum_{a=0}^{A-1}\Bigg[(\mathbf{h}_{a,u}^{n,k})^H\mathbf{h}_{a,u}^{n',k}\mathbf{s}_{u,ul}^{n',k}+(\hat{\boldsymbol{\nu}}_a^{n,k})^H\hat{\boldsymbol{\nu}}_a^{n',k}+(\hat{\boldsymbol{\nu}}_a^{n,k})^H\mathbf{h}_{a,u}^{n',k}\mathbf{s}_{u,ul}^{n',k}+\\ &+\sum_{\substack{u'=0\\u'\neq u}}^{U-1}\left(\mathbf{h}_{a,u}^{n,k}+\hat{\boldsymbol{\nu}}_a^{n,k}\right)^H\mathbf{h}_{a,u}^{n',k}\mathbf{s}_{u,ul}^{n',k}\Bigg],\end{aligned} \tag{3.11}$$

which can be finally written as

$$\mathbf{z}_{u,ul}^{n',k} = \underbrace{\sum_{a=0}^{A-1}\eta_{\vec{n}}(\mathbf{h}_{a,u}^{n,k})^H\mathbf{h}_{a,u}^{n,k}\mathbf{s}_{u,ul}^{n',k}}_{Useful}+\underbrace{\sum_{a=0}^{A-1}\left[\check{\boldsymbol{\nu}}_{a,u}^{n,k}+\sqrt{1-\eta_{\vec{n}}^2}\vec{\mathbf{h}}_{a,u}^{n',k}\mathbf{s}_{u,ul}^{n',k}\right]}_{Interference} \tag{3.12}$$

where

$$\check{\boldsymbol{\nu}}_{a,u}^{n,k} = (\hat{\boldsymbol{\nu}}_a^{n,k})^H\hat{\boldsymbol{\nu}}_a^{n',k}+(\hat{\boldsymbol{\nu}}_a^{n,k})^H\mathbf{h}_{a,u}^{n',k}\mathbf{s}_{u,ul}^{n',k}+\sum_{\substack{u'=0\\u'\neq u}}^{U-1}\left(\mathbf{h}_{a,u}^{n,k}+\hat{\boldsymbol{\nu}}_a^{n,k}\right)^H\mathbf{h}_{a,u}^{n',k}\mathbf{s}_{u,ul}^{n',k}. \tag{3.13}$$

By looking at Eq. 3.11 and Eq. 3.12, one can see that the received signal after filtering in the UL has a lot of interefering terms that do not only come from the IUI, but from the imperfect channel estimation and from the fact that the estimated channel "ages" with respect to the channel that must be compensated. That is the reason why the channel estimation is problematic when $\eta_{\vec{n}}$ (time correlation due to channel time variability) and/or $|\mathbf{p}_u|^2/\sigma_{\nu_a}^2$ (SNR of the channel estimation) are very small.

An equivalent derivation can be done for variations in the frequency domain by changing $\eta_{\vec{n}}$ for $\eta_{\vec{k}}$. Similarly, the same process can be done in case ZF is employed, in which the filtering matrix would follow the equation

$$\mathbf{b}_{a,u}^{n,k} = (\widehat{\mathbf{h}}_{a,u}^{n,k})^\dagger = \left((\widehat{\mathbf{h}}_{a,u}^{n,k})^H\widehat{\mathbf{h}}_{a,u}^{n,k}\right)^{-1}(\widehat{\mathbf{h}}_{a,u}^{n,k})^H \tag{3.14}$$

3.3 Non-coherent massive MIMO-OFDM

Contrary to classical massive MIMO-OFDM, NC-mMIMO can detect the symbols transmitted by some users in the UL without the need to acquire any kind of CSI. In this section, we particularize our system model to one BS with many antennas and some users. The non-coherent massive MIMO-OFDM based on DMPSK is based on performing a differential encoding in

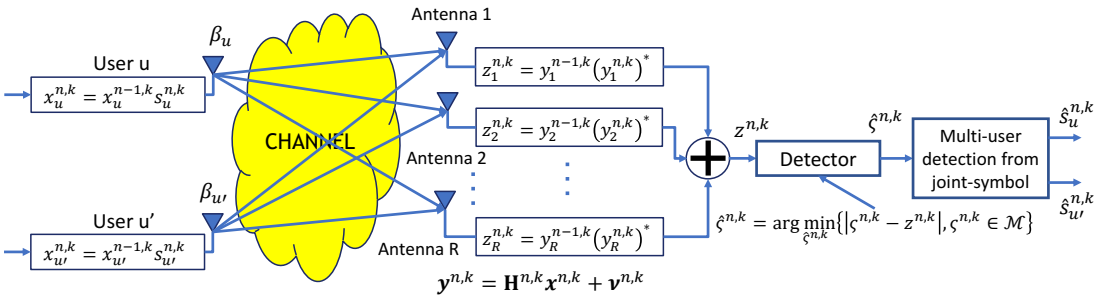

Figure 3.1: *Non-coherent multiuser massive MIMO scheme.*

We consider a MU single-input multiple-output (SIMO) uplink scenario, where a certain BS is equipped with R antennas to receive the signals transmitted from U users. The signal transmitted by any user u at time instant n is s_u^n, which belongs to a DMPSK constellation and is differentially encoded as

$$x_u^n = x_u^{n-1} s_u^n, \quad n > 0, \tag{3.15}$$

where x_u^0 is a single known reference symbol of the u-th user. Assuming a flat-fading[1] channel, the received signal is

$$\mathbf{y}^n = \mathbf{H}^n \boldsymbol{\beta} \mathbf{x}^n + \boldsymbol{\nu}^n, \tag{3.16}$$

$$\mathbf{x}^n = [x_1^n, \cdots, x_U^n]^T \text{ and } \mathbf{H}^n = [\mathbf{h}_1^n, \cdots, \mathbf{h}_U^n]^T \text{ and } \boldsymbol{\beta} = \text{diag}\left(\left[\sqrt{\beta_1}, \cdots, \sqrt{\beta_U}\right]\right), \tag{3.17}$$

where $\boldsymbol{\nu}^n$ is the additive white Gaussian noise (AWGN) vector with each element distributed as $\mathcal{CN}(0, \sigma_\nu^2)$, β_u denotes the ratio of the received average power of the u-th UE, with respect to some user ($\beta_u^{\min} = 1$, $\beta_u \geq 1$, without loss of generality), which is proportional to the composition of the large-scale channel effects and the power control of each user. Moreover,

[1] For non-flat fading channels, we can use OFDM, therefore creating multiple parallel channels that are regarded as flat-fading.

$\mathbf{H} \in \mathbb{C}^{R \times U}$ represents the small-scale fading. The reference SNR is defined as

$$\rho = \frac{1}{\sigma_\nu^2} \sum_{u=1}^{U} \beta_u = \sum_{u=1}^{U} \frac{\beta_u}{\sigma_\nu^2} = \sum_{u=1}^{U} \rho_u, \tag{3.18}$$

where ρ_u is the SNR of user u.

The phase difference of two consecutive symbols received at each antenna is non-coherently detected (differentially decoded) as

$$\begin{aligned} z^n &= \frac{(\mathbf{y}^{n-1})^H \mathbf{y}^n}{R} = \frac{1}{R}(\mathbf{H}^{n-1}\boldsymbol{\beta}\mathbf{x}^{n-1} + \boldsymbol{\nu}^{n-1})^H(\mathbf{H}^n\boldsymbol{\beta}\mathbf{x}^n + \boldsymbol{\nu}^n) = \\ &= \frac{1}{R}(\mathbf{x}^{n-1})^H\boldsymbol{\beta}(\mathbf{H}^{n-1})^H\mathbf{H}\boldsymbol{\beta}\mathbf{x}^n + \frac{1}{R}(\mathbf{x}^{n-1})^H\boldsymbol{\beta}(\mathbf{H}^{n-1})^H\boldsymbol{\nu}^n + \\ &+ \frac{1}{R}(\boldsymbol{\nu}^{n-1})^H\mathbf{H}^n\boldsymbol{\beta}\mathbf{x}^n + \frac{1}{R}(\boldsymbol{\nu}^{n-1})^H\boldsymbol{\nu}^n. \end{aligned} \tag{3.19}$$

For a very large number of antennas, using the asymptotic property of massive SIMO, by making use of the Law of Large Numbers, assuming that $\mathbf{H}^{n-1} \approx \mathbf{H}^n$ and that the channel follows a Rayleigh distribution ($\mathbf{H}^n \sim \mathcal{CN}(0, \mathbf{I}_R)$) and as shown in [58], we know that $\frac{1}{R}(\mathbf{H}^{n-1})^H\mathbf{H}^n \xrightarrow{R\to\infty} U$, and thus

$$z^n \xrightarrow{R\to\infty} \varsigma^n = \sum_{u=1}^{U} \beta_u s_u^n \in \mathfrak{M}_{NC}, \tag{3.20}$$

where $\mathfrak{M}$ is the joint-constellation set whose elements are obtained from the superimposed combinations of the constellation points of each user together with their mean received power.

The detection of the transmitted data is performed via a maximum likelihood detection as

$$\hat{\varsigma}^n = \arg\min_{\varsigma^n} \left\{ |\varsigma^n - z^n|,\ \varsigma^n \in \mathfrak{M}_{NC} \right\}, \tag{3.21}$$

taking into account that Eq. 3.19 can be rewritten as

$$z^n = \varsigma^n + \tilde{\nu}^n, \tag{3.22}$$

where $\tilde{\nu}$ contains all the cross terms of the noise and inter-user interference.

Similarly, the differential encoding can be performed in the frequency domain (or a combination) by changing the role of n and k, applying a phase error compensation over the streams in

frequency, as shown in [59].

Chapter 4

Single user non-coherent cell-free massive SIMO

In this chapter we propose a cell-free non-coherent (NC) massive single-input-multiple-output system in a wireless uplink where a single-antenna user transmits to several multi-antenna access-points (APs). NC detection assisted differential phase shift keying is the modulation to be used in this system. It has the advantage that no channel state information is required in the APs for the signal reception. Moreover, the NC data can be used to estimate the channel. We show that a higher number of APs does not always translate into better quality in this system, and we give insights on when to add extra APs. We also show how to select them when different APs are accessible to the user. Last, we provide some numerical results that demonstrate our analysis is correct and finalize with some conclusions.

4.1 Specific system model for the cell-free NC massive MIMO

We consider a generic massive MIMO system with A APs, with R_a antennas in AP a, and we focus on a particular user with one antenna. In case of cooperation, it is assumed that the APs are connected to a central processing unit (CPU) by means of fronthaul links, whose constraints are not taken into account. It is assumed that the channel coherence time is defined as τ_c.

4.1.1 Channel Model

The propagation channel between the user and the AP a at time instant n is represented by $\mathbf{h}_a^n$ ($R_a \times 1$). In detail,

$$\mathbf{h}_a^n = \sqrt{\alpha_a^n}\left(\bar{\mathbf{h}}_a^n + \mathbf{g}_a^n\right), \tag{4.1}$$

where α_a^n denotes the channel gain accounting for pathloss and shadow fading (large-scale fading), $\bar{\mathbf{h}}_a^n$ ($R_a \times 1$) represents a LOS component, where all elements are equal to $|\bar{h}_a^n|e^{j\theta_a^n}$, so

that $\mathbf{h}_a^n \sim \left(\bar{\mathbf{h}}_a^n, (\sigma_{h,a}^n)^2 \mathbf{R}_a^n\right)$ and $\theta_a^n \sim U(0, 2\pi)$, with

$$|\bar{h}_a^n|^2 = \frac{K_a^n}{K_a^n + 1} \qquad \text{and} \qquad (\sigma_{h,a}^n)^2 = \frac{1}{K_a^n + 1}, \tag{4.2}$$

where K_a^n is the Rician factor, which characterizes the fading model and $\mathbf{g}_a^n$ $(R_a \times 1)$, with $\mathbb{E}\left\{(\mathbf{g}_a^n)^H(\mathbf{g}_a^n)\right\} = (\sigma_{h,a}^n)^2 \mathbf{R}_a^n$ ($\mathbf{R}_a^n$ is a normalized Hermitian matrix of size $(R_a \times R_a)$), which represents small-scale fading, i.e. the NLOS component. We assume that the channel in two consecutive symbol time instants can be regarded as approximately equal $[\mathbf{h}_a^{n-1}]_{r_a} \approx [\mathbf{h}_a^n]_{r_a}$, for any antenna. The channel coefficients between APs are uncorrelated as $\mathbb{E}\left\{(\mathbf{h}_a^n)^H(\mathbf{h}_{a'}^n)\right\} = \mathbf{0} \quad \forall a \neq a'$.

4.1.2 Proposed non-coherent cell-free massive SIMO

We propose a NC-CF massive SIMO (NC-CF-mSIMO) in which the channel estimation is avoided since it is not needed to detect the transmitted data. Therefore, this proposal is not affected by the limitations inherent to the channel estimation. Besides this, the NC system will benefit from a multi-AP processing due to the fact that the spatial correlation is reduced between APs and a higher number of effective antennas are utilized.

We focus on the particular case of the UL, where the user transmits a differentially encoded signal at time instant n

$$x^n = x^{n-1} s^n \quad 1 \leq n \leq N, \tag{4.3}$$

where s^n is the symbol belonging to a DMPSK constellation and x^0 is a reference symbol known at the receiver side and necessary to perform the differential reception. Because the information is only encoded in the phase, we know that $(x^{n-1})^* x^n = s^n$.

The received signal at AP a and n-th time instant is

$$\mathbf{y}_a^n = \mathbf{h}_a^n x^n + \boldsymbol{\nu}_a^n, \tag{4.4}$$

where x^n denotes the transmitted symbol at time n by the user of interest and $\boldsymbol{\nu}_a^n$ $(R_a \times 1)$ represents the additive white Gaussian noise according to $\boldsymbol{\nu}_a^n \sim \mathcal{CN}(\mathbf{0}, (\sigma_{\nu,a}^n)^2 \mathbf{I}_{R_a})$. Finally, the signal-to-noise ratio (SNR) in AP a is defined as $\rho_a = \alpha_a^n (\sigma_{\nu,a}^n)^{-2}$, where we set the power of the transmitted symbols to one.

In reception at each AP a, two contiguous differential symbols in the time domain are non-coherently combined as

$$z_a^n = (\mathbf{y}_a^{n-1})^H \mathbf{y}_a^n = \sum_{r_a=1}^{R_a} \left[\mathbf{y}_a^{n-1}\right]_{r_a}^* \left[\mathbf{y}_a^n\right]_{r_a} = \sum_{r_a=1}^{R_a} \left[\mathbf{z}_a^n\right]_{r_a}. \tag{4.5}$$

In a scenario with $A > 1$ APs (multi-AP), some selected variables z_a are sent to the CPU and combined as

$$z^n = \frac{\sum_{a\in\mathcal{A}_s} z_a^n}{\sum_{a\in\mathcal{A}_s} R_a}, \tag{4.6}$$

where $\mathcal{A}_s$ indicates the subset of APs selected to send their z_a^n to the CPU for decision and z^n is the variable over which the transmitted symbols are estimated according to [2] as

$$\hat{s}^n = \arg\min_{s^n} \left\{ \left| s^n - z^n \right|,\ s^n \in \mathfrak{M} \right\}, \tag{4.7}$$

where $\mathfrak{M}$ indicates the DMPSK constellation set with M elements. The proposed detection process in Eq. 4.6 is made by first performing a distributed processing in each AP following Eq. 4.5 and then the resulting variable z_a^n in each AP is sent to the CPU for a centralized combining. This is proposed, rather than sending the raw data to the CPU and performing detection as in [2], since the result is mathematically the same while the fronthaul would be unnecessarily overloaded. A mean SNR for the APs is defined as

$$\bar{\rho} = \frac{1}{A}\sum_{a=1}^{A} \rho_a = \frac{1}{A}\sum_{a=1}^{A} \frac{\alpha_a^n}{(\sigma_{\nu,a}^n)^2}. \tag{4.8}$$

It is worth noting that our proposal does not need to estimate the channel as it is the case for the coherent scheme, which is explained in Section 4.4. Therefore, this proposal is more efficient in terms of throughput and complexity.

4.2 Distortion, Interference and Noise Terms in Non-coherent Cell-free M-DPSK Massive SIMO

The distortion, interference and noise (DIN) terms in each AP a is characterized in this section, since it will be useful to characterize the performance of each post-processing scheme proposed in Section 4.3. To account for the case of APs with $R_a = 1$, we have to analyze first the

distribution per antenna, later per AP and last for several APs. Mathematical preliminaries that are useful to understand this section can be found in Appendix 1.4.

4.2.1 Distribution of the received symbol in a single antenna

We characterize the distribution of $[\mathbf{z}_a^n]_{r_a}$ by taking into account that the product of a circularly symmetric variable by x^n or $(x^n)^*$ does not change the variable distribution. With some straightforward derivations, Eq. 4.5 can be expanded as

$$\begin{aligned}[\mathbf{z}_a^n]_{r_a} = &\underbrace{\left[\mathbf{h}_a^{n-1}\right]_{r_a}^* [\mathbf{h}_a^n]_{r_a}}_{[\mathbf{z}_a^n]_{r_a}^{(1)}} \underbrace{(x^{n-1})^* x^n}_{s^n} + \underbrace{[\boldsymbol{\nu}_a^{n-1}]_{r_a}^* [\boldsymbol{\nu}_a^n]_{r_a}}_{[\mathbf{z}_a^n]_{r_a}^{(2)}} + \\ &+ \underbrace{[\boldsymbol{\nu}_a^{n-1}]_{r_a}^* [\mathbf{h}_a^n]_{r_a}}_{[\mathbf{z}_a^n]_{r_a}^{(3)}} x^n + \underbrace{\left[\mathbf{h}_a^{n-1}\right]_{r_a}^* [\boldsymbol{\nu}_a^n]_{r_a}}_{[\mathbf{z}_a^n]_{r_a}^{(4)}} (x^{n-1})^*\end{aligned} \tag{4.9}$$

where (and since $[\mathbf{g}_a^n]_{r_a} \approx [\mathbf{g}_a^{n-1}]_{r_a}$ and $[\bar{\mathbf{h}}_a^n]_{r_a} \approx [\bar{\mathbf{h}}_a^{n-1}]_{r_a}$) each element expands as

$$\begin{aligned}[\mathbf{z}_a^n]_{r_a}^{(1)} &= \alpha_a^n \left([\bar{\mathbf{h}}_a^n]_{r_a}^* + [\mathbf{g}_a^n]_{r_a}^*\right)\left([\bar{\mathbf{h}}_a^n]_{r_a} + [\mathbf{g}_a^n]_{r_a}\right) = \\ &= \alpha_a^n |\bar{h}_a^n|^2 + \underbrace{2\alpha_a^n \Re\{[\bar{\mathbf{h}}_a^n]_{r_a}^* [\mathbf{g}_a^n]_{r_a}\}}_{[\mathbf{z}_a^n]_{r_a}^{(1,1)}} + \underbrace{\alpha_a^n \left|[\mathbf{g}_a^n]_{r_a}\right|^2}_{[\mathbf{z}_a^n]_{r_a}^{(1,2)}},\end{aligned} \tag{4.10}$$

$$[\mathbf{z}_a^n]_{r_a}^{(3)} = \underbrace{\sqrt{\alpha_a^n}[\boldsymbol{\nu}_a^n]_{r_a}^* [\bar{\mathbf{h}}_a^n]_{r_a}}_{[\mathbf{z}_a^n]_{r_a}^{(3,1)}} + \underbrace{\sqrt{\alpha_a^n}[\boldsymbol{\nu}_a^n]_{r_a}^* [\mathbf{g}_a^n]_{r_a}}_{[\mathbf{z}_a^n]_{r_a}^{(3,2)}}, \tag{4.11}$$

$$[\mathbf{z}_a^n]_{r_a}^{(4)} = \underbrace{\sqrt{\alpha_a^n}[\bar{\mathbf{h}}_a^n]_{r_a}^* [\boldsymbol{\nu}_a^n]_{r_a}}_{[\mathbf{z}_a^n]_{r_a}^{(4,1)}} + \underbrace{\sqrt{\alpha_a^n}[\mathbf{g}_a^n]_{r_a}^* [\boldsymbol{\nu}_a^n]_{r_a}}_{[\mathbf{z}_a^n]_{r_a}^{(4,2)}}. \tag{4.12}$$

From now on, we drop the time notation "n" for ease of reading. Using the properties of variance Gamma (VG) and Gamma distributions, which can be found in [60–62], we have the distribution of each term:

$$\Re, \Im \left\{ [\mathbf{z}_a]_{r_a}^{(2)} \right\} \sim VG\left(2, 0, \frac{\sigma_{\nu,a}^2}{2}, 0\right), \tag{4.13}$$

$$\Re, \Im \left\{ [\mathbf{z}_a]_{r_a}^{(3,2)}, [\mathbf{z}_a]_{r_a}^{(4,2)} \right\} \sim VG\left(2, 0, \frac{\sqrt{\alpha_a}\sigma_{h,a}\sigma_{\nu,a}}{2}, 0\right), \tag{4.14}$$

$$\Re, \Im \left\{ [\mathbf{z}_a]_{r_a}^{(3,1)}, [\mathbf{z}_a]_{r_a}^{(4,1)} \right\} \sim \mathcal{CN}(0, \alpha_a |\bar{h}_a|^2 \sigma_{\nu,a}^2), \tag{4.15}$$

$$\Re\left\{[\mathbf{z}_a]_{r_a}^{(1,1)}\right\} \sim \mathcal{N}(0, 2\alpha_a^2|\bar{h}_a|^2\sigma_{h,a}^2), \quad \Im\left\{[\mathbf{z}_a]_{r_a}^{(1,1)}\right\} = 0, \tag{4.16}$$

$$\Re\left\{[\mathbf{z}_a]_{r_a}^{(1,2)}\right\} \sim \Gamma(1, \alpha_a\sigma_{h,a}^2), \quad \Im\left\{[\mathbf{z}_a]_{r_a}^{(1,2)}\right\} = 0. \tag{4.17}$$

4.2.2 Distribution of the received symbol at each AP

We calculate the distribution of the real part and the imaginary part of z_a separately since they will be different due to the differential data processing in reception by following [63].

Following the VG properties [60–62], the summation of R_a elements (for a large R_a) for Eq. 4.13 and Eq. 4.14 can be regarded (please note Eq. 4.14) sums $2R_a$ terms), respectively, as

$$VG\left(4R_a, 0, \sqrt{\frac{2R_a\alpha_a\sigma_{\nu,a}^2}{8R_a\sigma_{h,a}^{-2}}}, 0\right) \xrightarrow{R_a\to\infty} \mathcal{N}\left(0, R_a\alpha_a\sigma_{h,a}^2\sigma_{\nu,a}^2\right), \tag{4.18}$$

$$VG\left(2R_a, 0, \sqrt{\frac{R_a\sigma_{\nu,a}^4}{4R_a}}, 0\right) \xrightarrow{R_a\to\infty} \mathcal{N}\left(0, R_a\frac{\sigma_{\nu,a}^4}{2}\right), \tag{4.19}$$

contributing equally to the real and imaginary parts.

To obtain Eq. 4.15, we sum $2R_a$ terms but take half the variance for the real part and half the variance for the imaginary part. Thus, the distribution for both the real and the imaginary part is

$$\mathcal{CN}(0, \alpha_a|\bar{h}_a|^2\sigma_{\nu,a}^2) \xrightarrow{R_a\to\infty} \mathcal{N}(0, R_a\alpha_a|\bar{h}_a|^2\sigma_{\nu,a}^2). \tag{4.20}$$

In a certain AP whose antennas are spatially correlated, the summation of the R_a elements in the AP for eqs. Eq. 4.16 and Eq. 4.17 can be calculated following the properties found in [18, 63, 64] (please note these terms only contribute to the real part) as

$$\mathcal{N}(0, 2\alpha_a^2|\bar{h}_a|^2\sigma_{h,a}^2) \xrightarrow{R_a\to\infty} \mathcal{N}(0, 2\alpha_a^2|\bar{h}_a|^2\sigma_{h,a}^2\mathbf{1}^T\mathbf{R}_a\mathbf{1}) \tag{4.21}$$

$$\Gamma(1, \alpha_a\sigma_{h,a}^2) \xrightarrow{R_a\to\infty} \mathcal{N}\left(R_a\alpha_a\sigma_{h,a}^2, \alpha_a^2\sigma_{h,a}^4\|\mathbf{R}_a\|_2^2\right). \tag{4.22}$$

Grouping all the previous elements accordingly, via straightforward manipulations, the distribution of the received symbol Eq. 4.5 for APs with R_a antennas and spatial correlation defined by matrix $\mathbf{R}_a$ can be computed assuming $s = 1$ without loss of generality, as

$\Re\{z_a\} \sim \mathcal{N}\left(\mu_{\Re\{z_a\}}, \sigma^2_{\Re\{z_a\}}\right)$ with

$$\mu_{\Re\{z_a\}} = R_a\alpha_a\left(\sigma^2_{h,a} + |\bar{h}_a|^2\right) = R_a\alpha_a, \tag{4.23}$$

$$\begin{aligned}\sigma^2_{\Re\{z_a\}} = \alpha_a^2\sigma^2_{h,a}\left(\sigma^2_{h,a}\|\mathbf{R}_a\|_2^2 + 2|\bar{h}_a|^2\mathbf{1}^T\mathbf{R}_a\mathbf{1}\right) + \\ + 2^{-1}R_a\left(2\alpha_a\sigma^2_{\nu,a} + \sigma^4_{\nu,a}\right),\end{aligned} \tag{4.24}$$

and $\Im\{z_a\} \sim \mathcal{N}\left(\mu_{\Im\{z_a\}}, \sigma^2_{\Im\{z_a\}}\right)$ with

$$\mu_{\Im\{z_a\}} = 0, \quad \text{and} \quad \sigma^2_{\Im\{z_a\}} = \frac{R_a(2\alpha_a\sigma^2_{\nu,a} + \sigma^4_{\nu,a})}{2}. \tag{4.25}$$

The first term of Eq. 4.24 only depends on the propagation channel characteristics and the second term equals to $\sigma^2_{\Im\{z_a\}}$, which depends on the pathloss and the noise.

4.2.3 Distribution of the received symbol in the CPU

Recalling Eq. 4.6, the distribution of z can be computed as the summation of several normally distributed random variables z_a [63] as $\Re\{z\} \sim \mathcal{N}\left(\mu_\Re, \sigma^2_\Re\right)$ with

$$\mu_\Re = \frac{\sum_{a\in\mathcal{A}_s} R_a\alpha_a}{\sum_{a\in\mathcal{A}_s} R_a}, \text{ and } \sigma^2_\Re = \frac{\sum_{a\in\mathcal{A}_s}\sigma^2_{\Re\{z_a\}}}{\left(\sum_{a\in\mathcal{A}_s} R_a\right)^2}, \tag{4.26}$$

and $\Im\{z\} \sim \mathcal{N}\left(\mu_\Im, \sigma^2_\Im\right)$ with

$$\mu_\Im = 0, \quad \text{and} \quad \sigma^2_\Im = \frac{\sum_{a\in\mathcal{A}_s} R_a(\sigma^4_a + 2\alpha_{n,a}\sigma^2_{\nu,a})}{2\left(\sum_{a\in\mathcal{A}_s} R_a\right)^2}. \tag{4.27}$$

4.2.4 Special case of base stations with a single antenna

This is an interesting case of $R_a = 1,\ \forall a \in \mathcal{A}_s$, to show that the law of large numbers still applies when sufficient APs are considered. Applying the properties of VG and Gamma distributions [60–62], for Eqs. 4.13-4.17 and summing for $R_a = 1,\ \forall a$ for large number of A APs, we have

$$VG\left(4A, 0, \sqrt{\sum_{a=1}^{A}\frac{\alpha_a\sigma^2_{h,a}}{4A\sigma^{-2}_{\nu,a}}}, 0\right) \xrightarrow{A\to\infty} \mathcal{N}\left(0, \sum_{a=1}^{A}\frac{\alpha_a\sigma^2_{h,a}}{\sigma^{-2}_{\nu,a}}\right), \tag{4.28}$$

$$VG\left(2A, 0, \sqrt{\frac{\sum_{a=1}^{A}\sigma_{\nu,a}^4}{4A}}, 0\right) \xrightarrow{A\to\infty} \mathcal{N}\left(0, \sum_{a=1}^{A}\frac{\sigma_{\nu,a}^4}{2}\right), \tag{4.29}$$

$$\mathcal{CN}(0, \alpha_a|\bar{h}_a|^2\sigma_{\nu,a}^2) \xrightarrow{A\to\infty} \mathcal{N}\left(0, \sum_{a=1}^{A}\alpha_a|\bar{h}_a|^2\sigma_{\nu,a}^2\right), \tag{4.30}$$

$$\mathcal{N}(0, 2\alpha_a^2|\bar{h}_a|^2\sigma_{h,a}^2) \xrightarrow{A\to\infty} \mathcal{N}\left(0, \sum_{a=1}^{A}2\alpha_a^2|\bar{h}_a|^2\sigma_{h,a}^2\right), \tag{4.31}$$

$$\Gamma(1, \alpha_a\sigma_{h,a}^2) \xrightarrow{A\to\infty} \mathcal{N}\left(\sum_{a=1}^{A}\alpha_a\sigma_{h,a}^2, \sum_{a=1}^{A}\alpha_a^2\sigma_{h,a}^4\right). \tag{4.32}$$

We obtain Eq. 4.32 using the condition $(\sum_a \alpha_a\sigma_{h,a}^2)^3 >> (\sum_a \alpha_a^2\sigma_{h,a}^4)^2$, which is true since $\alpha_a\sigma_{h,a}^2 > \alpha_a^2\sigma_{h,a}^4$ is always true, since $\alpha_a, \sigma_{h,a} \in [0,1]$, due to the fact that the pathloss can never be larger than 1 and $\sigma_{h,a} \leq 1$ by definition, and we also assume A to be very large. To summarize and to simplify, in case that AP a has only one antenna, the distribution of z_a is the same as the one defined with Eqs. 4.23, 4.24 and 4.25, particularizing with $\|\mathbf{R}_a\|_2^2 = \mathbf{1}^T\mathbf{R}_a\mathbf{1} = 1$. Thus, the distribution of z for $R_a = 1$ is valid using Eqs. 4.26 and 4.27.

4.2.5 Special case when compensating pathloss in each AP

In case the pathloss α_a is compensated in each AP locally before sending the data to the CPU, the signal in each AP would be defined as $\hat{z}_a = z_a/\alpha_a$, and the corresponding mean and variance would be $\mu_{\Re\{\hat{z}_a\}} = R_a$, $\sigma_{\Re\{\hat{z}_a\}}^2 = \sigma_{\Re\{z_a\}}^2/\alpha_a^2$, $\mu_{\Im\{\hat{z}_a\}} = I$ and $\sigma_{\Im\{\hat{z}_a\}}^2 = \sigma_{\Im\{z_a\}}^2/\alpha_a^2$.

Thus, the centralized signal would be defined as $\hat{z} = \sum_{a\in\mathcal{A}_s}\hat{z}_a/\sum_{a\in\mathcal{A}_s}R_a$, with mean and variances

$$\begin{aligned}
\mu_{\Re\{\hat{z}_a\}} = 1, \quad \sigma_{\Re}^2 &= \frac{\sum_{a\in\mathcal{A}_s}\alpha_a^{-2}\sigma_{\Re\{z_a\}}^2}{\left(\sum_{a\in\mathcal{A}_s}R_a\right)^2}, \\
\mu_{\Im\{\hat{z}_a\}} = 0, \quad \sigma_{\Im}^2 &= \frac{\sum_{a\in\mathcal{A}_s}\alpha_a^{-2}R_a(\sigma_a^4 + 2\alpha_{n,a}\sigma_{\nu,a}^2)}{2\left(\sum_{a\in\mathcal{A}_s}R_a\right)^2}.
\end{aligned} \tag{4.33}$$

4.2.6 Derivation of the SER, BER and SINR

Due to the symmetry of DMPSK constellations, the symbol error rate (SER) (P_s) and SINR (ρ) of the constellation can be calculated using any symbol of the constellation. In this case, we

particularize for the symbol $s = 1$, as done in Section 4.2.2, without loss of generality. The SER can be approximated by following the approach in Appendix A of [11] as

$$P_s(\mathcal{A}_s) \approx 1 - \frac{\int_{-\pi/M}^{\pi/M} \int_0^{\infty} e^{-\left(\frac{r\cos(\gamma)-\mu_{\Re}}{\sqrt{2}\sigma_{\Re}}\right)^2} e^{-\left(\frac{r\sin(\gamma)-\mu_{\Im}}{\sqrt{2}\sigma_{\Im}}\right)^2} r dr d\gamma}{2\pi\sigma_{\Re}^2\sigma_{\Im}^2}. \tag{4.34}$$

The double integral of Eq. 4.34 can be simplified by doing the following change of variables

$$a = \frac{\left(\sigma_{\Re}^2 - \sigma_{\Im}^2\right)\sin^2\gamma + \sigma_{\Im}^2}{2\sigma_{\Re}^2\sigma_{\Im}^2},\ b = \frac{2\sigma_{\Im}^2\mu_{\Re}\cos\gamma}{2\sigma_{\Re}^2\sigma_{\Im}^2},\ c = \frac{\sigma_{\Im}^2\mu_{\Re}^2}{2\sigma_{\Re}^2\sigma_{\Im}^2}, \tag{4.35}$$

and defining and solving the following integral

$$\begin{aligned}\int_0^{\infty} r e^{-\left(\frac{r\cos(\gamma)-\mu_{\Re}}{\sqrt{2}\sigma_{\Re}}\right)^2} e^{-\left(\frac{r\sin(\gamma)-\mu_{\Im}}{\sqrt{2}\sigma_{\Im}}\right)^2} dr = \int_0^{\infty} r e^{-ar^2+bx-c} dr = \\ e^{-c}\frac{\sqrt{\pi}be^{\frac{b^2}{4a}}\left(\text{erfc}\left(\frac{b}{2\sqrt{a}}\right)+1\right)+2\sqrt{a}}{4a^{3/2}},\end{aligned} \tag{4.36}$$

so the double dimensional integral of Eq. 4.34 turns into the one dimensional integral as

$$P_s(\mathcal{A}_s) \approx 1 - \int_{-\pi/M}^{\pi/M} e^{-c}\frac{\sqrt{\pi}be^{\frac{b^2}{4a}}\left(\text{erfc}\left(\frac{b}{2\sqrt{a}}\right)+1\right)+2\sqrt{a}}{8\pi\sigma_{\Re}^2\sigma_{\Im}^2a^{3/2}} d\gamma. \tag{4.37}$$

The integral can be solved numerically while a closed-form expression of Eq. 4.37 is mathematically intractable. The ρ can be calculated as the inverse of the sum of the variances of the real and imaginary parts as shown in Eq. 4.38. The numerator in Eq. 4.38 grows with the square of the sum of the total amount of antennas while the denominator grows with the sum of the square of the antennas in each AP. Then, the numerator grows faster than the denominator when several APs are used, showing that multi-AP processing benefits the NC scheme.

$$\rho = \frac{\left(\sum_{a=1}^{A} R_a\right)^2}{\sum_{a=1}^{A}\left(R_a(\sigma_{\nu,a}^4 + 2\sigma_{\nu,a}^2) + \sigma_{h,a}^2(\sigma_{h,a}^2\|\mathbf{R}_a\|_2^2 + 2|\bar{h}_a|^2\mathbf{1}^T\mathbf{R}_a\mathbf{1})\right)} \tag{4.38}$$

$$\underset{\delta_a=0}{\rho} = \frac{\left(\sum_{a=1}^{A} R_a\right)^2}{\sum_{a=1}^{A} R_a\left(\sigma_{\nu,a}^4 + 2\sigma_{\nu,a}^2 + \sigma_{h,a}^2(1+|\bar{h}_a|^2)\right)} \tag{4.39}$$

$$\underset{\delta_a=1}{\rho} = \frac{\left(\sum_{a=1}^{A} R_a\right)^2}{\sum_{a=1}^{A} R_a \left(\sigma_{\nu,a}^4 + 2\sigma_{\nu,a}^2 + R_a \sigma_{h,a}^2 (1 + |\bar{h}_a|^2)\right)} \tag{4.40}$$

We can further approximate Eq. 4.37 to a closed-form expression that does not require a numerical evaluation by assuming a circularly symmetric complex Gaussian distribution and using the expression for PSK error probability of [65] as

$$P_s(\mathcal{A}_s) \approx 2Q\left(\sqrt{2\rho}\sin\left(\frac{\pi}{M}\right)\right). \tag{4.41}$$

Last but not least, the BER can be straightforwardly calculated assuming Gray mapping as $P_b(\mathcal{A}_s) = P_s(\mathcal{A}_s)/\log_2(M)$.

4.2.7 Remarks about the effects of spatial correlation

It is worth noting that the previous expressions can be particularized for different scenarios. Assuming $\alpha_a = 1$ for all APs, the results agree with those obtained in [66]. Furthermore, for $A = 1$ and uncorrelated Rayleigh fading $\left(\bar{\mathbf{h}}_a, \sigma_{h,a}^2 \mathbf{R}_a\right) = (\mathbf{0}_a, \mathbf{I}_a)$, we obtain the results of [11, Appendix A].

Following the model $\left[\mathbf{R}_a\right]_{r_a, r'_a} = \delta_a^{|r_a - r'_a|}$ with $0 \leq \delta_a \leq 1$, where $|r_a - r'_a|$ is the distance between the antennas r_a and r'_a in AP a, the terms $\|\mathbf{R}_a\|_2^2$ and $\mathbf{1}^T\mathbf{R}_a\mathbf{1}$ are simplified to

$$R_a(\delta_a = 0) \leq \|\mathbf{R}_a\|_2^2 = R_a \frac{1 - \delta_a^{2R_a}}{1 - \delta_a^2} \leq R_a^2(\delta_a = 1), \tag{4.42}$$

$$R_a(\delta_a = 0) \leq \mathbf{1}^T\mathbf{R}_a\mathbf{1} = R_a \frac{1 - \delta_a^{R_a}}{1 - \delta_a} \leq R_a^2(\delta_a = 1). \tag{4.43}$$

Moreover, any spatial correlation model can be adjusted to the previously presented one by properly adjusting δ_a, so the latter can be used for analysis purposes. If correlation increases, both Eq. 4.42 and Eq. 4.43 increase, thus increasing $\sigma_{\Re\{z_a\}}^2$, which is the variance of Eq. 4.5. Therefore, the SER increases and the ρ (defined in Eq. 4.38) decreases, degrading the performance of the system. Eq. 4.39 shows the ρ for the extreme cases of $\delta_a = 0$ and $\delta_a = 1$. It can be observed an R_a term in the second summand in the case $\delta_a = 1$ that multiplies the variance of the real part, while for $\delta_a = 0$ that term is not present. Besides, it can be observed in both cases that the second summand of the denominator tends to 0 with increasing

K_a (decreasing both $|\bar{h}_a|^2$ and $\sigma^2_{h,a}$, so a strong Rician component benefits the performance). Interestingly, these conclusions are similar to those obtained for coherent CF schemes in [67].

Last but not least, it can be observed that the performance improves with the square of the sum of the number of antennas in each AP while it worsens with the sum of the square of the number of antennas in each AP (for the worst case of $\delta_a = 1$), so the performance tends to improve when several APs are used, instead of just one.

4.3 Cell-free AP selection in Non-coherent Massive SIMO based on DMPSK

In this section, we propose four alternatives to select a subset $\mathcal{A}_s$ among a set of accessible APs $\mathcal{A}$ to maximize the performance of the coordinated multipoint reception in non-coherent massive SIMO (NC-mSIMO). The first one is a brute force search (BFS) which tests all the possible AP combinations, so it is the best in terms of performance but the most complex one. The second one performs a successive AP selection (SAPS) in a greedy way (each iteration tests all the remaining combinations), so it has a lower performance and a lower complexity than the BFS. The last one performs a simplified successive AP selection (each iteration tests including the next best AP), so it is the one with the lowest performance but also the one with the lowest complexity. A fourth proposed alternative, even though not explained, is to select all the "visible" APs by the user. We will show the performance and complexity via simulations in Section 6.6.

The z_a of $\mathcal{A}_s$ are sent to the CPU and processed following Eq. 4.6. The performance measure in our case will be P_s, defined in Eq. 4.37. The goal is to select a subset $\mathcal{A}_s$ among a set of accessible APs $\mathcal{A}$ so that Eq. 4.37 is minimized. We define the following optimization problem, which is discrete and deterministic

$$\begin{aligned} \min_{\mathcal{A}_s, \Upsilon_{\mathcal{A}_s}} \quad & f_{\text{obj}} = P_s(\mathcal{A}_s), \\ \text{s.t.} \quad & \mathcal{A}_s \in \mathcal{A}, \quad |\mathcal{A}_s| = A_s, \\ & \Upsilon_{\mathcal{A}_s} = \{K_{\mathcal{A}_s}, \alpha_{\mathcal{A}_s}, \sigma_{\nu,\mathcal{A}_s}, R_{\mathcal{A}_s}, \mathbf{R}_{\mathcal{A}_s}\}, \end{aligned} \tag{4.44}$$

where A_s is the cardinality of subset $\mathcal{A}_s$ and $\Upsilon_{\mathcal{A}_s}$ is a set of parameters of the subset $\mathcal{A}_s$, needed by the CPU to select the best subset. These parameters are, for each AP in $\mathcal{A}_s$, the Rician factors

Technique	Compl.	A=1	A=5	A=10	A=20	A=300
BFS max	$2^A - 1$	0	31	1023	1M	$2^{300} \approx \infty$
SAPS max	$\frac{A^2+A}{2}$	0	15	55	210	45K
SAPS min	$2A - 1$	0	9	19	39	599
sSAPS max	$2A - 1$	0	9	19	39	599
sSAPS min	$A + 1$	0	6	11	21	301

Table 4.1: *Complexity of different APs selection techniques*

$K_{\mathcal{A}_s}$, the square of the large-scale fading $\alpha_{\mathcal{A}_s}$, the noise power $\sigma_{\nu,\mathcal{A}_s}$, the number of antennas $R_{\mathcal{A}_s}$ and the channel spatial correlation matrix $\mathbf{R}_{\mathcal{A}_s}$. The channel parameters required to solve the optimization problem defined in Eq. 4.44 vary in a very large temporal scale. The subsets $\mathcal{A}_s$ can have 1 to A APs, with a total combinations of $2^A - 1$ possible different subsets.

The computation of P_s depends on M, which is the constellation size of DMPSK. For fixed $\sigma^2_{\Re}$ and $\sigma^2_{\Im}$, a larger M results in a smaller integration area so a larger P_s, while a smaller M corresponds to a larger integration area and thus a smaller P_s. Therefore, we just have to compute the P_s for one constellation size and the effects of $\sigma^2_{\Re}$ and $\sigma^2_{\Im}$ will be the same for other constellation sizes.

4.3.1 Brute-force search (BFS) AP Selection

The optimization problem defined in Eq. 4.44 may be solved via a brute force search to obtain the set $\mathcal{A}_s^{\min}$, which is the APs set that minimizes the symbol error probability. This approach gives the best performance in terms of BER, so it serves as a benchmark, while its main limitation is its complexity. This would not be a limitation in case very strong computing capabilities are available for a reasonable number of APs. It needs to calculate the P_s Eq. 4.37 a total of $\sum_{a=1}^{A} \frac{A!}{a!(A-a)!} = 2^A - 1$ times. This is caused by the fact that we must look for combinations without repetitions of A APs. Nevertheless, this solution is useful since it represents an upper-bound in terms of performance, useful to compare it against suboptimal solutions. A pseudocode for the brute force search is provided in Algorithm 1.

Algorithm 1 Brute Force Search APs Selection

procedure $\mathbf{selectAP_BFS}(\mathcal{A}_s, \Upsilon_{\mathcal{A}_s})$
  $[\hat{\mathcal{A}}_\mathbf{s}] \leftarrow$ createAllCombs($\mathcal{A}_s$) ▷ *Create All Combinations*
  $[\boldsymbol{P}_{\boldsymbol{s},\hat{\boldsymbol{\mathcal{A}}}_\boldsymbol{s}}] \leftarrow$ computePs($\hat{\mathcal{A}}_\mathbf{s}$, $\Upsilon_{\mathcal{A}_s}$) ▷ *Compute P_s of $\hat{\mathcal{A}}_\mathbf{s}$*
  $[\hat{\mathcal{A}}_\mathbf{s}^{\min}] \leftarrow$ selectMinPs($\boldsymbol{P}_{\boldsymbol{s},\hat{\boldsymbol{\mathcal{A}}}_\boldsymbol{s}}$,$\hat{\mathcal{A}}_\mathbf{s}$) ▷ *Select AP set with minimum P_s*
  return $[\hat{\mathcal{A}}_\mathbf{s}^{\min}]$ ▷ *Return base station set with minimum P_s*
end procedure

4.3.2 Successive AP selection (SAPS)

One possibility to obtain a good performance while keeping the complexity low is to perform a greedy algorithm that successively selects the APs in the following way (see Algorithm 2). Please note greedy algorithms have been interesting in other selection strategies problems [68], even though the approach in this work is clearly different. First, the AP with the lowest individual P_s (called $P_{s,1}$) is selected, and is named A_1. A total of A calculations of P_s are needed in this first iteration. Among the $A-1$ APs left, we select the one that, combined with A_1, further reduces the P_s (called $P_{s,2}$), needing a total of $A-1$ calculations. This process is repeated until $P_{s,i} > P_{s,i-1}$ or until all APs are included in the set. The maximum complexity of this approach would be

$$\sum_{i=0}^{A-1}(A-i) = \frac{A^2+A}{2}, \tag{4.45}$$

while the minimum complexity would be $2A-1$, which is the case in which not a single second AP improves the performance.

4.3.3 Smart Successive AP selection (sSAPS)

The last proposal to obtain a good performance while keeping the complexity low is to perform a successive selection of APs in a smart way (see Algorithm 3). This approach can be seen as a simplified greedy approach in which the APs are successively selected first selecting the ones with a better performance. The P_s of all APs is computed and they are sorted in ascending order, taking a total of A computations of P_s. The AP with the lowest individual P_s (called $P_{s,1}$) is selected, and is named A_1. The AP with the second lowest P_s is combined with A_1 and the P_s of the combination is calculated and named $P_{s,2}$. This process is repeated until $P_{s,i} > P_{s,i-1}$ or until all APs are included in the set. The maximum complexity of this approach would be $2A-1$, which results from computing the P_s until all APs are included in the set. The minimum

Algorithm 2 Successive AP selection (SAPS)

procedure $\mathbf{selectAP_SAPS}(\mathcal{A}_s, \Upsilon_{\mathcal{A}_s})$
  $[\boldsymbol{P_s}] \leftarrow$ computePs($\mathcal{A}_\mathbf{s}$, $\Upsilon_{\mathcal{A}_s}$) ▷ *Compute P_s of $\mathcal{A}_\mathbf{s}$*
  $[\tilde{\boldsymbol{P}}_\boldsymbol{s}, \tilde{\mathcal{A}}_\mathbf{s}, \tilde{\Upsilon}_{\mathcal{A}_s}] \leftarrow$ orderPsAs($\boldsymbol{P_s}$,$\mathcal{A}_\mathbf{s}$,$\Upsilon_{\mathcal{A}_s}$) ▷ *Order APs*
  $[\boldsymbol{P}^{\text{min}}_{\boldsymbol{s},0}, \boldsymbol{P}^{\text{min}}_{\boldsymbol{s},1}] \leftarrow [1, \tilde{\boldsymbol{P}}_\boldsymbol{s}(1)]$ ▷ *Init Ps min to 1 and 1^{st} Ps*
  i $\leftarrow$ 1, set $\leftarrow$ 1 ▷ *Initialize Iter*
  while $\boldsymbol{P}^{\text{min}}_{\boldsymbol{s},i}$ ¡ $\boldsymbol{P}^{\text{min}}_{\boldsymbol{s},i-1}$ **do** ▷ *Loop over all APs*
    i $\leftarrow$ i + 1
    for k from (i to A) - set **do** ▷ *Loop in each iteration*
      [setTemp2,setTemp] $\leftarrow$ [set,[set,k]]
      $[\boldsymbol{P}^{\text{temp}}_{\boldsymbol{s}}] \leftarrow$ computePs($\tilde{\mathcal{A}}_\mathbf{s}$(setTemp),$\tilde{\Upsilon}_{\mathcal{A}_s}$(setTemp))
      if $\boldsymbol{P}^{\text{temp}}_{\boldsymbol{s}}$ ¡ $\boldsymbol{P}^{\text{min}}_{\boldsymbol{s},i}$ **then**
        $\boldsymbol{P}^{\text{min}}_{\boldsymbol{s},i} \leftarrow \boldsymbol{P}^{\text{temp}}_{\boldsymbol{s}}$
        setTemp2 $\leftarrow$ setTemp
      end if
    end for
    set $\leftarrow$ setTemp2 ▷ *Update set of APs with min Ps*
    $\tilde{\mathcal{A}}^{\text{min}}_\mathbf{s} \leftarrow \tilde{\mathcal{A}}_\mathbf{s}$(set) ▷ *Assign set of min Ps*
  end while
  return $[\tilde{\mathcal{A}}^{\text{min}}_\mathbf{s}]$ ▷ *Return base station set with minimum P_s*
end procedure

complexity would be $A+1$, when the second AP does not reduce the overall P_s. It is interesting to check from which amount of APs the algorithms compare in terms of complexity between them for sSAPSmin $<$ sSAPSmax $<$ SAPSmin $<$ SAPSmax $<$ BFS, as

$$A + 1 \leq 2A - 1 \leq \frac{(A+1)A}{2} \leq 2^A - 1 \rightarrow A \geq 2. \tag{4.46}$$

4.3.4 Figure of Merit (FoM) to compare selection techniques

One measure to compare the techniques is to account for both the complexity (C), either time or computational, and the performance of each technique, so we propose the following

$$FoM = (-\log_{10}(P_s))^{-1} \times 100C, \tag{4.47}$$

Algorithm 3 Smart Successive AP selection (sSAPS)

procedure $\mathbf{selectAPsBFS}(\mathcal{A}_s, \Upsilon_{\mathcal{A}_s})$
  $[\boldsymbol{P_s}] \leftarrow$ computePs($\mathcal{A}_\mathbf{s}$, $\Upsilon_{\mathcal{A}_s}$) ▷ *Compute P_s of $\mathcal{A}_\mathbf{s}$*
  $[\tilde{\boldsymbol{P}}_\boldsymbol{s}, \tilde{\mathcal{A}}_\mathbf{s}, \tilde{\Upsilon}_{\mathcal{A}_s}] \leftarrow$ orderPsAs($\boldsymbol{P_s}$,$\mathcal{A}_\mathbf{s}$,$\Upsilon_{\mathcal{A}_s}$) ▷ *Order APs*
  $[\boldsymbol{P}^{\min}_{\boldsymbol{s},0}, \boldsymbol{P}^{\min}_{\boldsymbol{s},1}] \leftarrow [1, \tilde{\boldsymbol{P}}_\boldsymbol{s}(1)]$ ▷ *Init Ps min to 1 and 1^{st} Ps*
  i $\leftarrow 1$ ▷ *Initialize Iter*
  while $\boldsymbol{P}^{\min}_{\boldsymbol{s},i}$ ¡ $\boldsymbol{P}^{\min}_{\boldsymbol{s},i-1}$ **do** ▷ *Loop*
    $[\boldsymbol{P}^{\min}_{\boldsymbol{s}}, \tilde{\mathcal{A}}^{\min}_\mathbf{s}] \leftarrow [\boldsymbol{P}^{\min}_{\boldsymbol{s},i}, \tilde{\mathcal{A}}_\mathbf{s}(1{:}i)]$ ▷ *Assign min Ps*
    i $\leftarrow$ i + 1
    $[\boldsymbol{P}^{\min}_{\boldsymbol{s},i}] \leftarrow$ computePs($\tilde{\mathcal{A}}_\mathbf{s}(1{:}i)$,$\tilde{\Upsilon}_{\mathcal{A}_s}(1{:}i)$) ▷ *$1^{st}$ to i^{th} Ps*
  end while
  return $[\tilde{\mathcal{A}}^{\min}_\mathbf{s}]$ ▷ *Return base station set with minimum P_s*
end procedure

which serves as a figure-of-merit (FoM) decision variable between techniques. A multiplication by 100 is done to avoid rounding errors in the results. Lower P_s come at the expense of greater complexity, but it may be possible that the P_s does not decrease much while complexity greatly reduces. This FoM is useful in fast varying channels in which we aim at minimizing the AP selection execution time in the CPU.

4.4 Comparison parameters for NC-CF vs CF

The aim of this section is to show that, in deployment scenarios of stringent conditions, such as fast varying channels and/or low SNR, the non-coherent cell-free (NC-CF) proposal can outperform its coherent counterpart. First, we explain the baseline coherent CF massive MIMO with a MMSE-based fully centralized processing scheme. Then, we consider the channel estimation overhead problem of any coherent CF scheme. Later, we do a qualitative analysis of the delay and complexity. Last, we describe the performances of the coherent and NC schemes in terms of BER.

4.4.1 Baseline coherent cell-free massive MIMO

We consider the optimal approach in terms of ρ for the coherent CF scheme, which is the MMSE-based fully centralized processing scheme (see [69] and references therein). It requires

tight synchronization between APs, large computational resources, and fronthaul links capable of managing considerable amount of data traffic. Notice there are plenty of other processing strategies when it comes to coherent CF, such as the commonly used distributed maximum ratio (MR) processing [70], but, in order to maintain fairness in comparison, we are only showing the MMSE-based as it represents the spectral efficiency upper-bound.

In contrast to NC-CF-mSIMO, its coherent counterpart requires performing channel estimation (which can be either performed locally at each AP or at the CPU) for the later construction of the combining vector. During the UL training phase, the user terminal will send its pilot signal to every AP resulting in

$$\mathbf{y}_{p,a}^{n} = \mathbf{h}_{a}^{n}\boldsymbol{\varphi}^{n} + \boldsymbol{\nu}_{p,a}^{n}, \tag{4.48}$$

as the received training signal at AP a during time instant n. The unique pilot sequence is $\boldsymbol{\varphi}^{n} \in \tau_p \times 1$, while τ_p are the pilot resources allocated for the channel estimation and $\boldsymbol{\nu}_{p,a}^{n}$ is the AWGN term at time instant n whose entries are distributed as $\mathcal{CN}(0, (\sigma_{p,a}^{n})^2)$. In the centralized MMSE scheme, each AP will typically act as a relay that forwards $\mathbf{y}_{p,a}^{n}$ to the CPU for channel estimation. The channel estimates will be acquired by MMSE estimation [71] and will be distributed as $\mathbf{h}_{a}^{n} \sim \mathcal{CN}(\bar{\mathbf{h}}_{a}^{n}, \tau_p(\sigma_{p,a}^{n})^{-2}\mathbf{R}_{a}^{n}(\boldsymbol{\Psi}_{a}^{n})^{-1}\mathbf{R}_{a}^{n})$. The channel estimation error is $\mathbf{e}_{a}^{n} = \boldsymbol{h}_{a}^{n} - \hat{\mathbf{h}}_{a}^{n}$ which follows $\mathbf{e}_{a}^{n} \sim \mathcal{CN}(\mathbf{0}_{R_a}, \mathbf{E}_{a}^{n})$ with $\mathbf{E}_{a}^{n} = \mathbf{R}_{a}^{n} - \tau_p(\sigma_{p,a}^{n})^{-2}\mathbf{R}_{a}^{n}(\boldsymbol{\Psi}_{a}^{n})^{-1}\mathbf{R}_{a}^{n}$. Thanks to the MMSE channel estimate we ensure that $\mathbf{e}_{a}^{n}$ and $\hat{\mathbf{h}}_{a}^{n}$ are independent, the same as $\mathbf{h}_{a}^{n}$ and $\hat{\mathbf{h}}_{a}^{n}$ (a necessary condition for the ρ_c definition that will be shown in Eq. 4.52). The channel estimate is then

$$\begin{aligned}\hat{\mathbf{h}}_{a}^{n} &= \bar{\mathbf{h}}_{a}^{n} + \frac{\mathbb{E}\left\{\breve{\mathbf{y}}_{p,a}^{n}(\breve{\mathbf{h}}_{a}^{n})^{H}\right\}}{\mathbb{E}\left\{\breve{\mathbf{y}}_{p,a}^{n}(\breve{\mathbf{y}}_{p,a}^{n})^{H}\right\}}\breve{\mathbf{y}}_{p,a}^{n} \\ &= \bar{\mathbf{h}}_{a}^{n} + \sqrt{\tau_p(\sigma_{p,a}^{n})^{-2}}\mathbf{R}_{a}^{n}(\boldsymbol{\Psi}_{a}^{n})^{-1}\breve{\mathbf{y}}_{p,a}^{n},\end{aligned} \tag{4.49}$$

with $\breve{\mathbf{h}}_{a}^{n} = \mathbf{h}_{a}^{n} - \mathbb{E}\left\{\mathbf{h}_{a}^{n}\right\}$, and $\boldsymbol{\Psi}_{a}^{n} \triangleq (\sigma_{p,a}^{n})^{-2}\mathbf{R}_{a}^{n} + \mathbf{I}_{R_a}$.

During the UL data payload phase, the user will send its data symbol to every AP and each AP to the CPU, i.e.

$$\mathbf{y}_{a}^{n} = \mathbf{h}_{a}^{n}x^{n} + \boldsymbol{\nu}_{a}^{n}, \tag{4.50}$$

where $\boldsymbol{\nu}_{a}^{n}$ accounts for the AWGN term during time instant n and is distributed as $\mathcal{CN}\left(0, (\sigma_{a}^{n})^2\right)$. We can express the decoded data symbol during the UL data payload phase

as

$$\hat{x}^n = \sum_{a=1}^{A} \left(\mathbf{b}_a^n\right)^H \mathbf{y}_a^n = \sqrt{\rho_u} \sum_{a=1}^{A} \left(\mathbf{b}_a^n\right)^H \mathbf{h}_a^n x^n + \left(\mathbf{b}_a^n\right)^H \mathbf{r}_a^n, \tag{4.51}$$

where the combining vector $\mathbf{b}_a^n$ must be searched to maximize the ρ of $\hat{x}^n$. Given the instant CSI knowledge at the CPU and defining $\mathbf{E}^n = \text{diag}(\mathbf{E}_1^n, \ldots, \mathbf{E}_A^n)$ and using [72], we have

$$\rho_c = \frac{(\sigma_{u,a}^n)^{-2} \left| (\mathbf{b}_a^n)^H \hat{\mathbf{h}}_a^n \right|^2}{(\mathbf{b}_a^n)^H \left((\sigma_{p,a}^n)^{-2} \mathbf{E}^n + \mathbf{I}_{AR_a} \right) \mathbf{b}_a^n}. \tag{4.52}$$

Defining $\mathbf{h}^n = [\mathbf{h}_1^n, \ldots, \mathbf{h}_A^n]$, and as shown in [53], the combining vector that maximizes Eq. 4.52 is

$$\begin{aligned} \mathbf{b}^n &= [\mathbf{b}_1^n, \ldots, \mathbf{b}_A^n] \\ &= (\sigma_{p,a}^n)^{-2} \left((\sigma_{p,a}^n)^{-2} \left(\hat{\mathbf{h}}^n (\hat{\mathbf{h}}^n)^H + \mathbf{E}^n \right) + \mathbf{I}_{AR_a} \right)^{-1} \hat{\mathbf{h}}^n. \end{aligned} \tag{4.53}$$

4.4.2 Channel estimation overhead

Assuming a total of τ_c wireless resources in a coherence block and τ_p pilot resources needed for the channel estimation, the efficiency of the link, caused by the pilots usage is

$$\tau = 1 - \frac{\tau_p}{\tau_c}. \tag{4.54}$$

If τ_c is close to τ_p, the efficiency of a coherent approach will be very low, even zero in the extreme case ($\tau_p = \tau_c$), as shown in [11]. Contrarily, $\tau_p = 0$ is always true for the NC scheme, since it will not have any pilot overhead.

4.4.3 Delay and complexity of the detection

Not only does the channel estimation reduce the efficiency of the link, but it also increases the delay in the data reception with the channel estimation delay t_{chEst}. Once the channel is estimated, it must be compensated with any of the filtering/precoding techniques in the literature, taking a compensation time t_{comp}. Then, there is a total delay of $t_{\text{chEst}} + t_{\text{comp}}$ before the data can be detected. On the contrary, the NC scheme only needs to perform the differential decoding and averaging, which is lower than t_{comp}, as shown in [73].

Yet another aspect of controversy of coherent CF schemes are their computational demands

together with the fronthaul links usage. Each AP is required to send $\tau_p R_a$ complex scalars to the CPU for channel estimation, while the CPU itself will be required to perform $(R_a + R_a^2)A$ complex multiplications for computing channel estimates. On the other side, APs will send $(\tau_c - \tau_p)R_a$ complex scalars to the CPU for the UL data reception. Last but surely not least, the computation complexity of the MMSE combining vector will grow cubically with R_a and A. Please, refer to [74], among other references, for a better understanding of the computational needs in coherent CF massive MIMO networks. Comparatively, the complexity of the NC-CF scheme is much lower. Each AP will perform R_a complex multiplications and a complex summation of R_a terms. It will send one complex scalar (z_a) to the CPU, which will only perform the summation of a maximum of A complex values. It is clear than the computational complexity and the fronthaul overload is much lower for the NC than for the coherent counterpart.

4.4.4 Performance comparison

A higher complexity of the coherent processing is justified when the performance is clearly improved. However, we will show that there are situations when it is not the case. Thus, to compare the coherent and NC-CF schemes in terms of performance, we will use the SER. Our intention is to use a realistic measure to compare among schemes. In order to make fair comparisons, the same data efficiency must be ensured for both the coherent and the NC schemes. This same data efficiency can be obtained by adjusting the effective ρ according to the channel estimation overhead. The SER of the NC is defined using Eq. 4.37, and the SER of the coherent scheme will be defined following [65] as

$$P_{s,c} = 2Q\left(\sqrt{2\tau\rho_c}\sin\left(\frac{\pi}{M_c}\right)\right), \tag{4.55}$$

where ρ_c denotes the SINR of the coherent scheme after joint processing and can be calculated as Eq. 4.52. The τ factor is included to adjust its value accounting for some resources that are used for channel estimation. Let us clarify this with an example: assume the number of symbols available for the UL of a TDD system, due to the coherence time length, is 2 symbols. In this case, for the coherent scheme at least one symbol is needed for channel estimation while the other one is needed for data transmission, while for the NC scheme, both symbols could be used for data. Thus, to obtain the same data efficiency, the overhead parameter would be set to $\tau = 0.5$ to adjust the effective ρ_c to compute the $P_{s,c}$.

Even though it is out of the scope of this work, another problem with the coherent scheme is the channel estimation error, which comes from the fact that the estimated channel is imperfect, caused by several reasons, including but not limited to noisy estimation and channel variability [75].

4.5 Numerical Results of the cell-free NC massive MIMO

In this section we show some numerical results. First, we verify our analysis of the symbol error probability P_s and the SINR ρ. Second, we show a comparison in terms of performance and complexity for the different APs selection techniques developed in Section 4.3, and show that the computation time relates directly to the complexity. Last, we show the performance in a scenario with realistic 3D MIMO channels and a realistic AP deployment, to show that our proposal can outperform the coherent CF massive MIMO scheme in fast varying channels and/or low SNRs.

The results in this section are obtained for a constellation size $M = 4$, a maximum of 8 available APs and a random number of antennas in each AP between 1 and 256 (in powers of 2), selected randomly. The UE is placed at the center of a 100m x 100m square, and the APs are uniformly placed in this square at each iteration of the Monte Carlo simulation. The pathloss follows a simplified version of the 3GPP urban microcell described in [51]. It is expressed as $L_a^n = L_0 + 10p\log_{10}(d_a^n) + \chi_a^n$, where L_0 is the pathloss at a reference distance of 1 meter, p is the pathloss exponent that depends on the environment, d_a^n is the distance between the center of the array of the AP a and the user and χ_a^n is the shadow fading component which is modeled as $\chi_a^n \sim \mathcal{N}(0, \sigma^2_{\chi_a^n})$. Thus, the channel gain is defined as $\alpha_a^n = 10^{-L_a^n/10}$. The Rician factor K_a^n is distributed as $10\log_{10}(\mathcal{K}_a^n) \sim \mathcal{N}\left(\mu_{\mathcal{K}_a^n}, \sigma^2_{\mathcal{K}_a^n}\right)$. The spatial correlation of the NLOS component is defined by δ_a^n and follows a random uniform distribution between 0 and 1 for each AP. All these parameters are used as described in the following sections unless otherwise stated.

4.5.1 Corroboration of Statistical Analysis for BER and SINR

In this section, we check that the theoretical analysis of the BER and SINR is correct and we get some insights on the effect of spatial correlation on the performance of NC-mSIMO when a multi-AP processing is performed. We show both the theoretical and the Monte-Carlo (obtained

via simulations) results of the BER and SINR for the correlation model defined in Section 4.2.7. Some channel parameters are fixed and modified with respect to the previous description, for representation purposes.

First and foremost, we have performed a Kolmogorov-Smirnov (KS) test to check if both the theoretical and the Monte-Carlo distributions obtained for z can be regarded as the same. When $\delta_a < 0.93$, values that can be regarded as representative of realistic channels, the theoretical and Monte-Carlo distributions were regarded as the same for a standard significance value of 5%, confirming our analysis. On the contrary, for $\delta_a > 0.93$, the test for the real part of the distribution fails, which indicates that the distributions cannot be regarded as the same. Nevertheless, the goal is to check whether the analysis is valid for the BER and the SINR and to check if there is a discrepancy between the theoretical and Monte-Carlo results. Figs. 4.1 and 4.2 show that even though the discrepancy between the BER and SINR obtained by simulations and with the analysis in Section 4.2 is greater for high values of δ, the approximations still provide accurate results. The small discrepancy comes from the fact that the approximation of Gamma to Gaussian distributions is less valid with larger spatial correlation.

Fig. 4.1 shows the BER for $K_a = 2$, against δ from 0.7 to 1, for $\bar{\rho} = -5$ dB and $\bar{\rho} = 10$ dB, with and without pathloss compensation. Both simulations and theoretical values are shown. We can observe how the BER increases with δ_a, since channel hardening is reduced. In Fig. 4.2, we can observe the $\bar{\rho}$ from the theoretical analysis and the Monte Carlo simulation versus different ρ_a (the same for all APs), for $K_a = 2$ for all APs, with and without pathloss compensation. The same conclusions can be extracted as those for Fig. 4.1. A very good agreement can be found in both figures for the theoretical analysis and the Monte Carlo simulation. It is worth noting that more simulations have been done for BER and $\bar{\rho}$ versus varying K_a and varying R_a, not presented here for conciseness since they bring the same conclusions.

4.5.2 AP selection in NC-CF for 8 APs

This section shows how the different proposed AP selection techniques behave. The noise power $(\sigma_a^n)^2$ is defined such that the mean SNR in the APs goes from -10 dB to 35 dB.

We show how the BFS approach outperforms the SAPS and the SAPS outperforms the sSAPS in terms of BER performance, while the opposite happens when we analyze the complexity in the AP selection approach. By looking at Table 4.2, one can see how the technique that

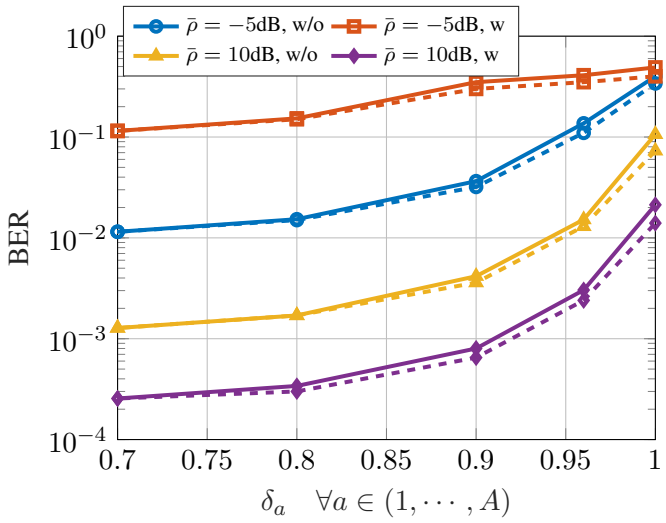

Figure 4.1: *BER vs δ_a for $K_a = 2$ $\forall a \in (1, \cdots, A)$ and two different $\bar{\rho}$ values, with (w) and without (w/o) pathloss compensation. Monte Carlo (dashed line) versus theoretical analysis (continuous line).*

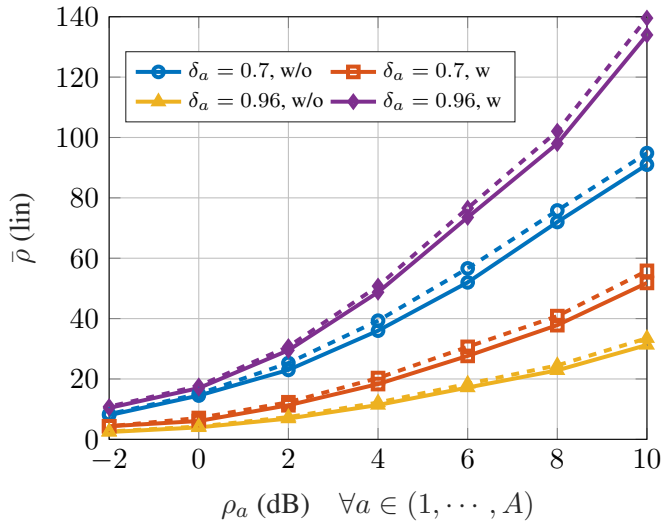

Figure 4.2: *$\bar{\rho}$ (linear) vs ρ_a for $K_a = 2$ $\forall a \in (1, \cdots, A)$ and two different δ_a values, with (w) and without (w/o) pathloss compensation. Monte Carlo (dashed line) versus theoretical analysis (continuous line).*

takes the longest is the BFS, followed by the SAPS and ending with the sSAPS which is the one that takes the least time. Comparatively, the All AP approach is better than the single AP but worse than the others, which remarks the fact that some APs will potentially decrease the overall performance, mainly due to the fact that some APs are at a very large distance or do not have enough antennas to compensate the large pathloss. That is why an AP selection

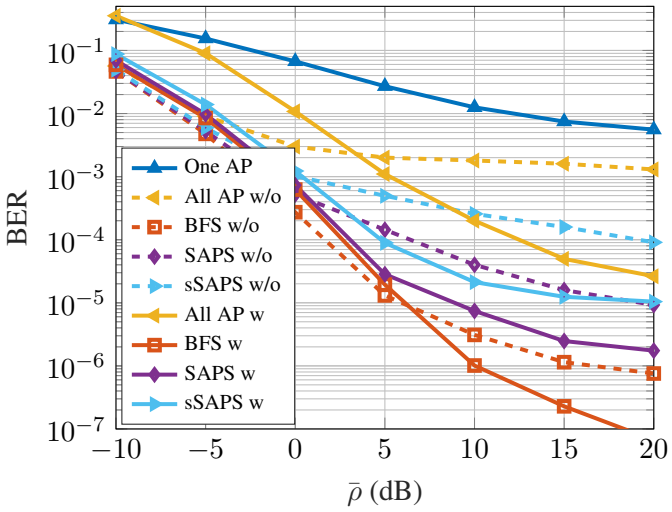

Figure 4.3: *BER vs mean SNR in dB for 8 APs comparing with (continuous line) and without (dashed line) pathloss compensation in each AP.*

Technique	**BER** ($\bar{\rho} = 10$dB)	**Time (secs)**	**Nops**	**FoM**
One AP	7.53e-03	0.24	8	12
All AP	2.03e-04	0.07	1	2
BFS	1.14e-06	13.5	255	227
SAPS	8.1e-06	2.53	15-36	50
sSAPS	2.12e-05	0.42	9-15	9

Table 4.2: *BER, Time, Nops and FoM for different AP selection techniques for A=8 and $\bar{\rho} = 10$ dB with pathloss compensation.*

technique is of interest. Consequently, the performance is the best for the BFS, followed by the SAPS and ending with the sSAPS, which has the lowest performance. This fact is supported by looking at Fig. 4.3, which shows the performance when pathloss compensation is and is not performed locally at each AP before combination processing at the CPU. It is interesting to note how the pathloss compensation in each AP before the central combination processing affects the performance. In the low SNR it is slightly better not to compensate the pathloss, while in the medium to large SNR it is very convenient to do so. To summarize, it can be seen that the best BER is given by the BFS, followed by the SAPS and ending with the sSAPS. The opposite happens for the complexity.

Nevertheless, to make a fair comparison among techniques, we utilize the FoM defined in

Technique	Centr. MMSE	Proposed NC-CF
Exec. Time (ms)	918	34

Table 4.3: *Execution time coherent versus NC.*

N_{CT}	Δ_f= 15	Δ_f= 30	Δ_f= 60	Δ_f= 120	Δ_f= 240
f_c = 0.7	7	15	29	-	-
f_c = 3.6	1.4	2.8	5.6	-	-
f_c = 27	-	-	-	1.5	3

Table 4.4: *T_c to T_s ratio (N_{CT}), for $v = 500$ km/h for different f_c in GHz and Δ_f in KHz.*

Section 4.3.4, for which the lower the value, the better the technique. By looking again at Table 4.2, in which C from Eq. 4.47 has been substituted by the execution time, it can be seen how the best approach according to the FoM is the All AP followed by the sSAPS. Comparatively, the sSAPS increases the performance about two orders of magnitude while less than doubling the execution time, with respect to the "One AP" approach. On the contrary, the decrement in performance with respect to the BFS is about two orders of magnitude but the execution time is about 28 times larger. While we do not include the results for a low $\bar{\rho}$ for succinctness, the best approach will be the sSAPS.

4.5.3 AP selection in NC-CF for 1 to 7 APs

In this section, an increasing number of APs from 1 to 7 has been simulated to find out which AP selection approach is best in this range. We do not include graphical results for succinctness. By looking at Table 4.5, we can see how the BER performance is the best for the BFS, followed by the SAPS, then the sSAPS and finally de All AP. Contrarily, the execution time follows the opposite behaviour. Nevertheless, the FoM shows that the best approach that balances the execution time and the BER performance is the "All AP" selection technique. Similar to the previous section, for a low $\bar{\rho}$ the best approach will be the sSAPS.

For fast varying channels, the best is to select the sSAPS for low $\bar{\rho}$ values and the "All AP" for high $\bar{\rho}$, the former without channel compensation and the latter with channel compensation. For slowly varying channels with low $\bar{\rho}$ the best is to avoid channel compensation and use the BFS or the SAPS for 2 to 4 APs since they have the best performance with a similar execution

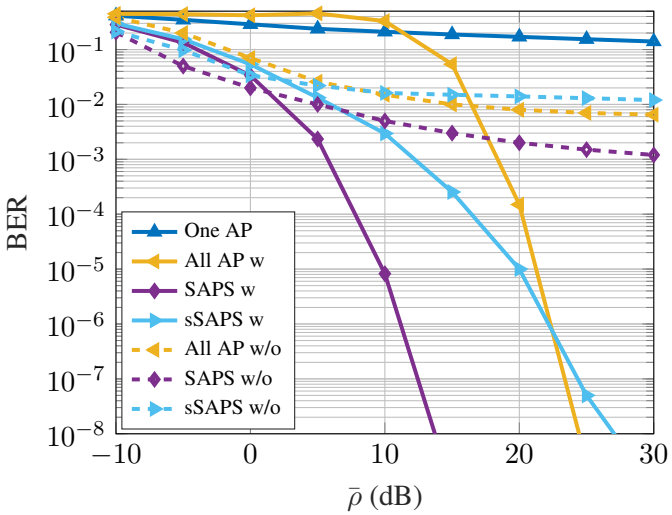

Figure 4.4: *BER vs mean SNR in dB for 200 single-antenna APs comparing with (continuous line) and without (dashed line) pathloss compensation in each AP (no BFS shown due to complexity limitations).*

time. For 5 and 6 the best is to use the SAPS, for 7 and up to 20, the sSAPS is the best option. Last, for more than 20 APs the best is to utilize the "All AP" selection technique.

4.5.4 AP selection in NC-CF for 200 APs with a single antenna

In this section, we simulate 200 APs with a single antenna, and perform all the proposed AP selection techniques except for the BFS, since the complexity is extremely large even for offline simulations.

By looking at Fig. 4.4, we can see that the best performance in the low $\bar{\rho}$ is obtained for the All AP, SAPS and sSAPS without pathloss compensation or for the sSAPS and SAPS with pathloss compensation. Please note the results for SAPS are included for illustration purposes, since the complexity would still be very large. In the high $\bar{\rho}$ all the techniques with pathloss compensation outperform the ones without it, and out of them, the All AP seems to be the best selection due to the fact that it has no complexity in terms of AP selection but performs very well. In the intermediate $\bar{\rho}$ range we propose to use the sSAPS with pathloss compensation, since it presents the best balance between complexity and performance.

4.5.5 Comparison between coherent and non-coherent schemes

In this subsection we compare the NC and coherent approaches of the CF scheme, by means of a Monte Carlo simulation. We consider a multipath time-varying channel and an implementation with OFDM modulation according to the 5G new radio numerology. The coherence time is calculated as $T_c = 0.15 f_D^{-1}$ [57], where f_D is the maximum Doppler frequency. The time correlation effects are implemented following the autocorrelation model of (2) in [76] and we assume the frequency offset (FO) of the LOS component is corrected with a FO correction. The OFDM symbol duration is $T_s = 1/\Delta_f$, where Δ_f is the subcarrier spacing of the OFDM. We define a ratio of coherence time to the OFDM symbol duration as $N_{CT} = T_c/T_s$, which is given in Table 4.4 for 5G scenarios at the maximum foreseen speed of 500 km/h. Only values compatible with the allowed combinations of carrier frequency (f_c) and subcarrier spacing (Δ_f) in the 5G standard are shown; otherwise they are marked with "-" in the table.

We consider a multipath channel with a delay spread of $\sigma_\tau < 1$ microsecond, so that the minimum coherence bandwidth is $B_c \approx 1/(5\sigma_\tau) = 200$ kHz. The 5G standard [77] is followed with the pilot placing for the coherent scheme, where 4 out of 14 OFDM symbols correspond to pilots in each slot. In this configuration, $\tau = 10/14$ which affects the mean SNR for the coherent scheme by penalizing the BER as shown in Eq. 4.55. The AP configuration is the same as that of Section 4.5.2, and we only perform the All AP selection approach together with a pathloss compensation in each AP to ensure a fair comparison between coherent and NC, since the AP selection is proposed for the NC scheme while an AP selection scheme for the coherent one is out of the scope of this work.

The reception process of the coherent scheme is composed of 3 steps, them being channel estimation, channel compensation and detection, while the NC scheme is composed of the differential decoding and detection. We compare the coherent centralized MMSE and the NC-CF proposal of this manuscript. Regarding the complexity, and for reproducible purposes, the times shown here have been obtained for a single-thread AMD Ryzen 7 2700X 3.7 GHz general purpose processor. The time shown in Table 4.3 is for one iteration of the reception process of each technique. It is clear from a complexity point of view that the proposed NC-CF is much more efficient than the coherent approach, mainly because pseudo-inverse calculations are avoided.

Fig. 4.5 shows the results for different N_{CT} values for 1 user for the coherent versus the NC

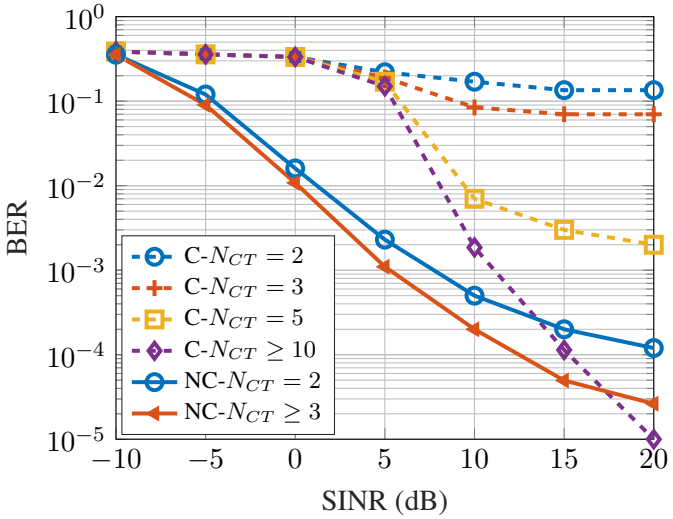

Figure 4.5: *Comparison between coherent centralized MMSE and NC for different N_{CT} values for 8 APs for the All AP selection approach with pathloss compensation.*

scheme for a QPSK constellation. It can be seen that, for high SINR, the NC outperforms the coherent scheme except for $N_{CT} \geq 10$, since in this sense the channel is quasi-static and thus the coherent outperforms the NC. For $N_{CT} \leq 5$, the NC outperforms the coherent scheme for all SINR values, due to the fact that the NC is more robust against channel variability. Also, the NC outperforms the coherent counterpart in the low SINR regime even for large N_{CT}, due to the fact that NC avoids the channel estimation, which is largely erroneous for low SINR.

4.6 Concluding Remarks for cell-free NC massive MIMO

In this chapter, we propose the combination of Cell-free massive SIMO (CF-mSIMO) and NC processing, which solves some weaknesses of the single-cell NC and the coherent CF-mSIMO. We have first performed a theoretical analysis of the effect of Rician channels with spatial correlation on the SINR and SER of single user UL NC massive MIMO systems. We have then proposed several AP selection techniques for the proposed CF massive MIMO based on NC processing, to maximize the performance. These AP selection techniques are the BFS, the SAPS, the sSAPS and the "All AP". The BFS has the best performance and largest complexity, while the "All AP" has the smallest complexity. Later, we presented some characteristics and parameters to justify in which cases it makes sense to use NC over the coherent CF, depending on the channel estimation overhead, the delay and complexity of the detection and the

performance comparison in fast varying and/or low SNR scenarios. Last, numerical results are provided to corroborate the theoretical analysis, to compare the time and performance of the AP selection techniques for different scenarios for the proposed CF NC massive MIMO and to compare the performance of the coherent and the NC CF for time varying channels. It is worth noting that the best AP selection approach for a low number of APs (the specific amount will be deployment dependent) and low SINR is the sSAPS without pathloss compensation, while for a very large number of APs or a high SINR the best is to select all the ”visible” APs by the user with pathloss compensation. For the special case of single antenna APs, the All AP without pathloss compensation is the best option in the low SINR range, the sSAPS with pathloss compensation in the intermediate range, and the All AP the best in the high range.

This work contributes to the improvement of the performance of NC schemes combined with a CF processing approach. It has shown the viability of the proposed NC-CF and its advantages over a single cell processing and over its coherent counterpart. This is a significant improvement with respect to previous NC approaches in the literature and paves the way to achieving even better capabilities, particularly in scenarios where NC schemes are known to outperform coherent communications.

A	Technique	BER ($\bar{\rho} = 10$dB)	Time (secs)	Nops	FoM
2	**One AP**	9,529e-02	0,057	2	5,6
	All AP	4,907e-03	0,046	1	2,0
	BFS	4,500e-03	0,182	3	7,7
	SAPS	4,903e-03	0,104	3	4,5
	sSAPS	4,903e-03	0,103	3	4,5
3	**One AP**	5,171e-02	0,086	3	6,7
	All AP	1,093e-03	0,051	1	1,7
	BFS	6,805e-04	0,392	7	12,4
	SAPS	8,637e-04	0,240	5-6	7,8
	sSAPS	1,009e-03	0,188	4-5	6,3
4	**One AP**	3,094e-02	0,113	4	7,5
	All AP	3,827e-04	0,055	1	1,6
	BFS	9,904e-05	0,797	15	19,9
	SAPS	1,608e-04	0,460	7-10	12,1
	sSAPS	2,653e-04	0,252	5-7	7,1
5	**One AP**	1,923e-02	0,143	5	8,3
	All AP	1,597e-04	0,057	1	1,5
	BFS	1,350e-05	1,623	31	33,3
	SAPS	3,456e-05	0,794	9-15	17,8
	sSAPS	9,327e-05	0,302	6-9	7,5
6	**One AP**	1,272e-02	0,164	6	8,6
	All AP	1,888e-04	0,058	1	1,5
	BFS	2,337e-06	3,208	63	57,0
	SAPS	1,340e-05	1,198	11-21	24,6
	sSAPS	7,527e-05	0,332	7-11	8,1
7	**One AP**	8,188e-03	0,198	7	9,5
	All AP	1,978e-05	0,061	1	1,3
	BFS	7,230e-07	6,780	127	110,4
	SAPS	8,436e-06	1,822	13-28	35,9
	sSAPS	1,533e-05	0,374	8-13	7,8

Table 4.5: *Comparison of different AP selection techniques and $\bar{\rho} = 10$ dB.*

Chapter 5

Pilot-less channel estimation with detected Non-coherent data

In this chapter, we propose a novel pilot-less channel estimation technique based on the use of reconstructed NC data that has been detected applying the procedure proposed in Section 3.3. This pilot-less channel estimation technique mainly allows to substitute the pilot signals in the PSAM approach by NC data, thus increasing the efficiency of the communication.

5.1 Proposed pilot-less channel estimation

Assuming a data TX as proposed in Section 3.3, and recalling the mathematical notation, we have that the received signal in a certain BS for a certain user would be

$$\mathbf{y}_u^n = \mathbf{h}_u^n \mathbf{x}_u^n + \boldsymbol{\nu}^n, \tag{5.1}$$

which can be differentially detected as

$$z_u^n = \frac{(\mathbf{y}_u^{n-1})^H \mathbf{y}_u^n}{R} = s_u^n + \widehat{\boldsymbol{\nu}}^n, \tag{5.2}$$

where the data sent by user u at time instant n is distorted by the presence of noise and the differential processing. The data symbols (s_u^n) can be obtained at the BS receiver applying, for instance, the maximum-likelihood (ML) criterion [78] as

$$\widehat{s}_u^n = \arg\max_{s_u^n} \left\{ f_{z|s}(z_u^n \mid s_u^n) \right\}, \tag{5.3}$$

where $f_{z|s}(z_u^n \mid s_u^n)$ is the conditional probability that z_u^n is received having transmitted s_u^n.

Once the decision is taken on the NC data symbols, they can be used for the channel estimation as follows. Firstly, the differential symbols are reconstructed ($\widehat{s}_u^n \rightarrow \widehat{x}_u^n$) by applying Eq. 3.15.

Then, the LS criterion is used to estimate the channel as

$$\widehat{\mathbf{h}}_u^n = \frac{1}{\widehat{x}_u^n}\mathbf{y}_u^n = \frac{x_u^n}{\widehat{x}_u^n}\mathbf{h}_u^n + \frac{1}{\widehat{x}_u^n}\boldsymbol{\nu}_u^n. \tag{5.4}$$

Inspecting Eq. 5.4, we can see that there is no noise enhancement since $|\widehat{x}_u^n| = 1$. However, unlike in traditional PSAM, there is an additional error term in the channel estimation produced by the possible mismatch between the transmitted and the reconstructed differential symbols. This error in the channel estimation is studied in the next subsection, where we characterize the mean squared error (MSE) of the channel estimation.

5.1.1 Mean squared error (MSE) of the channel estimation

The two terms given in Eq. 5.4 are independent to each other, which can be verified as

$$\begin{aligned}\mathbb{E}\left\{\frac{x_u^n}{\widehat{x}_u^{n'}}[\mathbf{h}_u^n]_r\left(\frac{1}{\widehat{x}_u^n}[\boldsymbol{\nu}_u^n]_r\right)^*\right\} = \mathbb{E}\left\{\frac{x_u^n}{|\widehat{x}_u^n|^2}[\mathbf{h}_u^n]_r\left([\boldsymbol{\nu}_u^n]_r\right)^*\right\} = \\ = \mathbb{E}\left\{x_u^n\right\}\mathbb{E}\left\{[\mathbf{h}_u^n]_r\right\}\mathbb{E}\left\{([\boldsymbol{\nu}_u^n]_r)^*\right\} = 0,\end{aligned} \tag{5.5}$$

due to the fact that the transmitted symbol, channel and noise are uncorrelated random variables. It is worth noting that usually, the channel estimation is performed in a certain time instant or frequency resource and it is used to compensate the channel in another time instant or frequency resource. Regarding the time dimension, this is what is called in the literature "channel aging" [79]. Hence, the channel estimation error incurred when using Eq. 5.4 is given by

$$\sigma_e^2 = \mathbb{E}\left\{\left|\widehat{\mathbf{h}}_u^n - \mathbf{h}_u^{n'}\right|^2\right\} = \sigma_{x\vec{n}}^2 + \sigma_\nu^2, \tag{5.6}$$

where $\sigma_{x\vec{n}}^2$ is the channel estimation error that comes from compensation and estimation in different time instants with a possible mismatch between transmitted and reconstructed differential symbol. We compute

$$\begin{aligned}\sigma_{x\vec{n}}^2 = \mathbb{E}\left\{\left|\mathbf{h}_u^n\frac{x_u^n}{\hat{x}_u^n} - \mathbf{h}_u^{n'}\right|^2\right\} = \mathbb{E}\left\{\left|\mathbf{h}_u^n\frac{x_u^n}{\hat{x}_u^n} - \eta_{\vec{n}}\mathbf{h}_u^n - \sqrt{1-\eta_{\vec{n}}^2}\vec{\mathbf{h}}_u^{n'}\right|^2\right\} = \\ = \mathbb{E}\left\{|\mathbf{h}_u^n|^2\left|\frac{x_u^n}{\hat{x}_u^n} - \eta_{\vec{n}}\right|^2 + \left|\sqrt{1-\eta_{\vec{n}}^2}\vec{\mathbf{h}}_u^{n'}\right|^2\right\} = \mathbb{E}\left\{\left|\frac{x_n^k}{\hat{x}_n^k} - \eta_{\vec{n}}\right|^2\right\} + \sigma_w^2,\end{aligned} \tag{5.7}$$

where $\mathbb{E}\left\{|\mathbf{h}_u^n|^2\right\} = 1$ since the channel is normalized, $|\mathbf{h}_u^n|^2$ is uncorrelated and independent of $\left|\frac{x_u^n}{\hat{x}_u^n} - \eta_{\vec{n}} - \sqrt{1-\eta_{\vec{n}}^2}\vec{\mathbf{h}}_u^{n'}\right|^2$ and $\frac{x_u^n}{\hat{x}_u^n} - \eta_{\vec{n}}$ and $\sqrt{1-\eta_{\vec{n}}^2}\vec{\mathbf{h}}_u^{n'}$ are uncorrelated and independent. In this case, $\sigma_w^2 = (1-\eta_{\vec{n}}^2)$, since the channel is normalized. Developing the first term of the last part of Eq. 5.7, we have

$$\begin{aligned}\mathbb{E}\left\{\left|\frac{x_u^n}{\hat{x}_u^n} - \eta_{\vec{n}}\right|^2\right\} &= \mathbb{E}\left\{\left|\frac{x_u^n}{\hat{x}_u^n}\right|^2 - 2\eta_{\vec{n}}\Re\left\{\frac{x_u^n}{\hat{x}_u^n}\right\} + \eta_{\vec{n}}^2\right\} \\ &= 1 + \eta_{\vec{n}}^2 - 2\eta_{\vec{n}}\mathbb{E}\left\{\cos\left(\angle(x_u^n) - \angle(\hat{x}_u^n)\right)\right\}.\end{aligned} \tag{5.8}$$

We define $\lambda_u^n = \mathbb{E}\{\cos\angle(x_u^n) - \angle(\hat{x}_u^n)\}$ and by following the same approach as that of Appendix B of [11] (omitted here for the sake of conciseness), we can define

$$\lambda_u^n \approx \begin{cases} 1, & P_u^n = 0 \\ \frac{1-P_u^n-(1-P_u^n)^{K_p}}{(K_p-1)P_u^n}, & 0 < P_u^n \leq 1 \end{cases}, \tag{5.9}$$

that will serve as an upper bound (UB) for σ_e^2, as stated in Appendix B of [11], and where K_p is the length of the NC data stream without accounting for any reference symbols. We can write $\sigma_{x\vec{n}}^2$ and σ_e^2 as

$$\sigma_{x\vec{n}}^2 = 1 + \eta_{\vec{n}}^2 - 2\eta_{\vec{n}}\lambda_u^n + 1 - \eta_{\vec{n}}^2 = 2(1 - \eta_{\vec{n}}\lambda_u^n), \tag{5.10}$$

$$\sigma_e^2 = \mathbb{E}\left\{\left|\hat{\mathbf{h}}_u^n - \mathbf{h}_u^{n'}\right|^2\right\} = 2(1 - \eta_{\vec{n}}\lambda_u^n) + \sigma_\nu^2. \tag{5.11}$$

The same analysis can be done for the frequency domain by substituting $\eta_{\vec{n}}$ with $\eta_{\vec{k}}$. Analyzing Eq. 5.11, it can be seen that in case either $\eta_{\vec{n}}$ or λ_u^n is zero, the channel error estimation is the highest, while both need to be 1 to avoid any increment in the channel estimation error, with respect to the classical PSAM. Therefore, the channel estimation error for our proposed scheme σ_e^2 is bounded by

$$\sigma_\nu^2 \leq \sigma_e^2 \leq \sigma_\nu^2 + 2. \tag{5.12}$$

It is worth noting that the error depends mainly on 4 factors:

- The symbol error probability of the NC detection, defined as P_u^n, which directly depends on the number of antennas R in the BS and the constellation size of the NC data.
- The length of the NC data stream, defined as K_p.

- The channel variability that depends on the channel correlation as $\eta_{\vec{n}}$ or $\eta_{\vec{k}}$.
- The noise of the channel estimation.

5.2 Increment in the uplink OFDM grid efficiency

5.2.1 Multiplexing the coherent and the NC data streams

To increment the uplink efficiency of an OFDM grid, we propose to change the pilot resource elements with NC data, in order to include more useful information in the grid. The user transmits N consecutive OFDM symbols to the BS, the OFDM signal has K subcarriers and the length of the cyclic prefix (L_{CP}) is long enough to absorb the effects of the multi-path channel ($L_{CP} \geq L_{CH} - 1$). The number of channel taps is denoted by L_{CH}. At the BS, after removing the cyclic prefix and performing a fast-Fourier transform (FFT), we can process each subcarrier as one of a set of K independent sub-channels. Moreover, the whole time-frequency resource grid ($K \times N$ resource elements) is split into unit blocks of K_B consecutive subcarriers and N_B contiguous OFDM symbols. Each unit block can be independently processed for channel estimation and detection. This model has practical interest since it is used, for example, in the 4G and 5G, where these generic unit blocks are denoted as physical resource blocks [77]. Hence, for the sake of conciseness and without loss of generality, we focus on a particular unit block.

Let $\mathcal{A}$ denote the set of pairs of frequency and time indexes that describe the resources of the unit block, defined as

$$\mathcal{A} = \{(n,k) \mid n \in \{1, \cdots, N_B\}, k \in \{1, \cdots, K_B\}\}, \tag{5.13}$$

with cardinality $|A| = K_B \times N_B$. Let $\mathcal{A}_d$ denote the subset of the pairs of frequency and time indexes intended for the data transmission, and $\mathcal{A}_p$ denote the subset that contains the pairs of frequency and time indexes reserved for the pilot symbols. These subsets must satisfy

$$\mathcal{A} = \mathcal{A}_d \cup \mathcal{A}_p, \quad \emptyset = \mathcal{A}_d \cap \mathcal{A}_p, \tag{5.14}$$

and their cardinality is given by

$$|A| = K_p \times N_p, \quad |A| = K_B N_B - K_p N_p. \tag{5.15}$$

In this equation K_p and N_p refer to the number of pilots in the frequency and time domain, respectively, in a unit block. According to [80], these pilot symbols must be equally spaced over the available resources. The distance between two contiguous pilot symbols in the frequency and time dimensions is denoted by L_K and L_N, measured in number of resources, and they must satisfy

$$K_B = L_K \times K_p, \quad N_B = L_N \times N_p. \tag{5.16}$$

A HDS is proposed, in which the classical coherent and the NC schemes are combined, with the NC occupying the resources previously occupied by the reference signals (see Fig. 5.1). The distribution of resources is

$$x_u^{nk} = \begin{cases} c_u^{nk}, & (n,k) \in \mathcal{A}_d \\ p_u^{nk}, & (n,k) \in \mathcal{A}_p, k = k_{min}^n \\ x_u^{n(k-L_K)} s_u^{nk}, & (n,k) \in \mathcal{A}_p, k \neq k_{min}^n \end{cases}, \tag{5.17}$$

where c_u^{nk} represents the coherent data in the OFDM grid in time instant n and frequency k, $\mathcal{A}_p$ is the set of resource elements that were used for pilot signals and now are used for NC data in the proposed HDS, k_{min}^n is the minimum value of the index k for the n-th OFDM symbol belonging to the subset $\mathcal{A}_p$ (that is, the first sub-carrier of each OFDM symbol that carries the NC data stream), $\mathcal{A}_d$ is the set of resource elements in the resource block that are used for coherent data, p_u^{nk} is the known reference symbol of the NC data stream and L_K is the distance between 2 contiguous NC resources.

For example, $k_{min}^n = 1$ in Fig. 5.1, $\mathcal{A}_p$ has $k = 1, 3, 5, 7, 9$ and $n = 3, 6, 9, 12$, so $L_K = 2$. In this example, the NC data stream is placed along the frequency dimension and not the time dimension. Interestingly, our proposed differential data-aided system can be adapted to any existing pilot distribution based on PSAM, by simply replacing the pilots by a NC data stream.

5.2.2 Analysis of the Throughput and the Complexity

In this section we analyze and compare in terms of throughput and complexity the traditional coherent scheme and our proposed HDS. We show that HDS can increase the throughput with a negligible increment of the complexity. For a typical packet-based transmission, let us define

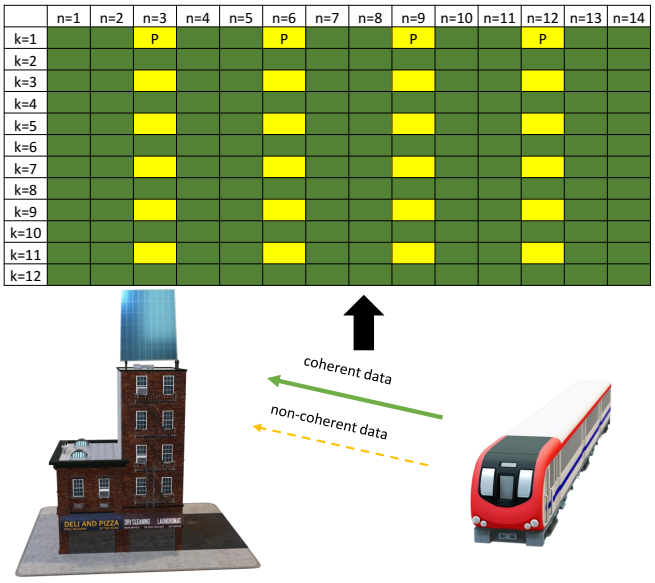

Figure 5.1: *Example of a unit block for the proposed HDS, where $K_p = 6$ and $N_p = 4$. The green boxes are data modulated by classical coherent, the yellow boxes are data modulated by the NC and "p" denotes the NC reference symbol.*

the total throughput of the HDS as

$$T = T_C + T_N \,[\text{packet/s}]\,, \tag{5.18}$$

where T_C and T_N refer to the throughput of the coherent and NC streams, respectively, for each unit block. The throughput of each scheme can be found as

$$T_C = \frac{\eta_C \Delta f K_B}{L_P} (1 - P_{bC})^{L_P} \log_2(M_C), \tag{5.19}$$

$$T_N = \frac{\eta_N \Delta f K_B}{L_P} (1 - P_{bN})^{L_P} \log_2(M_N). \tag{5.20}$$

In these equations, L_P denotes the number of bits in one packet, P_{bN} is given by Eq. 5.24 and P_{bC} by Eq. 5.22, M_C is the constellation size of the coherent and M_N is the constellation size of the NC. The efficiencies of the coherent and the NC in terms of the occupied resources in the unit block are

$$\eta_C = 1 - \frac{K_p N_p}{K_B N_B}, \quad \eta_N = \frac{N_p}{K_B N_B} (K_p - 1)\,. \tag{5.21}$$

Inspecting Eqs. 5.18-5.20, we can see that the total throughput of our proposed HDS is the sum

of the throughput of each scheme, coherent and NC given in Eq. 5.19 and Eq. 5.20, respectively. If some parameters are given by the system design, such as the number of antennas, SNR, bandwidth and length of the packet, the throughput of the NC only depends on the selected modulation scheme (M_N) and its corresponding BER ($P_{b,C}$ given in Eq. 5.24. In turn, the BER of coherent ($P_{b,C}$ given in Eq. 5.22) not only depends on the constellation size (M_C), but it also relies on the performance of the channel estimation provided by the NC stream. Hence, the proposed HDS outperforms the traditional coherent scheme due to the additional throughput provided by the NC if the channel estimation error (σ_e^2) is properly constrained in order to avoid the increment of $P_{b,C}$.

In order to obtain the best pair of constellation sizes (M_C and M_N) for a given scenario with some specific parameters, the throughput given in Eqs. 5.18-5.20 should be maximized. Due to the difficulty to find closed-form expressions from Eq. 5.22 and Eq. 5.24 and motivated by the fact that the search space is very small ($\log_2(\max(M_N)) \times \log_2(\max(M_C))$ combinations), we propose to resort to an exhaustive search over these few options. The throughput expressions are evaluated for a particular scenario and the values that provide the maximum throughput given in Eq. 5.18 are chosen. As we show in the next section, the search is limited to a small number of options since the possible values of M_C and M_N are usually constrained to a few, e.g. 8×6.

5.2.2.1 Bit error rate of the coherent and the NC schemes

According to [81], the BER for a M_C-QAM constellation using a ZF post-equalization may be approximated as

$$P_{bC} \approx \frac{2}{\sqrt{M_C} g_C} \sum_{i_1=1}^{g_C} \sum_{i_2=0}^{(1-2^{-i_1})\sqrt{M_C}-1} (-1)^{\left\lfloor \frac{i_2 2^{i_1-1}}{\sqrt{M_C}} \right\rfloor} \left(2^{i_1-1} - \left\lfloor \frac{i_2 2^{i_1-1}}{\sqrt{M_C}} + \frac{1}{2} \right\rfloor\right) \times \left[\frac{1-\mu_{i_2}}{2}\right]^R \sum_{i_3=0}^{R-1} \binom{R-1+i_3}{i_3} \left[\frac{1+\mu_{i_2}}{2}\right]^{i_3}, \tag{5.22}$$

$$\mu_{i_2} = \sqrt{\frac{3(2i_2+1)^2\gamma_s}{2(M_C-1)+3(2i_2+1)^2\gamma_s}}, \quad \gamma_s = \frac{\rho}{1+\rho\sigma_d^2}, \tag{5.23}$$

where M_C is the constellation size of the coherent data stream, $g_C = \log_2(\sqrt{M_C})$, $\rho = 1/\sigma_\nu^2$, σ_d^2 is the channel estimation error after interpolation [82] (whose detailed analysis is out of

scope of this work) and we assume the use of a rectangular pulse.

The expression of the BER is the same as that of the Eq. 4.37 which was calculated for a multi-cell approach. Here we simplify for a single AP for a Rayleigh uncorrelated channel (found in [11, Appendix A]) and is given by

$$P_{b,N} = \frac{2\sigma_x\sigma_y\pi - 1}{\sigma_x\sigma_y\pi \log_2(M_N)} \times \int_{\mathcal{D}} \int_0^{\infty} e^{-\left(\frac{r\cos(\gamma)-\mu_x}{\sigma_x\sqrt{2}}\right)^2 + \left(\frac{r\sin(\gamma)-\mu_y}{\sigma_y\sqrt{2}}\right)^2} r dr d\gamma, \tag{5.24}$$

where $\mathcal{D} \in [-\pi/M_N, \pi/M_N]$ denotes the decision region for the correspondent symbol of interest and (μ_x, μ_y)=$(1, 0)$ (set for the DPSK symbol placed in the positive part of the real axis of the complex plane without loss of generality), with the parameters $\sigma_x = \sqrt{\frac{2+2\sigma_v^2+\sigma_v^4}{2R}}$ and $\sigma_y = \sqrt{\frac{2\sigma_v^2+\sigma_v^4}{2R}}$.

In general, NC processing is much less complex than coherent processing. Anyway, as the NC stream is an addition to the proposed scheme with respect to the coherent scheme, its demodulation will incur some extra complexity. In order to show that the proposed HDS does not significantly increase the complexity of the system, the number of complex multiplications (NCM) required for each scheme is accounted as follows. For the particular case of the coherent, the expression of the NCM is given by

$$D_C = K_B N_B(3R + 1) - 3RK_p N_p, \tag{5.25}$$

where the LS channel estimation given in Eq. 5.4 is considered, as well as the post-coding matrix computation given in Eq. 3.14) and the equalization process given in Eq. 3.9. The complexity introduced by the interpolation process is not taken into account, so this is an optimistic evaluation of the complexity of coherent detection. If we consider it, the additional relative complexity of NC is even lower. For the case of HDS, the NCM can be expressed as

$$\begin{aligned} D_H = D_C + D_N = D_C + RN_p(K_p - 1) = \\ = K_B N_B(3R + 1) - RN_p(2K_p + 1), \end{aligned} \tag{5.26}$$

where D_N accounts for the differential decoding given in Eq. 3.19, required for the NC. Note that the differential encoding required for computing the differential symbols s_u^{nk} at the transmitter, and for the reconstruction of the differential symbols $\widehat{s}_u^{nk}$ at the receiver are considered negligible. The reason for this is the fact that the phase difference can be computed in polar

coordinates, which corresponds to adding/subtracting phases, and the conversion from polar to binomial coordinates can be implemented by using look-up tables, since the differential symbols (s_u^{nk}) belong to a DMPSK constellation, which is a finite set. On the contrary, these simplifications cannot be implemented for the differential decoding, since the received symbols, which are modified by the channel and noise effects, no longer belong to a finite set.

Comparing Eq. 5.25 and Eq. 5.26, we can see that the dominant term in Eq. 5.26 is the first one, which corresponds to the coherent processing, and therefore, both techniques have the same complexity order $\mathcal{O}(3RK_BM_B)$, rendering the additional complexity of the NC stream negligible, as predicted.

5.3 Pilot-less TDD massive MIMO

In this section, a novel TDD massive MIMO approach based on utilizing the pilot-less channel estimation proposed in Section 5.1 in the UL using differentially encoded data and a precoding in the DL, also with differentially encoded data, is proposed. In this system, the use of any type of explicit pilot symbol is completely avoided while maintaining spatial multiplexing capabilities in the DL. We perform an analysis of the full system in terms or SINR for the UL and the DL. The performance of the channel estimation using differentially encoded data is also analyzed, since it affects the performance of the DL data transmission. A multi-user allocation strategy in an OFDM grid is proposed. The analysis is corroborated via numerical results and the proposed scheme is shown to outperform its coherent counterpart. We assume a single BS with R antennas and U served users.

5.3.1 Proposed pilot-less TDD massive MIMO

We apply maximum ratio transmission (MRT) in the DL, so the precoding vector will be $\mathbf{b}_u^{nk} = \mathbf{h}_u^{nk}$. For the coherent demodulation, we assume that the coherence time of the channel is at least four OFDM symbols (which is the most pessimistic case). This comes from the fact that in a typical TDD time stream, reference signals are needed in the UL to estimate the CSI and additional pilot symbols are required in the DL (sometimes called demodulation pilots), plus at least one data symbol in the UL and one data symbol in the DL, as shown in Fig. 5.2. The additional pilot in the DL are introduced since channel precoding may not perfectly separate the users or compensate the channel effects, and additional estimation and processing

is required [83]. By observing Fig. 5.2, it can be easily observed that in the worst case (UL pilot - UL data - DL pilot - DL data), the data efficiency of a coherent scheme would be 50% of the available resources. Even worse would be the scenario in which the coherence time is smaller

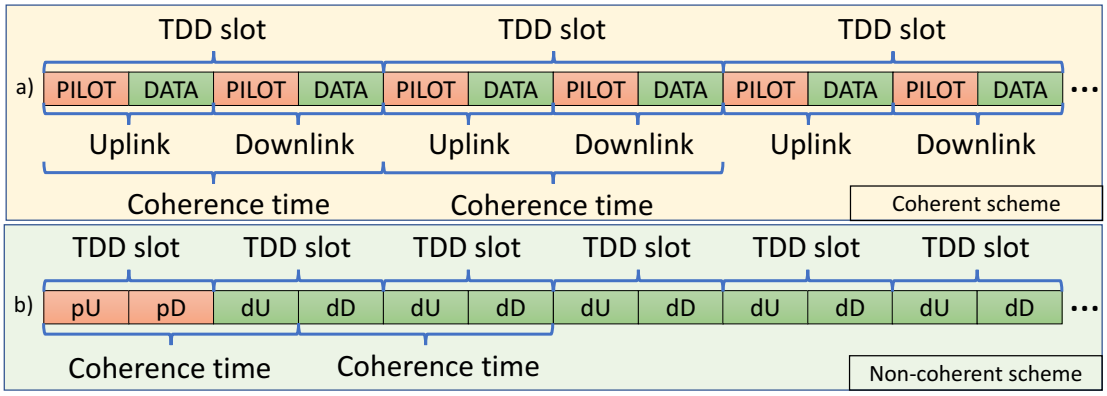

Figure 5.2: *TDD frame comparison for coherent (a) and non-coherent (b).*

In the proposed pilot-less TDD massive MIMO scheme each UL and DL data symbol of each user s_u^{nk} is differentially encoded as Eq. 3.15, resulting in x_u^{nk}, which only needs one reference symbol or pilot known at the BS (for the UL) and at each user (for the DL), and s_u^{nk} belongs to a DMPSK constellation. We focus on a single BS, and for the coherent processing, we can extend Eq. 3.7 as

$$\mathbf{y}_{u,dl}^{n,k} = (\mathbf{h}_u^{n,k})^H \sum_{u=1}^{U} \mathbf{b}_u^{n,k} x_{u,dl}^{n,k} + \boldsymbol{\nu}_u^{n,k} = (\mathbf{h}_u^{n,k})^H \mathbf{b}_u^{n,k} x_{u,dl}^{n,k} + (\mathbf{h}_u^{n,k})^H \sum_{\substack{u'=1 \\ u' \neq u}}^{U} \mathbf{b}_{u'}^{n,k} x_{u',dl}^{n,k} + \boldsymbol{\nu}_u^{n,k}, \tag{5.27}$$

where Eq. 3.7 is separated in three terms, the first one being the desired signal for user u, the second term is the interference generated in user u from the rest of the users and the third term is the noise.

The reception is performed via differential detection of two consecutive received signals in time, as shown in [73],

$$z_u^{n,k} = \left(\mathbf{y}_u^{n-1,k}\right)^H \mathbf{y}_u^{n,k} = \left(\mathbf{h}_u^{n-1,k}\right)^H \mathbf{h}_u^{n,k} s_u^{n,k} + \eta_u^{n,k}, \tag{5.28}$$

with the noise terms ($\eta_u^{n,k}$) as

$$\eta_u^{n,k} = \left(\mathbf{h}_u^{n-1,k}\right)^H \left(\mathbf{x}_u^{n-1,k}\right)^H \boldsymbol{\nu}_u^{n,k} + \left(\boldsymbol{\nu}_u^{n-1,k}\right)^H \mathbf{h}_u^{n,k}\mathbf{x}_u^{n,k} + \left(\boldsymbol{\nu}_u^{n-1,k}\right)^H \boldsymbol{\nu}_u^{n,k}, \quad (5.29)$$

and the transmitted symbol for each user is estimated in the BS (for the UL) and in each user terminal (for the DL) according to [2] as

$$\hat{s}_u^{n,k} = \arg\min_{s_u^{n,k}} \left\{ \left| s_u^{n,k} - z_u^{n,k} \right|,\ s_u^{n,k} \in \mathfrak{M} \right\}, \quad (5.30)$$

where $\mathfrak{M}$ indicates the DMPSK constellation set, of size M, either for the UL or DL. For the DL, spatial multiplexing is utilized, via the use of MRT. Once the decision is taken on the UL NC data symbols, the channel is estimated following the approach in 5.1. A maximum length for the UL stream K_p is defined to reduce the error probability in the data reconstruction. With this estimated channel, the DL is precoded following Eq. 3.7.

5.3.2 SER of the received symbol in the DL

To analyze the effect of imperfect channel estimation for the proposed pilot-less TDD massive MIMO schemes in the DL transmission, we assume the following definition [75]

$$\hat{\mathbf{h}}_u^{nk} = \sqrt{1 - e_d^2}\mathbf{h}_u^{nk} + \mathbf{h}_{ue}^{nk}, \quad (5.31)$$

where $\mathbf{h}_{ue}^{nk} \sim \mathcal{CN}\left(\mathbf{0}, e_d^2\mathbf{I}\right)$ is an error component which is uncorrelated with $\mathbf{h}_u^{nk}$. We extend the components of Eq. 5.27 following the definition in Eq. 5.31 as

$$\mathbf{h}_u^{n,k}\mathbf{b}_{u'}^{n,k} = \mathbf{h}_u^{n,k}\left(\sqrt{1 - e_d^2}\mathbf{h}_{u'}^{n,k} + \mathbf{h}_{u',e}^{n,k}\right)^H = \sqrt{1 - e_d^2}\mathbf{h}_u^{n,k}(\mathbf{h}_{u'}^{n,k})^H + \mathbf{h}_u^{n,k}(\mathbf{h}_{u',e}^{n,k})^H, \quad (5.32)$$

and $[\mathbf{x}_n^k]_u$ is just a phase rotation. Thus, following the properties of the product of normal variables [84] and the properties of VG distributions [60, 61], we have that

$$\sqrt{1 - e_d^2}\mathbf{h}_u^{n,k}(\mathbf{h}_u^{n,k})^H \sim \mathcal{N}\left(R\sqrt{1 - e_d^2}, R(1 - e_d^2)\right), \quad (5.33)$$

$$\sqrt{1 - e_d^2}\mathbf{h}_u^{n,k}(\mathbf{h}_{u'}^{n,k})^H \sim \mathcal{CN}\left(0, R(1 - e_d^2)\right), \quad (5.34)$$

$$\mathbf{h}_{u'}^{n,k}(\mathbf{h}_{u',e}^{n,k})^H \sim \mathcal{CN}\left(0, Re_d^2\right). \tag{5.35}$$

We define a useful component (UF) of the received signal

$$\text{UF}_u^n = \left(\sqrt{1-e_d^2}\mathbf{h}_u^{n,k}(\mathbf{h}_u^{n,k})^H\right)\mathbf{x}_u^{n,k} \tag{5.36}$$

and the rest of the terms that arise from combining Eq. 5.27 and Eq. 5.31 are defined as non-useful (NUF) terms. Using the properties of the product of normal variables and the properties of VG distributions, the distribution of UF_n^u is defined as Eq. 5.33. The distribution of NUF_n^u is composed of the sum of several complex circularly symmetric Gaussian variables, including Eq. 5.35 from the desired user and $U-1$ of Eq. 5.34 and Eq. 5.35 from the interfering users over the desired user. Since $\mathbf{x}_{u'}^{n,k}$ only rotates the distributions, NUF_n^u is

$$\text{NUF}_n^u \sim \mathcal{CN}\left(0, R(U+e_d^2-1)+\sigma_{\nu_u}^2\right). \tag{5.37}$$

Assuming $\mathbf{x}_u^{n,k}=1$ without loss of generality[1], we have $\Re\{[\mathbf{y}_n^k]_u\} \sim \mu_\Re + \mathcal{N}\left(0,\sigma_\Re^2\right)$ and $\Im\{[\mathbf{y}_n^k]_u\} \sim \mathcal{N}\left(\mu_\Im,\sigma_\Im^2\right)$, so

$$\Re\{\mathbf{y}_u^{n,k}\} \sim R\sqrt{1-e_d^2} + \mathcal{N}\left(0, \frac{R(U-e_d^2+1)+\sigma_{\nu_u}^2}{2}\right) \tag{5.38}$$

$$\Im\{\mathbf{y}_u^{n,k}\} \sim \mathcal{N}\left(0, \frac{R(U+e_d^2-1)+\sigma_{\nu_u}^2}{2}\right). \tag{5.39}$$

The differential decoding performed in reception for the received signal at each user Eq. 5.28 results in the product of complex normally distributed variables, where in order to find the distribution of the received symbol, we have to consider the product of two complex variables $x=a+jb$ and $y=c+jd$, so the product $(x)^*y=(ac+bd)+j(ad-bc)$. Using again the properties of the product of normal variables and VG distributions, we have that

$$\Re\{z_u^{n,k}\} = \Re\{\mathbf{y}_u^{n-1,k}\}\Re\{\mathbf{y}_u^{n,k}\} + \Im\{\mathbf{y}_u^{n-1,k}\}\Im\{\mathbf{y}_u^{n,k}\}, \tag{5.40}$$

$$\Im\{z_u^{n,k}\} = \Re\{\mathbf{y}_u^{n-1,k}\}\Im\{\mathbf{y}_u^{n,k}\} - \Im\{\mathbf{y}_u^{n-1,k}\}\Re\{\mathbf{y}_u^{n,k}\}. \tag{5.41}$$

[1]The error is computed for $\mathbf{x}_u^{n,k}=1$ for simplicity but it is the same for the rest of the symbols.

Thus, the first term of Eq. 5.40 is composed of three terms as

$$\mathfrak{R}_1\{z_u^{n,k}\} = R^2(1-e_d^2),\ \mathfrak{R}_2\{z_u^{n,k}\} \sim R\sqrt{1-e_d^2}\mathcal{N}\left(0, 2\sigma_{\mathfrak{R}}^2\right),\ \mathfrak{R}_3\{z_u^{n,k}\} \sim VG\left(1, 0, \sigma_{\mathfrak{R}}^2, 0\right), \tag{5.42}$$

while the second term of Eq. 5.40 is distributed as $\mathfrak{I}\{\mathbf{y}_u^{n-1,k}\}\mathfrak{I}\{\mathbf{y}_u^{n,k}\} \sim VG\left(1, 0, \sigma_{\mathfrak{I}}^2, 0\right)$. Each term of Eq. 5.41 is composed of two terms, them being

$$\mathfrak{I}_1\{z_u^{n,k}\} = R\sqrt{1-e_d^2}\mathcal{N}\left(0, \sigma_{\mathfrak{I}}^2\right), \quad \mathfrak{I}_2\{z_u^{n,k}\} \sim VG\left(1, 0, \sigma_{\mathfrak{R}}\sigma_{\mathfrak{I}}, 0\right). \tag{5.43}$$

The VG distributions may be approximated for convenience to normal distributions as

$$VG\left(1, 0, \sigma_{\mathfrak{R}}^2, 0\right) \approx \mathcal{N}\left(0, \sigma_{\mathfrak{R}}^4\right),$$

$$VG\left(1, 0, \sigma_{\mathfrak{I}}^2, 0\right) \approx \mathcal{N}\left(0, \sigma_{\mathfrak{I}}^4\right),$$

$$VG\left(1, 0, \sigma_{\mathfrak{R}}\sigma_{\mathfrak{I}}, 0\right) \approx \mathcal{N}\left(0, \sigma_{\mathfrak{R}}^2\sigma_{\mathfrak{I}}^2\right).$$

Summarizing, the distribution for $s_u^{n,k} = 1$ follows $\mathfrak{R}\{z_u^{n,k}\} \sim \mathcal{N}\left(\mu_{\mathfrak{R}\{z_u^{n,k}\}}, \sigma^2_{\mathfrak{R}\{z_u^{n,k}\}}\right)$, $\mathfrak{I}\{z_u^{n,k}\} \sim \mathcal{N}\left(\mu_{\mathfrak{I}\{z_u^{n,k}\}}, \sigma^2_{\mathfrak{I}\{z_u^{n,k}\}}\right)$ and defined as

$$\mathfrak{R}\{[\mathbf{z}_n^k]_u\} \sim \mathcal{N}\left(R^2(1-e_d^2), 2R^2(1-e_d^2)\sigma_{\mathfrak{R}}^2 + \sigma_{\mathfrak{R}}^4 + \sigma_{\mathfrak{I}}^4\right), \tag{5.44}$$

$$\mathfrak{I}\{[\mathbf{z}_n^k]_u\} \sim \mathcal{N}\left(0, 2\sigma_{\mathfrak{I}}^2\left(R^2(1-e_d^2) + \sigma_{\mathfrak{R}}^2\right)\right), \tag{5.45}$$

so the SER for the DL of user u can be computed following the approach in Appendix A of [11] as

$$P_n^k \approx 1 - \frac{\int_{-\pi/M}^{\pi/M}\int_0^{\infty} e^{-\left(\frac{r\cos(\gamma)-\mu_{\mathfrak{R}\{z_u^{n,k}\}}}{\sqrt{2}\sigma_{\mathfrak{R}\{z_u^{n,k}\}}}\right)^2} e^{-\left(\frac{r\sin(\gamma)-\mu_{\mathfrak{I}\{z_u^{n,k}\}}}{\sqrt{2}\sigma_{\mathfrak{I}\{z_u^{n,k}\}}}\right)^2} r dr d\gamma}{2\pi\sigma_{\mathfrak{R}\{z_u^{n,k}\}}\sigma_{\mathfrak{I}\{z_u^{n,k}\}}}. \tag{5.46}$$

5.4 Numerical Results for pilot-less channel estimation with detected NC data

In this section we include the numerical results for both the proposed HDS for the UL of a massive MIMO-OFDM scheme and for the pilot-less TDD massive MIMO.

K_p	1, 2, 3, 4, 6, 12	K_B, N_B	12, 14	K	1024
N_p	1, 2, 4, 7, 14	M_C	4, 16, 64	L_P	20
R	16, 64, 256	M_N	4, 8, 16, 64	Δf	30 KHz

Table 5.1: *Simulation parameters*

5.4.1 Uplink efficiency with NC data pilot-less channel estimation

In this section, we provide some numerical results to verify our analysis and show the validity of the proposed HDS, which is capable of outperforming the traditional coherent scheme for several scenarios of interest, as well as other alternative schemes such as ST. In Table 5.1, we provide a summary of some numerical values for the different system parameters, where they have been chosen taking into account the numerology given in 5G [77]. Besides, the size of the unit block has been set $K_B = 12$, $N_B = 14$ and the interpolation method to 'spline' [85].

The number of pilots placed in the unit block (given by K_p and N_p) must be incremented as the variations of the channel in both dimensions increase. Note that the time variability of the channel is modelled by using Eq. 3.2. According to [80], the number of pilots placed in the frequency dimension should be at least twice the number of taps of the multi-path channel, and in the time dimension there must be at least two pilots within the coherence time [57]. However, realistic communication links increase the number of pilots beyond the minimum, especially in the frequency dimension, to improve the quality of the estimators. Then, by changing the values of K_p and N_p we illustrate different scenarios of time and frequency variability of the channel. The ST scheme of [86] is also taken into account for the comparison of throughput. This scheme has a parameter denoted as ι that indicates the power allocated for the superimposed pilot symbols, while $1 - \iota$ corresponds to the power of the data symbols. According to [86], we set $\iota = 0.2$ which is the most frequently used value in the literature. ST requires an averaging process, which is implemented in both time and frequency dimensions and the number of resources to average is dynamically adapted for different values of Doppler and delay spreads to avoid the degradation of the channel estimates due to these effects. Hence, considering the definitions of Eq. 5.16 for the ST, the number of averaged samples has been set equal to the amount of resources between two contiguous pilot symbols for each dimension $(L_K \times L_N)$.

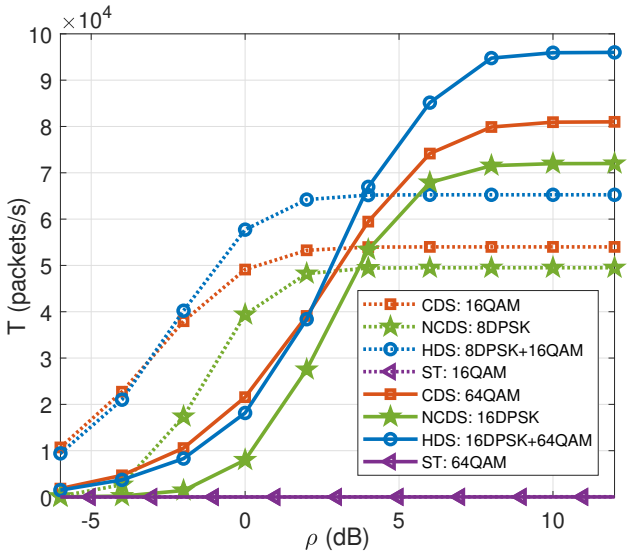

Figure 5.3: *Throughput comparison of coherent (CDS), HDS, ST and NC (NCDS) for different constellation sizes, $R = 64$, $K_p = 6$ and $N_p = 7$, for different SNR values (ρ).*

5.4.1.1 Throughput evaluation for different channel scenarios

In Fig. 5.3, we show the throughput comparison for the coherent, NC, HDS and ST for a unit block where $R = 64$, $K_p = 6$ and $N_p = 7$, which is an interesting case in terms of medium to high delay and Doppler spreads. There is a substantial improvement of performance for the HDS with respect to the coherent, since the latter is highly penalized by the great amount of necessary pilots. The throughput of the HDS is the highest, not only due to a low average BER, but also to the additional throughput provided by the NC stream (recall Eq. 5.19 and Eq. 5.20). Moreover, we also show the performance of the pure NC, where the DPSK symbols are occupying the entire unit block. We can see that NC is not able to outperform neither coherent nor HDS in this scenario. This is due to the fact that a QAM constellation has always a better performance than DPSK in terms of BER when $M_C = M_N$, provided that the channel can be adequately estimated. Also, it is known that the differential detection process increases the noise [2]. On the other hand, ST has a very poor performance since in this scenario there are not enough resources to perform the required averaging process in order to avoid the self-interference produced by the data, degrading its performance in terms of throughput.

According to the throughput analysis, for each particular scenario of interest imposed by the system design (number of antennas, length of the packet, delay and Doppler spreads, etc.), an optimum value of M_N and M_C can be chosen for each case of SNR (ρ) in order to obtain the

ρ \ M_N	**4**	**8**	**16**	**32**	**64**	**128**
5 dB	61.5	**65**	64.6	55.6	47.3	44.9
10 dB	61.5	65	69	**69.9**	57.9	51
15 dB	61.5	65	69	**72.7**	71.8	58.4
20 dB	61.5	65	69	72.7	**76.4**	72.9

Table 5.2: *Throughput for HDS ($10^3\times$ packets/second) for increasing ρ and increasing M_N for $R = 64$, $K_p = 6$, $N_p = 7$ and $M_C = 16$.*

maximum throughput. Tables 5.2 and 5.3 show the throughput evaluation of the HDS calculated for $M_C = 16$ and $M_C = 64$, respectively, where $R = 64$, $K_p = 6$ and $N_p = 7$. The maximum throughput values are highlighted in bold letters, and their corresponding optimal values of M_N and M_C depend on the SNR (ρ). Both constellation sizes can be increased when the SNR is high enough, maximizing the data-rate of the system. Note that the optimum value of M_N is not only chosen to increase the throughput of the NC stream, but it also has to constrain the channel estimation error, guaranteeing the performance of the coherent stream (M_C). Hence, given the expressions of the throughput, we can easily choose the best configuration for a given case. For example $M_C = 16$ and $M_N = 8$ should be chosen for $\rho = 5$ dB, while $M_C = 64$ and $M_N = 32$ are best for $\rho = 15$ dB.

ρ \ M_N	**4**	**8**	**16**	**32**	**64**	**128**
5 dB	75.5	**79.2**	76.7	33.8	18.4	15.7
10 dB	88.4	92.1	**95.9**	95.7	44.8	24.6
15 dB	88.5	92.2	96	**99.7**	98.4	45.3
20 dB	88.5	92.2	96	99.7	**103.4**	98.4

Table 5.3: *Throughput for HDS ($10^3\times$ packets/second) for increasing ρ and increasing M_N for $R = 64$, $K_p = 6$, $N_p = 7$ and $M_C = 64$.*

Tables 5.4 and 5.5 show a throughput comparison among the coherent, HDS and ST for different values of K_p and N_p where $R = 64$, $M_C = 16$, $M_N = 8$ and $\rho = 5$ dB. NC is not shown in this Table since its throughput remains constant for any of the considered values of delay and Doppler spread (K_p and N_p respectively). Its throughput is 49.5×10^3 packets/s for $M_N = 8$ and $\rho = 5$. This value is the same given in Table IV for HDS when $K_p = 12$ and $N_p = 14$, since

N_p \ K_p	**1**			**2**			**3**		
	Coh	HDS	ST	Coh	HDS	ST	Coh	HDS	ST
1	72	71.6	62	71	71.5	42	70.7	71	31
2	71	71	45	70	71	20	69.4	71	10
4	70.3	70.3	20	67	67	5.6	67	69.4	2
7	69	69	7	66	68	1.5	63	67.5	0.5
14	66	66	2	60	64.5	0.2	54	63	0

Table 5.4: *Throughput comparison among coherent, HDS and ST ($10^3\times$ packets/second) for $\rho = 5$, $R = 64$, $M_N = 8$ and $M_C = 16$. Increasing K_p and N_p means increasing the maximum supported values of delay and Doppler spread (PART 1).*

N_p \ K_p	**4**			**6**			**12**		
	Coh	HDS	ST	Coh	HDS	ST	Coh	HDS	ST
1	70	71	19	69.4	71	9.6	67	70.4	2.7
2	69	70.5	7	67	70	2.3	62	69	0.3
4	65	69	1	62	68	0.4	51.4	65.6	0.1
7	60	67	0.2	54	65	0.1	36	61	0
14	48	61.5	0	36	58.5	0	0	49.5	0

Table 5.5: *Throughput comparison among coherent, HDS and ST ($10^3\times$ packets/second) for $\rho = 5$, $R = 64$, $M_N = 8$ and $M_C = 16$. Increasing K_p and N_p means increasing the maximum supported values of delay and Doppler spread (part 2).*

N_p \ K_p	**1**	**2**	**3**	**4**	**6**	**12**
1	0%	0.5%	0.9%	1.4%	2.3%	5.3%
2	0%	0.9%	1.9%	2.8%	4.8%	11.5%
4	0%	1.9%	3.8%	5.9%	10.4%	27.5%
7	0%	3.4%	7.1%	11.2%	20.8%	68.7%
14	0%	7.5%	16.7%	28.1%	62.5%	∞

Table 5.6: *Percentage improvement of the throughput for the HDS with respect to the coherent; same parameters as in Tables 5.4 and 5.5.*

in this extreme case all the symbols in the HDS are differentially encoded and HDS boils down to NC. Again, the different values of K_p and N_p correspond to different maximum supported values of delay and Doppler spreads. Once more, the use of ST does not bring in general an adequate performance. When there are enough resources for averaging (K_p and M_p low), the results are acceptable, but they degrade fast when K_p and M_p increase. In Table 5.6, for the same scenario, we provide the percentage of throughput increment of the proposed HDS with respect to the coherent, which is defined as

$$\Delta T_H(\%) = \frac{T - T_C}{T_C} \times 100. \tag{5.47}$$

We can see in Tables 5.4, 5.5 and 5.6 that for low mobility scenarios with a low or medium delay spread (low K_p and N_p), the NC does not provide a significant increase of the throughput (approximately $0 - 5\%$) over the HDS. However, when either the Doppler or delay spreads are significantly increased, the throughput of the coherent is decreased while the throughput of NC is increased, improving ΔT_H (approximately $6 - 70\%$). For the extreme case of extremely high Doppler and delay spread ($K_p = 12$ and $N_p = 14$), only NC can provide an acceptable performance (HDS collapses to pure NC), while coherent cannot be used. In summary, for increasing K_p and N_p values the performance of coherent worsens faster than that of HDS. ST can only provide an acceptable performance for the particular case of $K_p = N_p = 1$, where the channel has very mild variations in both dimensions and the averaging processing can be performed satisfactorily.

According to this numerical evaluation of the throughput, we provide a graphical summary of the advisable technique for different scenarios in Fig. 5.4. Coherent processing is not recommendable in scenarios with high delay and/or Doppler spreads, where an excessive number of pilots must be transmitted to provide a continuous tracking of the channel at both time and frequency dimensions ($K_p \uparrow$ and $N_p \uparrow$), so that an acceptable quality of the channel estimates ($\sigma^2_{e,p} \to 0$ given in Eq. 5.6) is provided. In these cases, $T_C = 0$ since $\eta_C \to 0$. On the other hand, NC is suitable for these extreme cases where resources are not wasted to transmit reference signals. Indeed, [2, 59, 87] showed that NC has a great robustness against high Doppler scenarios, no matter the delay spread when OFDM is used. On the contrary, for low mobility or fixed communication scenarios with low or moderate values of delay spread, the number of reference signals can be greatly reduced ($K_p \downarrow$ and $N_p \downarrow$) since the channel remains quasi-static in both dimensions. Therefore, the throughput increment provided by the addition of the NC

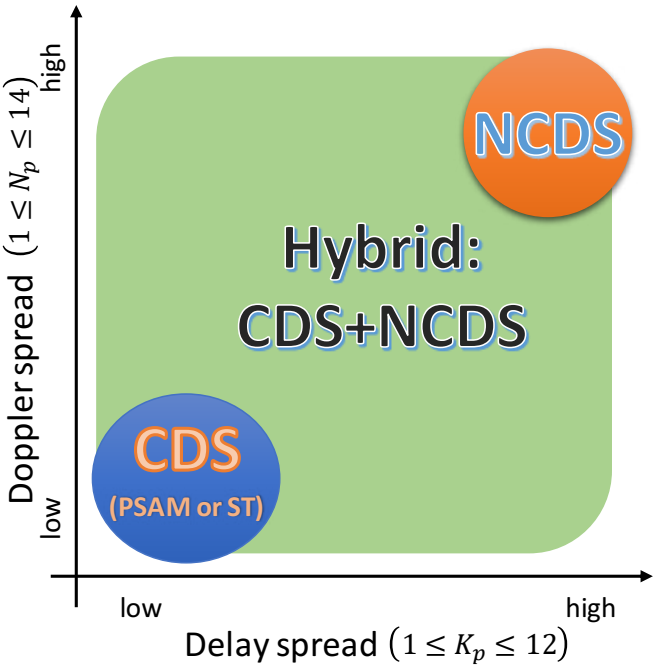

Figure 5.4: *Summary of the chosen scheme for different scenarios.*

stream is not significant as compared to the throughput of the coherent ($T_C >> T_N$). Finally, in those scenarios where the channel variations are not excessively high, at least in one dimension, the combination of coherent and NC, that is the proposed HDS, outperforms the existing solutions in terms of throughput. In these scenarios, the proportion of resources allocated to the reference signals in coherent is significant and the effective data-rate of the link is reduced if only the coherent stream is sent. In the example provided in Fig. 5.1, which is a typical configuration in 5G-NR [77], the pilot symbols correspond to 28.6% of the grid, which is an important overhead, and our proposal can take advantage of this overhead by transmitting an additional data stream using NC.

5.4.1.2 Complexity evaluation for different channel scenarios

In order to compare the complexity of coherent and HDS, we define the complexity increment of HDS with respect to coherent as

$$\Delta D_H(\%) = \frac{D_H - D_C}{D_C} \times 100. \tag{5.48}$$

This complexity increment is presented in Table 5.7 where we can see that it is proportional to

the number of symbols transmitted in the NC stream (given by K_p and N_p). This complexity increment is below 10% for a low to medium amount of resources dedicated to NC, which corresponds to a throughput increment of up to 21% as shown in Table 5.6. For the extreme case of very fast time-varying and/or strongly frequency-selective channels, many more resources can be dedicated to the NC stream and the additional complexity can be increased up to 30%, while the throughput increase is almost 70%. In summary, the additional complexity produced by the proposed scheme is always much lower than the additional amount of throughput that it can provide, showing that HDS is more efficient than the traditional PSAM-based coherent.

N_p \ K_p	**1**	**2**	**3**	**4**	**6**	**12**
1	0.0%	0.2%	0.4%	0.6%	1.0%	2.3%
2	0.0%	0.4%	0.8%	1.2%	2.1%	5.1%
4	0.0%	0.8%	1.7%	2.6%	4.6%	12.1%
7	0.0%	1.5%	3.2%	5.0%	9.2%	30.2%
14	0.0%	3.3%	7.4%	12.4%	27.5%	–

Table 5.7: *Complexity increment of HDS with respect to coherent for different K_p and N_p values.*

5.4.1.3 Throughput evaluation with a geometric channel model

In this subsection we provide some simulation results with a more realistic channel model to compare coherent and HDS. Particularly, we adopt a geometric wide-band channel model which enables the characterization of the effects of the propagation channel and the antenna arrays [88]. It is characterized by the geometric superposition of several separate clusters, where each of them has a different value of delay and gain. Moreover, each cluster is made of a certain number of rays with different angle of arrival and departure. The chosen array configuration corresponds to a uniform linear array (ULA), where the distance of two contiguous elements is half the wavelength. The delay spread is set to 363 ns and the angular spread is set to 5 degrees, which are example values defined in [1]. Additionally, with interest in high mobility scenarios, we set a Doppler frequency of 1.6 KHz, which corresponds to a carrier frequency of 3.5 GHz and an approximated speed of 500 km/h. Moreover, we set $K_p = 6$ and $N_p = 4$, which is the configuration given in Fig. 5.1.

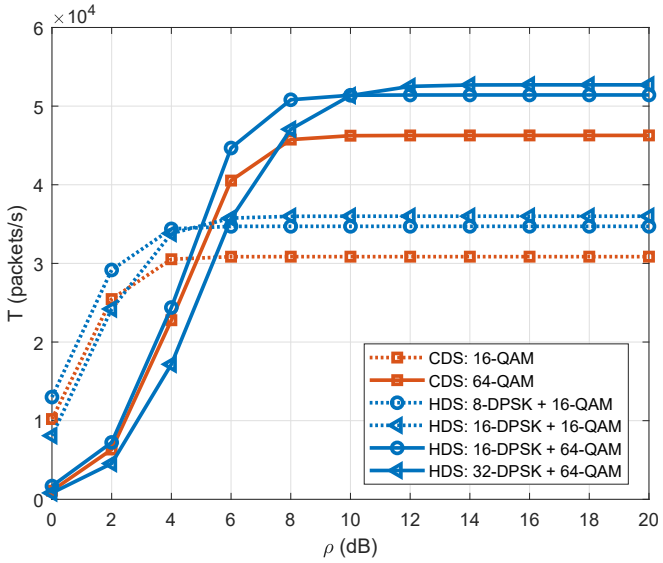

Figure 5.5: *Throughput comparison of coherent (CDS) and HDS for different constellation sizes, $K_p = 6$ and $N_p = 7$, for the geometric channel defined in [1].*

In Fig. 5.5, we provide the throughput comparison for the different values of constellation size. We can see that the HDS provides a significant additional throughput as compared to coherent. Under this particular realistic channel model, the achieved throughput of both coherent and HDS is lower than in the previous case, due to the effect of the spatial correlation produced by the chosen array configuration. However, HDS still outperforms the traditional coherent scheme by approximately a 11% of throughput increment, which is similar to what was obtained in the equivalent case with spatially uncorrelated channels. Hence, these results also show the advantages of our proposed scheme in a more realistic environment.

5.4.2 Results for pilot-less TDD massive MIMO

In order to compare the classical coherent scheme and the proposed pilot-less scheme, we will use the SER. Since the overhead is different in them, for a fair comparison we will ensure the same spectral efficiency in both systems. For such purpose, different constellation sizes are used. For instance, in a TDD slot of 4 OFDM symbols, where 2 are used for the uplink and the other 2 for the downlink, half of the OFDM symbols should be used for pilots (one for uplink and another one for downlink). In this case, for a fair comparison, the size of the constellation used in the coherent scheme should be the square of that used in the non-coherent scheme. Furthermore, the proposed pilot-less scheme can work with a coherence time of 3 symbol slots

(1.5 TDD slots), as shown in Fig. 5.2, while the classical scheme is more restrictive and needs at least 4 symbols.

In this section, we first validate the theoretical analysis previously shown in Sec. 5.3.2 and afterwards we compare the classical scheme with the proposed scheme in a deployment scenario with ideal conditions. Unless otherwise stated, $R = 100$, $M_u = M_d = 4$. The SNR in the simulations is defined as the inverse of the noise power.

5.4.2.1 Corroboration of the theoretical analysis

It can be seen in Fig. 5.6, that the theoretical analysis for the channel estimation fits well with the Monte Carlo simulations, with the theoretical results being an upper bound of the simulations. The lower bound is given by the performance of the PSAM with a pilot in every coherence time, that is, without any degradation due to time variability (at the expense of a large pilot overhead). It can be observed that a correlation α_d caused by time difference between the estimated channel and the real one results in a MSE floor, caused by the time variability of the channel. When there is no time variability, the MSE is affected only by the error probability in the detection of Eq. 5.28 via Eq. 2.1. Last but not least, the case of PSAM with time variability is shown, were it can be seen that it is below the proposed channel estimation with channel time variability, but is equal to it for high SNR.

In Fig. 5.7, we can see the histogram and the theoretical PDFs for the real and imaginary parts of the received symbol when $[\mathbf{z}_n^{k_d}]_u = 1$. A very good agreement can be seen for both cases, but for the real part, since more approximations were made, the agreement is slightly worse. This fact directly affects the accuracy of the SER performance for the DL of the proposed scheme, which is shown in Fig. 5.8. The theoretical SER (labeled 'TH' in the legend) is very similar to that of the Monte Carlo simulations even though there are little discrepancies, due to the left tail of the distribution of the real part.

5.4.2.2 Comparison with a classical pilot assisted system

The classical and the proposed schemes are compared with Monte Carlo simulations. The coherence time n_c is defined in number of OFDM symbols of the TDD scheme, according to the frame shown in Fig. 5.2, and the values of 2, 3 and 10 are considered in Fig. 5.9. The number of symbols in a TDD slot period for the UL τ_u and the DL τ_d are set to 1 and 2 to see

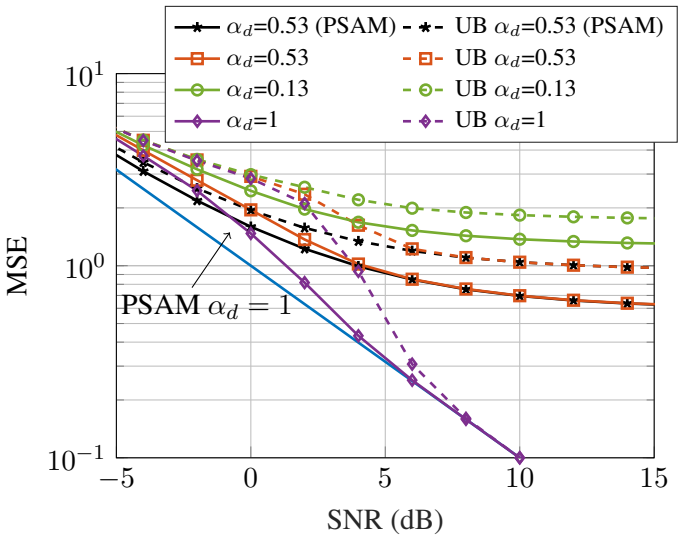

Figure 5.6: *MSE of channel estimation for $M_{UL} = 16$ and $R = 100$. Continuous line corresponds to the Monte Carlo simulation while dashed line corresponds to the theoretical upper bound. Blue line represents the PSAM without channel time variability, which is the best case.*

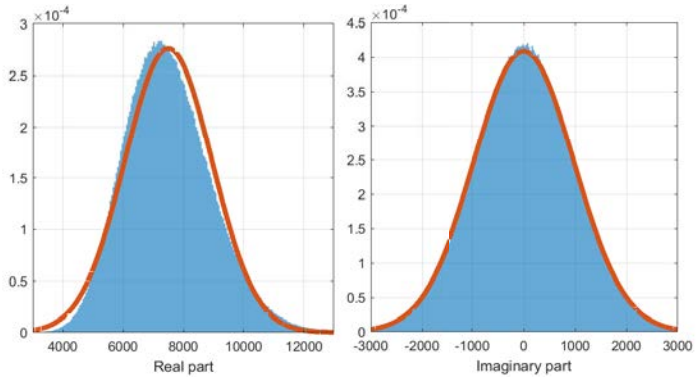

Figure 5.7: *Monte Carlo histogram (blue) versus theoretical PDF (red) of the real (left) and imaginary (right) part of $[\mathbf{s}_n^{k_d}]_u = 1$ for $R = 100$, $M_{UL} = 4$ and $e_d = 0.5$.*

the dependence with this parameter, and the constellation size in the DL M_d is set to 4 and 16. A sufficiently large SNR to avoid any errors is used in the UL and $U = 2$ are considered. The classical (coherent) and the proposed (non-coherent) schemes are referred in Fig. 5.9 as C and N, respectively.

It can be observed how, for large n_c (10 in Fig. 5.9), the scheme C is approximately the same as the scheme N, which reinforces the validity of the proposed scheme even for large n_c. For

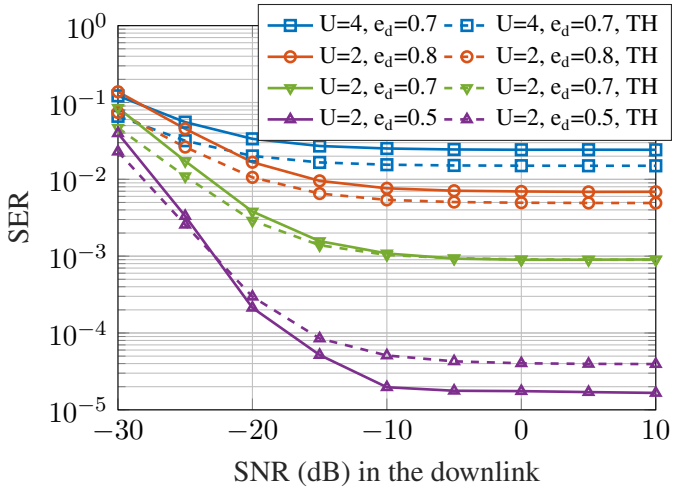

Figure 5.8: *DL performance with different U and e_d for the proposed scheme for $M_{DL} = 8$ and $R = 200$. Continuous line corresponds to the Monte Carlo simulation while dashed line corresponds to the theoretical upper bound.*

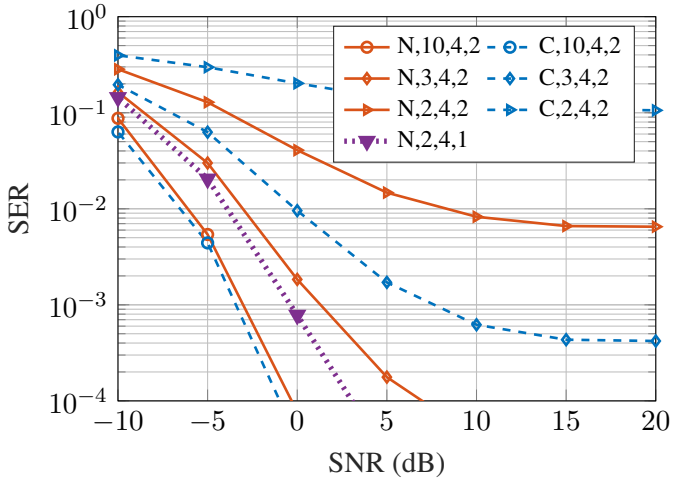

Figure 5.9: *Comparison between classical (C, dashed) and proposed (N, continuous) schemes, labelled from left to right with n_c, M_d, $\tau_u = \tau_d$, for $R = 100$.*

very fast varying channels ($n_c = 2$), the latter outperforms the former for the same spectral efficiency. More concretely, for $\tau_u = \tau_d = 2$, the scheme C utilizes one symbol pilot while the scheme N does not. Thus, the scheme C transmits a 16-QAM while the scheme N transmits a QPSK. For both schemes transmitting a QPSK (scheme C with a lower spectral efficiency than scheme N) and for $n_c = 3$, scheme N outperforms scheme C, which reinforces our proposal. In fact, scheme N can go down to $\tau_u = \tau_d = 1$, while C cannot since then, only pilots would

be sent both in UL and DL. This is an advantage for the proposed scheme N which can work in extremely fast varying channels. As a clarification example, in a 5G system with carrier frequency $f_c = 3.6$GHz, carrier spacing $\Delta_f = 30$KHz at a speed of 500km/h, the coherence time is $n_c = 2.8$ OFDM symbols.

5.5 Concluding Remarks for pilot-less channel estimation with detected NC data

In this chapter, for an UL massive SIMO-OFDM system, we have first proposed a differential data-aided channel estimation scheme, where the traditional reference signals are replaced by a differential data stream. This data stream is demodulated using non-coherent detection at the BS and is used to perform the channel estimation. Therefore, by proposing a hybrid scheme denoted as HDS, the channel can be accurately estimated to perform coherent demodulation of the coherent stream, while the resources typically occupied by pilots are now leveraged for transmission of the NC data stream. The benefits of our proposal have been evaluated in terms of the channel estimation MSE, BER, throughput and complexity. We have provided the analytical expressions of the channel estimation MSE and we have shown that it has very close performance to PSAM-based estimation. We have provided analytical expressions of the BER and evaluated the throughput of HDS for different configurations of the resources in the time-frequency grid, which correspond to different values of Doppler and delay spreads, showing that it outperforms the coherent with up to a 75% of throughput increment, which is obtained for high mobility scenarios. The different theoretical derivations are shown to match the numerical results, showing the accuracy of the analysis, and facilitating an optimization of the system parameters. Illustrative values of the number of antennas and the length of the NC data stream were chosen to shown the feasibility of this solution in the frame of the current mobile communications standards and deployments. With the analytical tools provided in this thesis, the same optimization can be performed for any other values of these parameters.

In summary, with the HDS scheme we are able to replace the reference signals with a differential data stream, which in most of the analyzed scenarios provides a higher throughput than what can be achieved with a coherent system based on PSAM. Other alternatives such as ST perform worse when there is a mild frequency selectivity or channel variability. Then, this work contributes to the improvement of the spectral efficiency of massive MIMO-OFDM systems,

which is crucial for the evolution of wireless communications. It is worth noting that the NC stream can be used, for example, to establish a low latency service in parallel with the regular high data rate application provided by the coherent, since the detected NC data stream can be quickly forwarded to upper protocol layers while the channel is estimated for its use to equalize the coherent data stream. Therefore, it is possible to use this system for a single service with enhanced throughput or to multiplex two parallel services at the physical level.

Secondly, we have proposed a pilot-less massive MIMO TDD scheme where the UL data is detected via non-coherent processing, the channel is estimated using the data received in the UL and the data of several users in the DL is precoded to spatially separate them. To avoid the use of pilots in both the UL and DL, differential PSK is utilized. The MSE of the channel estimation for time-varying channels and the performance of the DL using precoding and differential encoding are characterized and validated with numerical simulations. The proposed pilot-less TDD scheme is compared with its coherent PSAM counterpart and it is shown that it largely outperforms it when the coherence time is very small, which is exemplified to be realistic in the context of 5G.

Chapter 6
Constellation Design for the Multi-user Non-coherent Massive SIMO Scenario

In this chapter we treat the problem of constellation design for the multiuser scenario of non-coherent Massive SIMO based on DMPSK. We first show that a classical analytical constellation design for the MU is intractable. Then, we propose to solve this problem by using optimization techniques relying on evolutionary computation. Two approaches are designed, namely GAO and MCO, which provide both individual constellations for each user and a bit mapping policy to minimize the BER. Later, a complexity analysis and strategies for its reduction are proposed. A set of constellations for different number of users and constellation sizes is proposed, and we evaluate the link-level performance of some illustrative examples to verify that our solutions outperforms the existing ones. Finally, we show via simulations that NC outperform the coherent schemes in high mobility and/or low SNR scenarios.

6.1 Specific System Model for constellation design

At the n-th time instant, the bits transmitted by the u-th user are grouped in the vector $\mathbf{b}_u^n$ of size $N_b^u \times 1$, where N_b^u indicates the number of bits for user u, and it is mapped into a complex symbol s_u^n as

$$s_u^n = g_B(\boldsymbol{\varpi}_u, \mathbf{b}_u^n) \in \mathfrak{M}_u, \;\; \mathfrak{M}_u = \left\{c_1^u, \ldots, c_{M_u}^u\right\}, \tag{6.1}$$

$$c_i^u \in \mathbb{C}, \;\; |c_i^u| = 1, \;\; c_i^u \neq c_{i'}^u \;\; \forall i \neq i',$$

where $M_u = |\mathfrak{M}_u| = 2^{N_b^u}$, $g_B(\cdot)$ is the bit mapping function, $\mathfrak{M}_u$ denotes the individual constellation set for the u-th user (constrained to constant modulus to facilitate the use of the differential modulation), and $\boldsymbol{\varpi}_u$ of size $M_u \times 1$ denotes the bit mapping policy for the u-th user which satisfies that $\boldsymbol{\varpi}_u^i \in \{1, \ldots, M_u\}, 1 \leq i \leq M_u, \boldsymbol{\varpi}^i \neq \boldsymbol{\varpi}^{i'}, \forall i \neq i'$. We define $\boldsymbol{\Pi} = \begin{bmatrix} \boldsymbol{\varpi}_1^T & \cdots & \boldsymbol{\varpi}_U^T \end{bmatrix}^T$ a vector of size $(\sum_{u=1}^{U} M_u \times 1)$ that contains the bit mapping policies of all users. The complex symbols of each user are encoded following Eq. 3.15. We assume a flat-fading channel, the received signal is defined by 3.16 and 3.17, where $\boldsymbol{\nu}^n$ is the additive

white Gaussian noise (AWGN) vector with each element distributed as $[\boldsymbol{\nu}^n]_r \sim \mathcal{CN}(0, \sigma_\nu^2)$, β_u denotes the ratio of the received average power of the u-th user, with respect to user 1 ($\beta_u^{\min} = 1$, $\beta_u \geq 1$, without loss of generality), which is proportional to the composition of the large-scale channel effects and the power control of each user. A different β_u value for each user affects their performance, which is taken into account in the design of constellations. A certain $\beta_{\max}$ is considered to avoid users' performance to be excessively unequal. Moreover, $\mathbf{H}^n \in \mathbb{C}^{R \times U}$ represents the small-scale fading as a spatially uncorrelated channel matrix, where each element is distributed as $[\mathbf{H}^n]_{r,u} \sim \mathcal{CN}(0, 1)$, since the channel is a spatially uncorrelated Rayleigh one. The reference SNR is 3.18. The phase difference of two consecutive symbols received at each antenna is non-coherently detected following 3.19. The property defined in 3.20 is utilized to perform detection in the RX side, where $\mathfrak{M} = \{c_1, \ldots, c_M\}$, $c_i \in \mathbb{C}$, $c_i \neq c_{i'}$ $\forall i \neq i'$, ς^n is the joint-symbol which results from the superposition of the symbols sent by the users, and $\mathfrak{M}$ denotes the joint-constellation set. Fig. 6.1 shows the joint-constellation built from two particular individual constellations. We define $\mathbf{b}_{i,u}$ as a vector of size $(N_b^u \times 1)$ that contains the bits for the u-th user and the i-th joint-symbol according to the mapping $\mathbf{\Pi}$, and $\mathbf{b}_i = [\mathbf{b}_{i,1}^T \ \cdots \ \mathbf{b}_{i,U}^T]^T$ as a vector of size $(\sum_{u=1}^{U} N_b^u \times 1)$ that contains the $\mathbf{b}_{i,u}$ of all users for the i-th joint-symbol.

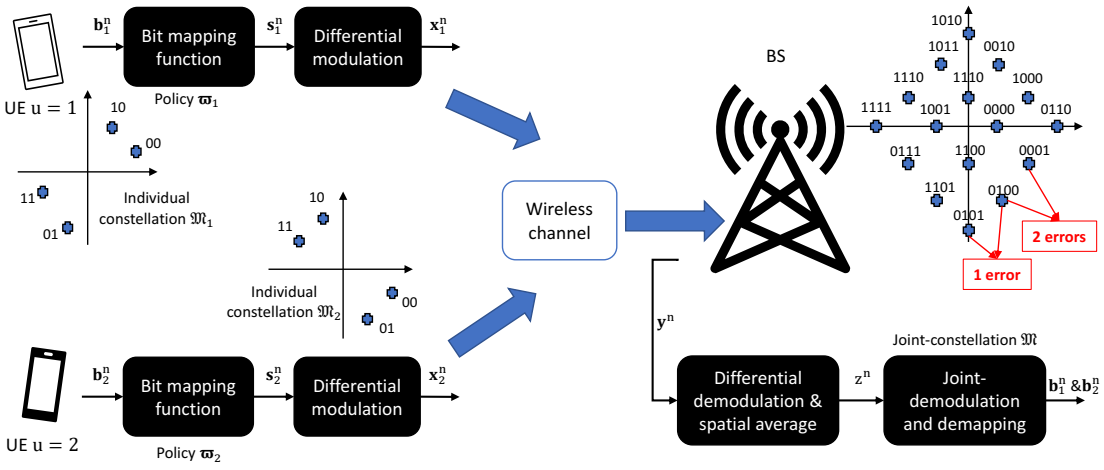

Figure 6.1: *Block diagram of NC scheme in UL for the particular case of $U = 2$, $\beta_1 = \beta_2 = 1$ and two particular cases of individual constellations ($\mathfrak{M}_1$ and $\mathfrak{M}_2$). These two individual constellations are properly designed by the proposed methods to produce a QAM joint-constellation ($\mathfrak{M}$).*

6.2 Interference analysis for Rayleigh (NLoS) channels

In this section, we first analyze the probability density function (PDF) of the received differentially processed signal based on DMPSK and show that it is mathematically intractable for a classical constellation design approach. Later, to further clarify the mathematical intractability, we particularize the analysis for a set of constellations to demonstrate an inherent problem of NC differential detection that makes the individual constellations of the users and the joint-constellation non-linearly dependent.

6.2.1 Analysis of the Distribution of the Interference

The terms of Eq. 3.19 are shown to be independent in the Appendix of [87], and thus,

$$z^n = z_g^n + z_s^n + z_x^n = \sum_{l=1}^{3} z_{g,l}^n + z_s^n + z_x^n \tag{6.2}$$

where

$$z_{g,1}^n = \frac{1}{R}\sum_{r=1}^{R} [\boldsymbol{\nu}^{n-1}]_r^* [\boldsymbol{\nu}^n]_r \tag{6.3}$$

$$z_{g,2}^n = \sum_{u=1}^{U} \underbrace{\frac{1}{R}\sum_{r=1}^{R} [\boldsymbol{\nu}^{n-1}]_r^* [\mathbf{H}]_{r,u}}_{\tilde{z}_{g,2}^u} \sqrt{\beta_u}[\mathbf{x}^n]_u, \tag{6.4}$$

$$z_{g,3}^n = \sum_{u=1}^{U} \underbrace{\frac{1}{R}\sum_{r=1}^{R} [\boldsymbol{\nu}^{n}]_r [\mathbf{H}]_{r,u}^*}_{\tilde{z}_{g,3}^u} \sqrt{\beta_u}[\mathbf{x}^{n-1}]_u^*, \tag{6.5}$$

$$z_s^n = \sum_{u=1}^{U} \underbrace{\frac{1}{R}\sum_{r=1}^{R} |[\mathbf{H}]_{r,u}|^2}_{\tilde{z}_s^u} \beta_u s_u^n = \sum_{u=1}^{U} \tilde{z}_s^u \beta_u \exp\left(j\phi_s^{u,n}\right), \tag{6.6}$$

$$z_x^n = \sum_{u=1}^{U} \sum_{\substack{u'=1 \\ u\neq u'}}^{U} \frac{1}{R}\sum_{r=1}^{R} \underbrace{\sqrt{\beta_u}[\mathbf{H}]_{r,u}^* \sqrt{\beta_{u'}}[\mathbf{H}]_{r,u'}}_{\tilde{z}_x^{u,u'} = \tilde{z}_x^u \tilde{z}_x^{u'}} [\mathbf{x}^{n-1}]_u^* [\mathbf{x}^n]_{u'}, \tag{6.7}$$

where $\phi_s^{u,n} = \angle(s_u^n)$. The terms Eq. 6.3, 6.4 and 6.5 are noise components, Eq. 6.6 is the distorted (since $R < \infty$) received joint-symbol and 6.7 is the inter-user interference.

The distribution of the received joint symbol can be obtained using the independence of the terms in Eq. 6.2 and the analysis in [11]. It utilizes the properties of the product of independent complex circularly symmetric Gaussian variables [89], the properties of the modified Bessel function of the second kind and zero-th order [90], and the central limit theorem (CLT) to approximate the distribution of each term. The distribution of $z_{g,1}^n$, $\tilde{z}_{g,2}^u$ and $\tilde{z}_{g,3}^u$ can be asymptotically approximated for an increasing number of antennas at the BS as

$$z_{g,1}^n \sim \mathcal{CN}\left(0, \frac{\sigma_\nu^4}{R}\right), \qquad \tilde{z}_{g,2}^u,\ \tilde{z}_{g,3}^u \sim \mathcal{CN}\left(0, \frac{\sigma_\nu^2}{R}\right), \tag{6.8}$$

and by using some straightforward manipulations

$$z_{g,2}^n,\ z_{g,3}^n \sim \mathcal{CN}\left(0, \frac{\sigma_\nu^2}{R}\sum_{u=1}^{U}\beta_u\right), \tag{6.9}$$

since a phase rotation does not change the distribution of a bivariate Gaussian. Focusing on Eq. 6.6 and using [91], it can be easily shown that $\tilde{z}_s^u$ is a one-dimensional random variable distributed as $\tilde{z}_s^u \sim \Gamma\left(R, R^{-1}\right)$. This term only affects the amplitude of the signal, and thus, z_s^u is distributed as

$$f\left(\mathcal{R}\left\{z_s^n\right\} \mid \varsigma^n\right) = \sum_{u=1}^{U}\Gamma\left(R, \frac{\beta_u}{R}\cos\left(\phi_s^{u,n}\right)\right), \tag{6.10}$$

$$f\left(\mathcal{I}\left\{z_s^n\right\} \mid \varsigma^n\right) = \sum_{u=1}^{U}\Gamma\left(R, \frac{\beta_u}{R}\sin\left(\phi_s^{u,n}\right)\right), \tag{6.11}$$

where both Eq. 6.10 and 6.11 represent the summation of U independent random variables, each following a Gamma distribution with a different scale parameter (β_u and $\phi_s^{u,n}$). We can see that the distribution of this interference term, given in Eq. 6.6, depends on the received joint-symbol, which is the result of superimposing the symbols transmitted by all the users (s_u^n). Hence, the design of a robust joint-constellation against interference and noise terms is not straightforward since each joint-symbol has a different distribution.

The term Eq. 6.7 is a sum of $U(U-1)$ independent terms, so its conditional distribution given

the differential symbols can be expressed as

$$\begin{aligned} f\left(z_x^n \mid \phi_x^{u,n-1}, \phi_x^{u',n},\ 1 \leq u, u' \leq U,\ u \neq u'\right) = \\ = f\left(\tilde{z}_x^{1,2}\right) \exp\left(j\left(\phi_x^{1,n-1} - \phi_x^{2,n}\right)\right) * \\ * f\left(\tilde{z}_x^{1,3}\right) \exp\left(j\left(\phi_x^{1,n-1} - \phi_x^{3,n}\right)\right) * \cdots * \\ * \cdots * f\left(\tilde{z}_x^{u,u-1}\right) \exp\left(j\left(\phi_x^{u,n-1} - \phi_x^{u-1,n}\right)\right), \end{aligned} \tag{6.12}$$

where $\phi_x^{u,n} = \angle(x_u^n)$, $\tilde{z}_x^{u,u'}$, $1 \leq u, u' \leq U, u \neq u'$ is the product of $\tilde{z}_x^u$ and $\tilde{z}_x^{u'}$ distributed as $\mathcal{CN}(0, \beta_u)$ and $\mathcal{CN}(0, \beta_{u'})$, respectively. The analytical expression of $f\left(\tilde{z}_x^{u,u'}\right)$ can be obtained by using [92], and it is shifted by the phase difference between the differential symbols of each pair of users. Thus, we can see that the distribution of Eq. 6.7 is generated by the existence of multiple users, due to the fact that the off-diagonal elements of $\mathbf{H}^H\mathbf{H}$ are non-zero values. Consequently, Eq. 6.7 depends on the cross-product of the transmitted differential symbol by each pair of users (phase difference between two differential symbols), which complicates the design of the joint-constellation due to the high number of possible combinations $(\phi_x^{u,n-1} - \phi_x^{u',n})$.

Since the terms of Eq. 6.2 are independent, the conditional PDF of z^n given the transmitted symbols of each user can be analytically obtained as a convolution of the PDF of the terms computed in Eqs. 6.8-6.12. Assuming equiprobable joint-constellation elements, the decision of ς^n while receiving z^n can be done using Eq. 3.20 and maximum likelihood detection as

$$\begin{aligned} \widehat{\varsigma}_{ML}^n = \arg\max_{\varsigma^n}\{f(z^n \mid \varsigma^n, \phi_x^{u,n-1}, \phi_x^{u',n})\} \in \mathfrak{M}, \\ 1 \leq u, u' \leq U, u \neq u'. \end{aligned} \tag{6.13}$$

From the previous analysis, it can easily be observed that the variances of the real and imaginary parts of z^n increase with increasing U. To reduce the SER and based on the previous analysis, the different elements of the joint-constellation should be placed such that the interference among them is minimized. However, the complexity of the constellation design significantly increases since the PDF differs for each joint-symbol. Moreover, even if an optimum joint-constellation is found, the individual constant modulus constellations must produce that joint-constellation and fulfill the individual requirements, described in Section 6.1, which may not be possible. This is aggravated by the interdependent relation between the individual constellations of the users and the PDF of the received joint-constellation in the BS.

6.2.2 Effect of the Individual Constellations of the Users

The relation between the individual users' constellations, the minimum distance in the joint-constellation and the PDF of the joint-symbols are shown with some examples of individual and joint-constellations. We choose 2 users with 4 symbols per user, as shown in Fig. 6.2.

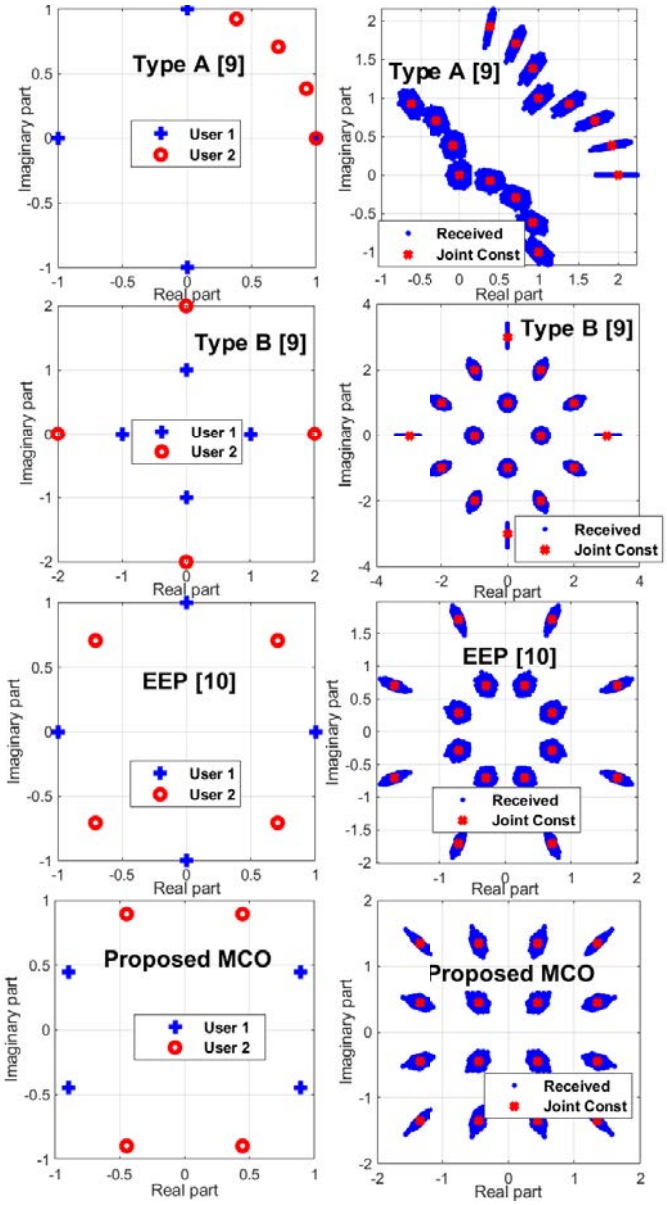

Figure 6.2: *Constellations for 2 users with 4 symbols per user. Top to bottom: Type A [2], Type B [2], EEP [3] and proposed MCO, left: individual constellations, right: JC.*

The minimum distance between the elements in the joint-constellation must be normalized as it is done in Eq. (17) of [2], $d_{\min}^{\text{norm}} = d_{\min}/\sqrt{\sum_{u=1}^{U} \beta_u^2}$. The value of this distance for the constel-

lations shown in Fig. 6.2 is: 0.39 for Type A, 0.6325 for Type B, 0.4142 for EEP and 0.6325 for the MCO. Type A reduces the distance exponentially with increasing number of users and/or constellation sizes, EEP suffers from a distance reduction in the inner circle, inherent to the constellation definition structure (making the distance even 0 in some configurations) and Type B is limited to differential quadrature phase-shift keying (QPSK) and the need of specific average receive powers. The normalized minimum distance (NMD) is directly related to the performance as it was shown in [2], and hence, the larger the NMD the better the performance. The NMD of the joint-constellation reduces with a greater number of users U, and/or constellation sizes M_u, thus a decrease in performance. A regular M-QAM joint-constellation maximizes the NMD, as $((M-1)/6)^{-1/2}$, so the minimum distance of any joint-constellation will fulfill $0 < d_{\text{min}}^{\text{norm}} \leq ((M-1)/6)^{-1/2}$, with M calculated by using Eq. 3.20.

Furthermore, it can be observed in Fig. 6.2 that the distribution of the received symbols around the theoretical (obtained with $R \to \infty$) ones in the joint-constellation varies depending on the individual users' symbols. Thus, the analysis made in Eq. (17) of [2] is just valid as an approximation since it assumes that the interference of all the joint-constellation elements are bivariate Guassians, which is not the case as shown in Fig. 6.2. The more similarity between the phases of the individual constellation elements that compose the joint-constellation element, the larger interference power projects on its direction, while the opposite also holds. It can be observed that the interference shapes of the joint constellation elements depend on the individual constellations, and that by changing the joint-constellation shape to minimize the effect of the interference will result in the need to use different individual constellations, thus creating a different interference and resulting in a recursive problem in the design process.

6.3 Proposed Constellation Design

Traditionally, the constellation design for coherent schemes is performed for a single user, assuming that MIMO processing based on CSI can separate the streams of the user equipments (UEs). The noise and interference terms are usually modelled as bivariate Gaussians, and as such, QAM constellations are preferred. Lastly, the bit mapping policy is often done using Gray coding. However, the constellation design is more challenging for NC schemes, especially for the multi-user case, as it was demonstrated in Section 6.2.1. At the same time, it is instrumental to achieve an efficient use of the time-frequency resources, allowing to multiplex several users. In Fig. 6.1, we outline the key points to improve the performance of the NC scheme

based on differential modulation. First, the joint-constellation $\mathfrak{M}$ must be robust against the interference and noise terms (see Eqs. 6.2-6.7). When differential modulation is used, QAM constellations are not necessarily optimum since the noise and interference terms do not follow a Gaussian distribution. Once the joint-constellation is chosen, the individual constellation for each UE ($\mathfrak{M}_u$) must be found so that when combined for all users, they create the adequate joint-constellation. However, these individual constellations may not exist, forcing us to choose an alternative joint-constellation. Finally, a bit mapping policy is required to minimize the BER. In this section, taking into account the mathematical intractability shown in section 6.2.1, we propose two approaches (GAO and MCO) to obtain the desired constellation for each UE by numerically solving the identified non-convex, non-linear and stochastic optimization problems. Due to its potential to solve these types of problems, we choose evolutionary computation (EC) as the algorithm to solve the optimization problems defined in GAO and MCO. To make certain that a good solution is attained, we ensure that the performance obtained by our proposed algorithm is (at the very least) better than that of the SoA.

6.3.1 Gaussian-Approximated Optimization (GAO)

As a first approximation to simplify the design process (valid for low SNR and R values since the noise term (z_g^n) dominates), the conditional distribution of z^n given the transmitted symbols of each UE provided in Eq. 6.13 is approximated as a bivariate Gaussian distribution for all the joint-symbols in the joint-constellation ($\mathfrak{M}$). Thus, the classical regular QAM constellation [93] can be straightforwardly set as the joint-constellation. The problem relies on finding the individual constellations that resemble, as reliably as possible, a regular QAM joint constellation. To ease the notation, let us define the constellation vectors for the objective normalized QAM joint-constellation, that is, the joint constellation that we would like to approach as close as possible, and the actual individual constellation of the u-th UE, respectively, as

$$\mathbf{c} = \begin{bmatrix} c_1 & \cdots & c_M \end{bmatrix}^T, \quad \tilde{\mathbf{c}}_u = \begin{bmatrix} [\tilde{\mathbf{c}}_u]_1 & \cdots & [\tilde{\mathbf{c}}_u]_{M_u} \end{bmatrix}^T, \tag{6.14}$$

where $[\tilde{\mathbf{c}}]_i$ is the obtained joint-constellation and is defined as

$$\begin{aligned} [\tilde{\mathbf{c}}]_i &= \sum_{u=1}^{U} \beta_u [\tilde{\mathbf{c}}_u]_{i_u}, \quad 1 \leq i \leq M, \quad |[\tilde{\mathbf{c}}_u]_{i_u}|^2 = 1, \\ 0 &\leq \angle [\tilde{\mathbf{c}}_u]_{i_u} < 2\pi, \quad u = 1, \cdots, U, \quad i_u = 1, \cdots, M_u. \end{aligned} \tag{6.15}$$

The individual constellations must be found for each UE $\tilde{\mathbf{c}}_u$ such that, when combined with their corresponding β_u, they resemble the objective QAM joint-constellation as accurately as possible. This is achieved by solving the following problem

$$\min_{\tilde{\mathbf{c}}_u,\boldsymbol{\beta}} \quad \alpha_1 \left\| \frac{\mathbf{c}}{\|\mathbf{c}\|_2} - \frac{\tilde{\mathbf{c}}}{\|\tilde{\mathbf{c}}\|_2} \right\|_2 + \alpha_2 \sum_{u=1}^{U} \beta_u, \quad \text{s.t.} \quad 1 \leq \beta_u \leq \beta_{\max}, \quad \alpha_1 + \alpha_2 = 1. \tag{6.16}$$

The vectors $\tilde{\mathbf{c}}$ and $\mathbf{c}$ are normalized in Eq. 6.16 to properly compare them, $\beta_{\max}$ is the maximum allowed ratio of the effective received power between users, and the terms α_1 and α_2 are added to allow different ways to constrain the values of $\beta_u,\ \forall u$. When $\alpha_1 << \alpha_2$, the optimization problem forces the same unitary power to all UEs ($\beta_u = 1,\ \forall u$). Otherwise, when $\alpha_1 >> \alpha_2$, it does not constrain β_u values. The optimization problem is non-convex and NP-hard, so we have to exploit numerical methods based on EC to solve this problem. More details are provided in Section 6.3.3.

After the individual constellations for each UE ($\tilde{\mathbf{c}}_u,\ \forall u$) and the received power coefficients ($\beta_u,\ \forall u$) are found as a solution to Eq. 6.16, an adequate bit mapping policy for each UE is required to guarantee a sufficiently low BER. To find this bit mapping policy, since the decision is made over the joint-symbols ($\mathbf{c}$) and since we assumed a bivariate Gaussian distribution for all joint symbols, we define an approximated BER (P_b) based on the use of the SER upper bound [65] for a certain bit mapping policy and joint-constellation

$$P_b\left(\boldsymbol{\Pi}, \mathbf{c}\right) = \sum_{i=1}^{M} \sum_{\substack{i'=1 \\ i \neq i'}}^{M} \underbrace{Q\left(\left\|[\mathbf{c}]_i - [\mathbf{c}]_{i'}\right\|_2\right)}_{p_j\left([\mathbf{c}]_i, [\mathbf{c}]_{i'}\right)} \underbrace{\frac{\left\|\mathbf{b}_i - \mathbf{b}_{i'}\right\|_1}{M \log_2 M}}_{\hat{P}_b\left(\boldsymbol{\Pi}, [\mathbf{c}]_i, [\mathbf{c}]_{i'}\right)} \tag{6.17}$$

where $p_j\left([\mathbf{c}]_i, [\mathbf{c}]_{i'}\right)$ is the joint-symbol error rate produced by the decision of $[\mathbf{c}]_{i'}$ when $[\mathbf{c}]_i$ is transmitted and $\hat{P}_b\left(\boldsymbol{\Pi}, [\mathbf{c}]_i, [\mathbf{c}]_{i'}\right)$ is the BER produced by the miss-decision of the joint-symbol (as the errors shown in Fig. 6.1). In this problem, $\mathbf{b}_i = g_B^{-1}(\boldsymbol{\Pi}, [\mathbf{c}]_i)$ is obtained with the inverse of the bit mapping function $g_B^{-1}(\bullet)$ which inputs the joint symbol $[\mathbf{c}]_i$ and the bit mapping policy applied at the UEs $\boldsymbol{\varpi}_u$.

Hence, the optimization problem for obtaining the optimum bit mapping policy for each UE can be described as

$$\begin{aligned} &\min_{\boldsymbol{\Pi}} P_b\left(\boldsymbol{\Pi}, \mathbf{c}\right), \\ &\text{s.t. } \boldsymbol{\varpi}_u \in \mathfrak{B}_u,\ B_u = |\mathfrak{B}_u| = M_u!,\ [\boldsymbol{\varpi}_u]_{i_u} \neq [\boldsymbol{\varpi}_u]_{i'_u},\ i_u \neq i'_u,\ 1 \leq i_u, i'_u \leq M_u, \end{aligned} \tag{6.18}$$

where $\mathfrak{B}_u$ is a set of bit mapping policies for the u-th UE that contains all the possible permutations of policies. The restriction $[\boldsymbol{\varpi}_u]_{i_u} \neq [\boldsymbol{\varpi}_u]_{i'_u}$ indicates that different symbols of the individual constellation of UE u cannot be mapped to the same bits. This is a finite integer optimization problem which can be solved by exploiting an exhaustive search. Nevertheless, we propose to use numerical methods based on EC when the complexity is too high, as shown in Section 6.4.

Algorithm 4 provides a summary of the GAO. First, M-QAM is chosen for the joint-constellation. Then, the individual constellations fulfilling Eq. 6.16 are obtained. Finally, the bit mapping policy for all UEs is obtained with Eq. 6.18.

Algorithm 4 Constellation design based on GAO

1: **procedure GAO**(M, U, α_1, α_2)
2: $\quad$ $\mathbf{c} \leftarrow M$-QAM $\quad\triangleright$ *Constrain the joint-constellation*
3: $\quad$ $\tilde{\mathbf{c}}_u \leftarrow$ SearchInd($\mathbf{c}$, U, α_1, α_2) $\quad\triangleright$ *Individual constellation*
4: $\quad$ $\boldsymbol{\Pi} \leftarrow$ SearchPolicy($\tilde{\mathbf{c}}_u$, $\mathbf{c}$) $\quad\triangleright$ *Bit mapping*
5: **end procedure**

6.3.2 Monte-Carlo based Optimization (MCO)

The complex circularly-symmetric Gaussian approximation employed by GAO is not accurate enough for several realistic scenarios, and thus, it provides a suboptimal solution. We propose to use the MCO, where no assumptions on the distribution are considered. MCO defines a single optimization problem capable of providing the individual constellations and the bit mapping policy of all UEs at once. It is based on the Monte-Carlo method to numerically evaluate the performance in terms of BER of the candidates at each iteration. The MCO optimization problem is expressed as

$$\begin{aligned} \min_{\tilde{\mathbf{c}}_u, \boldsymbol{\beta}} \quad & \alpha_1 \sum_{u=1}^{U} [\boldsymbol{\epsilon}]_u + \alpha_2 \sum_{u=1}^{U} \beta_u, \quad \text{with} \quad \boldsymbol{\epsilon} = g_M\left(\sigma_\nu^2, R, \boldsymbol{\Pi}, \boldsymbol{\beta}, \hat{\mathbf{c}}, N_s, N_r\right) \\ \text{s.t.} \quad & |[\tilde{\mathbf{c}}_u]_{i_u}|^2 = 1, \quad 0 \leq \angle[\tilde{\mathbf{c}}_u]_{i_u} < 2\pi, \quad u = 1, \cdots, U; \quad i_u = 1, \cdots, M_u; \\ & 1 \leq \beta_u \leq \beta_{\text{max}} \quad [\hat{\mathbf{c}}] = [\tilde{\mathbf{c}}_1, \cdots, \tilde{\mathbf{c}}_U]^T, \quad \alpha_1 + \alpha_2 = 1, \quad \boldsymbol{\varpi}_u \in \mathfrak{B}_u, \end{aligned} \tag{6.19}$$

where $\boldsymbol{\epsilon}$ is a vector of size $U \times 1$ that contains the BER of each UE and $g_M(\cdot)$ denotes a function to obtain this BER for a particular set of system parameters. Similar to Eq. 6.16,

this optimization problem is non-convex and NP-hard. Hence, we propose to solve it by using numerical methods based on EC detailed in Section 6.3.3.

Fig. 6.3 provides a block diagram of the implementation of MCO, and Algorithm 5 shows its pseudocode. The Monte-Carlo block performs a link-level simulation as described in Section 6.1. The scenario conditions of the optimization problem are R and σ_ν^2, and the Monte Carlo simulation performs N_r realizations of the channel and noise, without any constraint on their characteristics. Given the scenario conditions, the chosen individual constellations ($\tilde{\mathbf{c}}_u$), the ratio of average received power per user (β_u) and the bit mapping policies ($\mathbf{\Pi}$) of all UEs at each iteration, the Monte-Carlo block obtains the BER performance of all the UEs ($\boldsymbol{\epsilon}$ of size $U \times 1$). To attain an accurate enough BER, we can configure the number of symbols transmitted by each UE (N_s) at each iteration and the number of iterations (N_r). The optimization control and

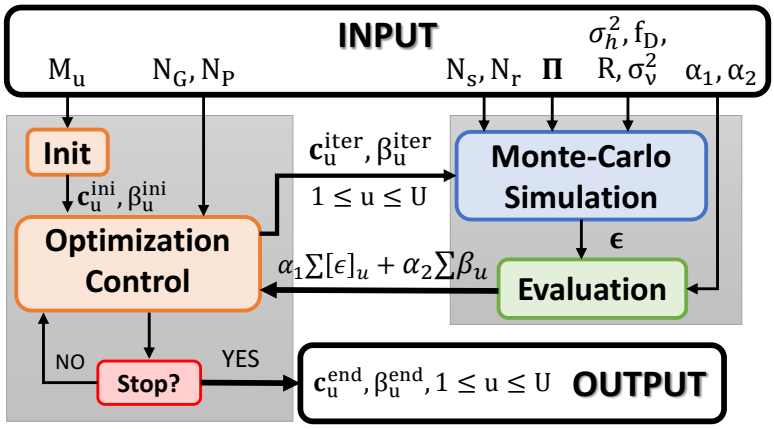

Figure 6.3: *Block diagram of MCO.*

6.3.3 Evolutionary Computation (EC)

EC is a subfield of artificial intelligence [94], which is composed of global optimization techniques based on mimicking biological evolution. It has been applied to produce optimized solutions for a wide range of complex non-convex optimization problems when classical optimization techniques are not applicable, since the objective function is discontinuous, non-differentiable, stochastic, or highly non-linear. The EC complexity is characterized by the

Algorithm 5 Constellation design based on MCO

procedure MCO (M_u,N_P,N_G,σ_ν^2,R,$\mathbf{\Pi}$,N_s,N_r,α_1,α_2)
  [$\mathbf{c}_u^{\text{ini}}$, β_u^{ini}] $\leftarrow$ Init(M_u, U) ▷ *Init.*
  [$\mathbf{c}_u^{\text{iter}}$, β_u^{iter}] $\leftarrow$ OptCtrl($\mathbf{c}_u^{\text{ini}}$, β_u^{ini},N_P,N_G) ▷ *Control Init.*
  while stop==false **do**
    $\boldsymbol{\epsilon} \leftarrow$ MonteCarlo($\mathbf{c}_u^{\text{it}}$, β_u^{it}, σ_ν^2, R, $\mathbf{\Pi}$, N_s, N_r)
    $f_{\text{obj}} \leftarrow$ Evaluation($\boldsymbol{\epsilon}$, β_u^{it}, α_1, α_2) ▷ *Evaluate*
    [$\mathbf{c}_u^{\text{it}}$, $\boldsymbol{\beta}_u^{\text{it}}$, stop] $\leftarrow$ OptCtrl($\mathbf{c}_u^{\text{it}}$, β_u^{it}, N_P, N_G, f_{obj}) ▷ *Control*
  end while
  output: $\beta_u^{\text{end}} \leftarrow \beta_u^{\text{it}}$, $f_{\text{obj}}^{\text{end}} \leftarrow f_{\text{obj}}^{\text{it}}$, $\mathbf{c}_u^{\text{end}} \leftarrow \mathbf{c}_u^{\text{it}}$
end procedure

population and generation sizes (N_P and N_G, respectively); hence, N_P denotes all possible solutions to the problem evaluated to generate new descendants, and N_G is the number of times the population evolves. If N_P and N_G are properly set, good and even optimal solutions can be found for problems where the optimization parameters are continuous, as explained in [95] and related works. Even though EC techniques consist of an optimization search with a random component, they ensure finding optimal solutions almost always to a wide range of problems in case they are properly configured. This is in contrast with machine learning techniques which easily end in local minima.

From the discussion in Section 6.2, we can observe that the constellation design for a multi-user NC scheme based on differential modulation turns into a mathematically intractable problem, so a numerical optimization is proposed. The optimization problems presented in Eq. 6.16, 6.18 and 6.19 not only are non-convex, non-linear and stochastic, but they also show a significant complexity. Given the EC benefits, we adopt the genetic algorithm (GA) [96] as a solver. It is worth noting that the approach followed in this manuscript can be extended to other non-coherent techniques such as those based on energy detection [97] or even to coherent techniques.

6.4 Complexity Analysis and Strategies for its Reduction

In this section, we analyze the complexity of the proposed design techniques and then, we propose strategies to reduce their complexity without losing performance.

6.4.1 Complexity Analysis

The EC complexity depends on the population size (N_P) and number of generations (N_G) [98]. They must be selected to facilitate a sufficient search of the possible results to the optimization problem. The values for N_P and N_G should be proportional to the dimensionality of the problem (N_D), which corresponds to the number of variables to optimize ($N_D \propto N_P N_G$), to ensure an adequate solution is found. Nevertheless, they are typically obtained with some trial, error and observation of the convergence [99, 100].

Technique	N_D	$N_\times$ per iteration	N_+ per iteration
GAO Constellation	$U + \sum_{u=1}^{U} M_u$	$\prod_{u=1}^{U} M_u$	$\prod_{u=1}^{U} M_u$
GAO Bit Mapping	$\sum_{u=1}^{U} M_u$	$\left(\prod_{u=1}^{U} M_u\right)^2$	$\left(\prod_{u=1}^{U} M_u\right)^2$
MCO	$U + \sum_{u=1}^{U} M_u$	$N_s N_r \left(R(U+1) + 2\prod_{u=1}^{U} M_u\right)$	$N_s N_r \left(R(U+2) + 3\prod_{u=1}^{U} M_u\right)$

Table 6.1: *Complexity comparison for GAO and MCO.*

To provide insight into the complexity, we look at the dimensionality of the problem. Furthermore, for each population element, we account for the number of required complex products ($N_\times$) and sums (N_+) [101]. Table 6.1 summarizes the complexity for GAO and MCO.

The first optimization of GAO Eq. 6.16 comprises the matching between the normalized target QAM constellation $\mathbf{c}$ and the obtained joint-constellation $\tilde{\mathbf{c}}$. The dimensionality of the problem depends on M_u and U. At each iteration, the mean squared error (MSE) between the points of the target QAM and the obtained one is calculated. The number of products and sums is conditioned by the MSE computation.

The second optimization problem of GAO Eq. 6.18 is an integer optimization problem that can be solved by an exhaustive search, since the possible amount of combinations is finite. According to Eq. 6.18, the number of possible bit mapping policies depends on the constellation sizes of the users. Each user can map a different set of bits for each symbol, without repetition. Therefore, considering that user u has a constellation size M_u, the first symbol can be mapped to M_u different bit mapping sets $\{1, 2, \cdots, M_u\}$. Once the first symbol is mapped to one bit mapping policy, the second symbol can be mapped to $M_u - 1$ different bit mapping policies. We repeat until symbol M_u, so user u has a total of $M_u \times (M_u - 1) \times \cdots \times 1 = M_u!$ bit mapping policies. Considering that the users' bit mapping policies are independent, the amount of possible bit mapping policies is $N_M = \prod_{u=1}^{U} M_u! > N_P N_G$. Even though the exhaustive search is feasible, we propose the use of EC for solving this optimization problem to increase

the efficiency when N_M is very large. In Section 6.5, we provide a numerical comparison to verify this point. The number of operations required (complex products and sums) at each iteration is determined by the computation of Eq. 6.17.

Finally, the dimensionality of MCO is the same as that of the first step of GAO. However, the complexity at each iteration is much higher for MCO due to the Monte-Carlo simulations. The number of operations is due to the simulation of the differential encoding/decoding, channel propagation, spatial averaging, joint-symbol decision and BER computation. Additionally, these operations are repeated $N_s \times N_r$ times to obtain an accurate enough BER estimation.

6.4.2 Strategies for Complexity Reduction

First, we note that the complexity of both steps of GAO is low enough to make the computation time negligible for today's computational capabilities. On the other hand, the MCO complexity is much higher, since a Monte-Carlo simulation is executed for each member of the population in each generation. Typically, N_G and N_P should be large enough to produce a high number of diverse potential solution candidates to be evaluated [98], to obtain a reliable-enough global minimum. However, this method (denoted as S1) excessively increases the execution time for the proposed MCO. Accordingly, we propose S2 and S3 to reduce the complexity.

S2 is based on a hierarchical search to reduce N_P and N_G without sacrificing the performance, being built on two phases: exploration and refinement. In the exploration phase, the genetic algorithm is run with a very small number of N_G, N_P, and a small number of N_r and N_s to reduce the execution time as much as possible. Hence, a better than random but still low-accuracy solution is found. This solution initializes a new run of the GA in which N_s and N_r are increased, and then a more accurate solution is obtained. Both phases can be repeated several times, increasing N_P and N_G in each cycle, until a convergence criterion is met. We must ensure that the summation of the product $N_P N_G N_s N_r$ of each iteration is lower than that of S1. As we will show in Section 6.5, the complexity is reduced to about one third of the S1, without losing on the performance of the obtained solutions.

Additionally, the solution obtained for GAO can be used as an input for MCO with reduced N_G and N_P. We first find a suboptimal but better than the SoA solution with GAO, and then refine it with MCO. This strategy is referred to as S3. The complexity is reduced to about one fourth compared to the S1, without losing performance, as shown in Section 6.5.

A last strategy makes use of the solution obtained from MCO for a particular scenario (fixed number of antennas, particular propagation channel and SNR). To explore other similar scenarios, we propose that the solution is employed as the initial point for the optimization problem in the new scenario, and we denote this strategy as S4. As we will show in Section 6.5, the complexity is reduced about some tens with respect to the S1, without losing performance.

6.5 Proposed Constellations and Implementation Aspects

In this section, we first propose a set of constellations, obtained with the proposed design techniques, for the multiuser scenario of the UL of NC massive SIMO. Second, we give insights on how to implement them in real scenarios.

6.5.1 Proposed Constellations

We provide a set of constellations in Table 6.5, which have been obtained with the strategy S3 of Section 6.4. While each constellation has been determined for a certain R and ρ, it can be used for any values in a realistic range. These constellations outperform the SoA, as shown in Section VI, and can be used to propose constellations for new scenarios with different users and constellation sizes (even among users).

To read the table, please note we provide for each scenario U vectors of the form $\Phi = [\Phi_1^u \Phi_2^u \cdots \Phi_{M_u}^u]$, where $\Phi_{m_u}^u$ is the phase in radians for the constellation element m_u of user u ($1 \leq m_u \leq M_u$, $1 \leq u \leq U$, where M_u is the constellation size of user u). A specific constellation element m_u of user u can be found as $s_{m_u}^u = \exp j\Phi_{m_u}^u$. The mapping of element m_u is obtained with a decimal to binary conversion of $m_u - 1$. An example of a constellation for 2 users with QPSK ($\mathbf{M} = [4\ 4]$, $\boldsymbol{\beta} = [1\ 1]$) is shown in Fig. 6.4 and another one for 3 users with QPSK ($\mathbf{M} = [4\ 4\ 4]$, $\boldsymbol{\beta} = [1\ 1\ 1]$) is depicted in Fig. 6.6.

6.5.2 Applicability in Real Scenarios

We obtained constellations by means of an offline optimization using different scenario parameters (R, ρ_u, v, etc.). The complexity of the online stage is not affected in any case by the complexity of the offline design technique, and only the constellations look-up table is different from the previous solutions in the SoA. These constellations minimize the average BER

of the users for the scenario parameters for which they have been designed. Nevertheless, the proposed constellations work well for any operative values of ρ and R. If a better performance is desired at the expense of increasing the complexity, we may obtain constellations optimized for different R and ρ values (results are more sensitive to R than to ρ, as shown in Section 6.6), for the different combinations of users and constellation sizes. In this case, the proposed set of solutions would be much larger. It is worth noting that each scenario will have a fixed R, so in practice the constellations should be designed for that R and for a few ρ values.

Given the improved constellations and β_u values for a certain scenario, the scheduler at the BS may perform a user grouping, power control strategy (considering the ρ_u of the users) and modulation and coding scheme (MCS) assignment, similarly to what is done, for example, in non-orthogonal multiple access systems [102]. Based on this strategy, it would be decided which users should be multiplexed with which MCS and powers to share the same time-frequency resources, with the goal of optimizing some non-coherent multiuser massive SIMO network parameter. The user grouping and power allocation can take advantage of the different path-loss suffered by each user to help minimize the power consumption of the users. It is worth noting that a user re-grouping would be performed by the BS only when the large-scale effects vary significantly (which happens slowly). This can be triggered by two factors: some users appear or disappear from the network or the power usage required by at least one user exceeds a predefined threshold. A detailed investigation of the user grouping, power control and MCS assignment is part of a future work.

6.6 Numerical Results for Performance and Complexity

In this section, we first present the performance of the most representative constellations. Second, we show numerical results for the time complexity of the EC algorithm and validate the theoretical complexity analysis. Last, we provide results that justify the use of NC over coherent massive MIMO for channels with very high mobility and/or low SNR.

6.6.1 Performance Evaluation

First, the case of 2 users with QPSK is shown since it has been used in the SoA as a baseline case. It is important to demonstrate the capabilities of our design technique and the proposed solution with respect to the previous work. Second, the case of 3 users with QPSK, 2 users

with 8PSK and 4 and 5 users with BPSK are shown since the SoA solutions for these scenarios proved to be very limited in terms of performance. Thus, we show that our proposed solution can greatly overcome the SoA limitations. Last, the case of 3 users with different constellation sizes is shown to illustrate that we overcome another limitation of the SoA, namely that the previous works could not propose any set of constellations with different sizes for an arbitrary number of users (e.g. $U = 3$ was not possible for several constellation sizes), while our solution can. We show the individual and joint constellations and the average BER of the uncoded constellations. We compare our solutions with the constellation designs in [87]. To ease the understanding of the results, the individual elements in the constellations are tagged by a number i, which corresponds to the sub-index of the complex symbols (c_i and c_i^u), described in Eq. 6.14. Each i indicates a bit mapping that results from the decimal to binary conversion of $i - 1$.

6.6.1.1 Scenario with $U = 2$ and $M_u = 4\ \forall u$

In this scenario, there are two UEs, where each UE has a constellation of size $M_u = 4$. Moreover, in this subsection, the MCO results are obtained by setting $R = 100$ and SNR $= 0$ dB. The solutions obtained here are superior to the ones of Type A in [2], which is worse than Type B, so we restrict the comparison to the latter for conciseness. When $\alpha_1 >> \alpha_2$, both GAO and MCO obtain the same solution as the constellation Type B given in [2] ($\beta_1 = 1$ and $\beta_2 = 2$), where each individual constellation corresponds to a 4-QAM and the joint-constellation corresponds to a 16-QAM. When $\alpha_1 << \alpha_2$, the solution for both GAO and MCO is $\beta_1 = \beta_2 = 1$. In Fig. 6.4, we show the individual constellations (top) for the case of $\beta_1 = \beta_2 = 1$, and the resulting joint-constellations (bottom), for the EEP [3], GAO and MCO schemes (from left to right). For GAO and MCO, the constellation is the same and it is a 16-QAM (rotated for the MCO). For EEP, the joint-symbols placed at the inner circle have a very small distance to each other, which degrades the performance.

In Fig. 6.5, we plot the average BER of both UEs for the EEP, GAO and MCO, where GAO and MCO significantly outperform EEP. The bit mapping policy is key to the performance of the system, as shown by intentionally replacing the bit mapping policy by a bad one denoted "bad map" in Fig. 6.5, where we can see the performance degradation. Moreover, by inspecting Fig. 6.4, we can understand that GAO and MCO reduce the BER with respect to EEP by increasing the distance among joint symbols and reducing the pairwise bit errors.

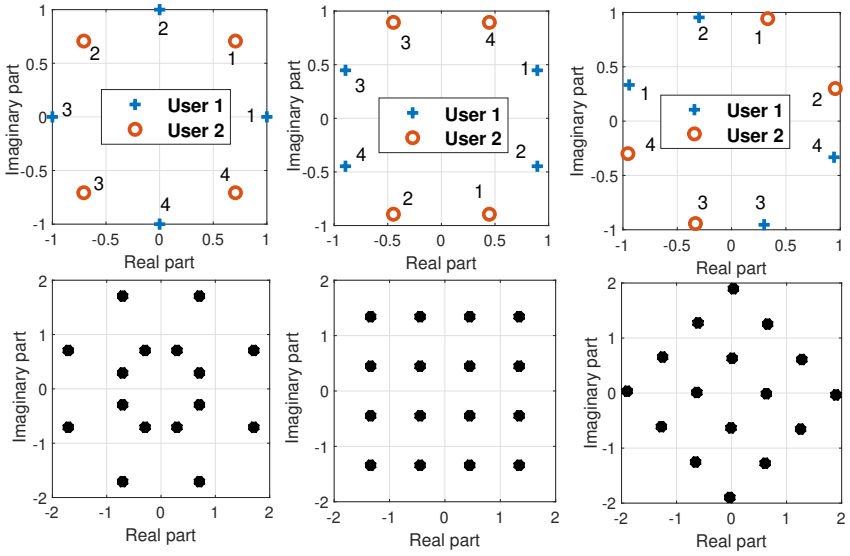

Figure 6.4: *Constellations for 2 users with 4 symbols per user with $\beta_u = 1$. From left to right: EEP, GAO and MCO. Top: individual users constellations, bottom: joint-constellation.*

6.6.1.2 Scenario with $U = 3$ and $M_u = 4\ \forall u$

In this scenario, we increase the number of UEs to three, and each UE has an individual constellation of size $M_u = 4$. The results provided by the MCO are obtained for $R = 400$ and SNR $= 3$ dB.

In Fig. 6.6, we show the individual constellations (top) for both UEs and the joint-constellation (bottom) for EEP, GAO and MCO (from left to right), when $\beta_u = 1,\ \forall u$. EEP cannot be used for three UEs as different combinations of individual symbols generate the same joint-symbols, since 11 joint-symbols out of 64 are equal in the complex-plane, thus creating an error floor of $11/64 \approx 0.172$, something avoided by GAO and MCO. In Fig. 6.7, we provide the average BER vs. ρ; our proposed schemes significantly outperform EEP, and MCO performs the best. In fact, these results confirm the mentioned error floor of EEP. Additionally, we show with black crosses the performance when MCO is trained for ρ values different from the one used for the optimization, leaving R unchanged.

It can be seen that the effect of ρ is almost negligible in the case of the MCO, except for very low ρ values. Additionally, we show an example of the combination of the proposed constellations with channel coding, which is common practice in wireless communications standards, so the BER performance can be significantly improved. The chosen coding scheme is a 1/2-rate low

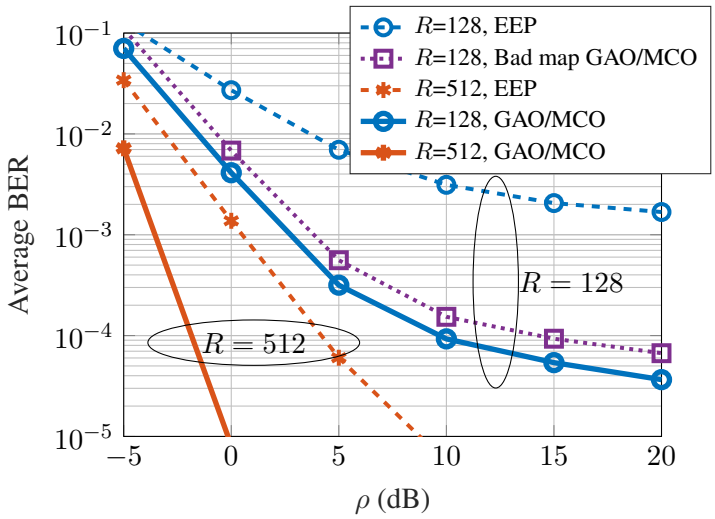

Figure 6.5: *BER vs. ρ for 2 users and 4 symbols per user with $\beta_u = 1$.*

density parity check code (LDPC) with a block of 8424 bits, which is used in 5G [77], and the performance is improved by about two orders of magnitude. In Fig. 6.8, we provide the average BER vs. the number of antennas (R); again, EEP has an error floor irrespective of the number of antennas, GAO outperforms EEP and MCO outperforms both GAO and EEP. In this case, the black crosses show the BER obtained when MCO is trained for the same ρ and R is set to values different from the one used for the optimization. Additionally, the effect of R is considerable when its value is relatively large, contrary to the SNR. These results demonstrate that it is feasible to use the constellation design of a particular ρ and/or R and for a wide range of operational values.

6.6.2 Scenario: $U = 3$, $M_u = 4$ and $\beta_u \neq 1$, $\forall u \in [1, \cdots, U]$

If we do not restrict β_u values ($\alpha_2 = 0$) in the objective function of GAO and MCO, the obtained solution is the same as given by Type B in [2]. Furthermore, if we set $\alpha_1 \approx \alpha_2$, GAO and MCO provide different solutions than the previous ones.

In this case, the constellations of user 1 and user 2 will be equal to the ones in the top-center constellation in Fig. 6.4, while the constellation of the third user will be a classical QPSK. For this configuration, two different solutions were found, depending on how α_1 and α_2 were set, one with power terms $\beta_1 = \beta_2 = 1$ and $\beta_3 = 2.53$ and the other one with $\beta_1 = \beta_2 = \sqrt{10}$ and $\beta_3 = 1$. In both cases, the joint constellation resembles a 64-QAM constellation, as shown in

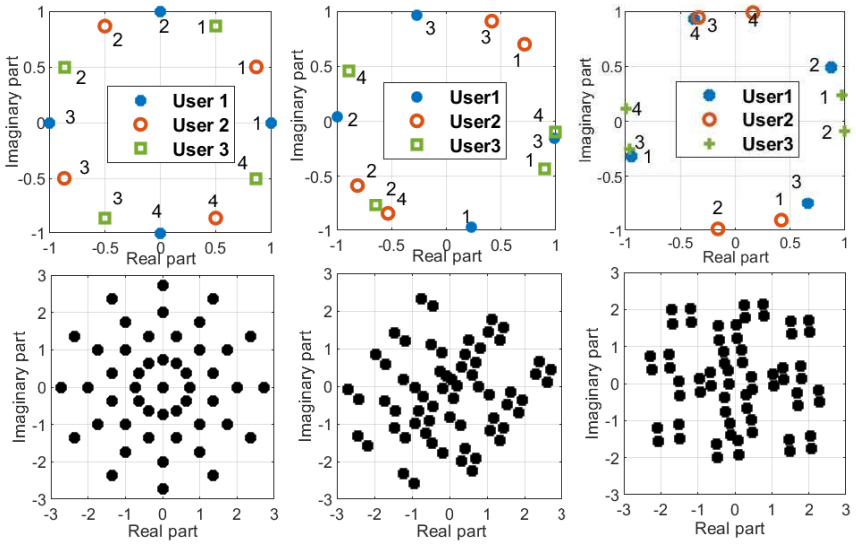

Figure 6.6: *Constellations for 3 users with 4 symbols per user with $\beta_u = 1$. From left to right: EEP, GAO and MCO. Top: individual users constellations, bottom: JC.*

Fig. 6.9. The BER performance is shown in Fig. 6.10. The results for the multiuser scenario show an error floor caused by the interference between users. Thus, we recommend to restrict the operational values to $\prod_{u=1}^{U} M_u \leq 64$ (Table 6.5).

6.6.2.1 Scenario with $U = 2$, $M_u = 8$ and $\beta_u = 1, \forall u$

We set two UEs and a constellation size of $M_u = 8$. The results provided by MCO are obtained for $R = 300$ and SNR $= 0$ dB. In Fig. 6.11, we show the individual (top) and joint constellations (bottom) obtained with EEP, GAO and MCO (left to right). In this case, the constellations obtained with GAO and MCO are virtually the same, with the MCO being a rotated version of that of the GAO. For the case of EEP, the distance of the joint-symbols placed at the inner circle is very low, increasing the average BER. On the contrary, both GAO and MCO try to keep the same distance among the neighbour joint-symbols. The bit mapping policies are different, as observed from Fig. 6.11b and Fig. 6.11c, but the performance is the same, since several bit mapping policies are equivalent, due to the symmetry of the constellations. Moreover, $M_u > 8$ can be performed with GAO and MCO, and the results follow the same strategy as for $M_u = 4$ and $M_u = 8$. However, their BER performance is degraded since the distance among joint-symbols is reduced.

In Fig. 6.12, we plot the average BER comparison of both UEs, for $R = 128$ and $R = 512$. It

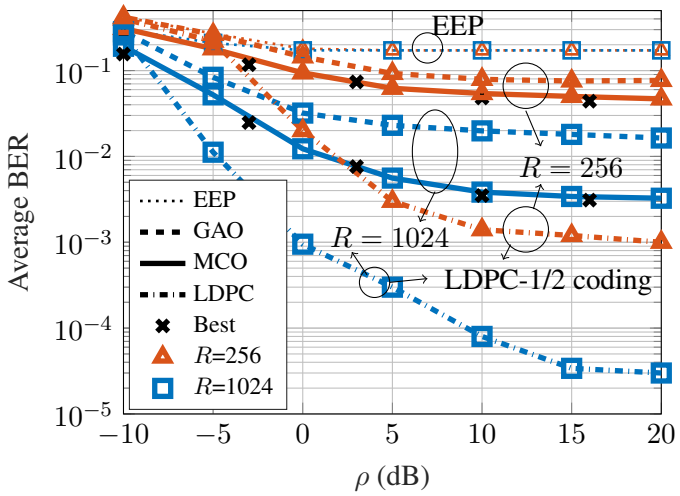

Figure 6.7: *BER vs. ρ for 3 users and 4 symbols per user with $\beta_u = 1$, for $R = 256$ and $R = 1024$. Black crosses show the best performance with MCO optimized for those values. The performance with LPDC-1/2 coding is shown.*

can be seen that the improvement of the BER with the number of antennas for the EEP is lower than that for GAO and MCO. This is caused by the reduced distance in the inner circle of the joint constellation. Both GAO and MCO have the same performance and outperform EEP.

6.6.2.2 Scenario with $U = 4$ and $U = 5$ for $M_u = 2\ \forall u$

We simulate 4 and 5 users, all with BPSK and the same average receive power, for the EEP and the proposed constellations in Table 6.2 (obtained with S3). The results shown in Fig. 6.13 are obtained for $R = 1000$ for both an IID Rayleigh channel and a geometric wideband (GEO) channel defined in TR 38.901 3GPP. The EEP is clearly outperformed by our proposal.

6.6.2.3 Scenario with $U = 3$ with different constellation sizes

In this case, we set 3 UEs with different constellation sizes (BPSK for the first user, and QPSK for the other two), to show that both GAO and MCO can cope with this type of constraints. EEP is limited to having the same constellation sizes for all UEs. In Fig. 6.15, the individual constellations are shown on top, and the joint constellations are shown at the bottom. From left to right, we have the solution of the GAO for $\beta_u = 1,\ \forall u$, the MCO for $\beta_u = 1,\ \ u$ and both the GAO and MCO for $\boldsymbol{\beta} = [1, 2, 2.4]$. The BER performance is better for the MCO than for

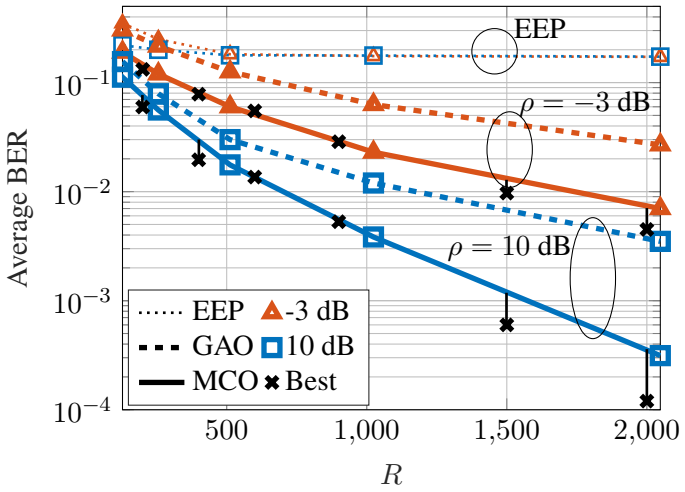

Figure 6.8: *BER vs. R for 3 users and 4 symbols per user with $\beta_u = 1$, for SNR=-3 dB and SNR=10 dB, for the EEP, the GAO and the MCO. Black crosses show the best performance with MCO optimized for those values.*

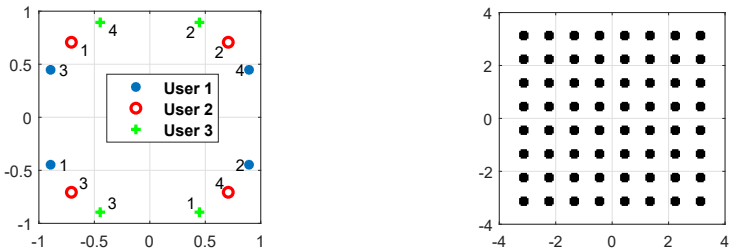

(a) *Individual.* **(b)** *Joint.*

Figure 6.9: *MCO Constellation for 3 users and 4 symbols per user, with $\beta_1 = \beta_3 = 1$ and $\beta_2 = 2.53$ or with $\beta_1 = \beta_3 = \sqrt{10}$ and $\beta_2 = 1$.*

the GAO with $\beta_u = 1, \quad u$, and the solution with $\boldsymbol{\beta} = [1, 2, 2.4]$ outperforms the other. In Fig. 6.14, we show the BER for the case of 3 users where one uses a BPSK and the other two use a QPSK, for $R = 128$ and $R = 512$.

6.6.3 Complexity of the Offline Optimization

The constellations proposed in Section 6.5.1 have been obtained with the parameterization in Table 6.2. For strategy S2, we indicate the cycle and step as (cycle-step). The total complexity is decreased by around 3 times for S2 with respect to the strategy S1, but the total number of generations is greater and the total population size is similar. The solutions obtained for the S1,

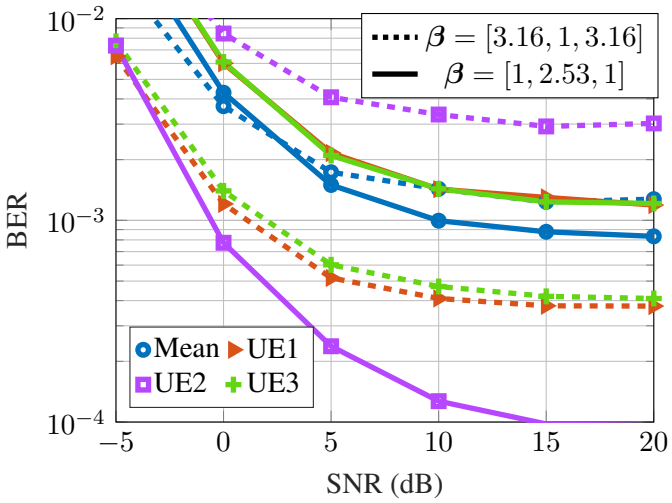

Figure 6.10: *BER vs ρ for 3 users and 4 symbols per user, with $\beta_u \neq 1, \forall u$. Average and individual users performance are shown. $R = 500$, GAO and MCO same results.*

S2, S3 and S4 strategies are virtually identical and their differences manifest mainly in rotations and very small variations in the position of the symbols. The variables of both GAO and MCO S1 have been randomly initialized.

	N_G	N_P	N_r	N_s
GAO 1st	$4(U + \sum M_u)$	$20(U + \sum M_u)$	X	X
GAO 2nd	30	300	X	X
MCO S1	$6(U + \sum M_u)$	$20(U + \sum M_u)$	1000	1000
MCO S2 (1-1)	$2(U + \sum M_u)$	$5(U + \sum M_u)$	100	100
MCO S2 (1-2)	$2(U + \sum M_u)$	$5(U + \sum M_u)$	100	100
MCO S2 (2)	$3(U + \sum M_u)$	$10(U + \sum M_u)$	1000	1000
MCO S4	$U + \sum M_u$	$U + \sum M_u$	1000	1000

Table 6.2: *Configuration of N_G, N_P, N_r and N_s for different strategies.*

As the previous results evidence, MCO has the best performance, outperforming the existing solutions and GAO, at the expense of increasing the complexity. In Section 6.4, four different strategies were introduced to reduce the complexity, while obtaining the same results. In Table 6.3, we provide the total number of operations and execution time per design technique and strategy. GAO (1) and GAO (2) refer to the first and second step of GAO, respectively. All times are obtained for a processor AMD Ryzen 7 2700X 3.7 GHz. GAO uses a single processor and MCO uses parallel processors (12 times faster). Nevertheless, GAO performs on average

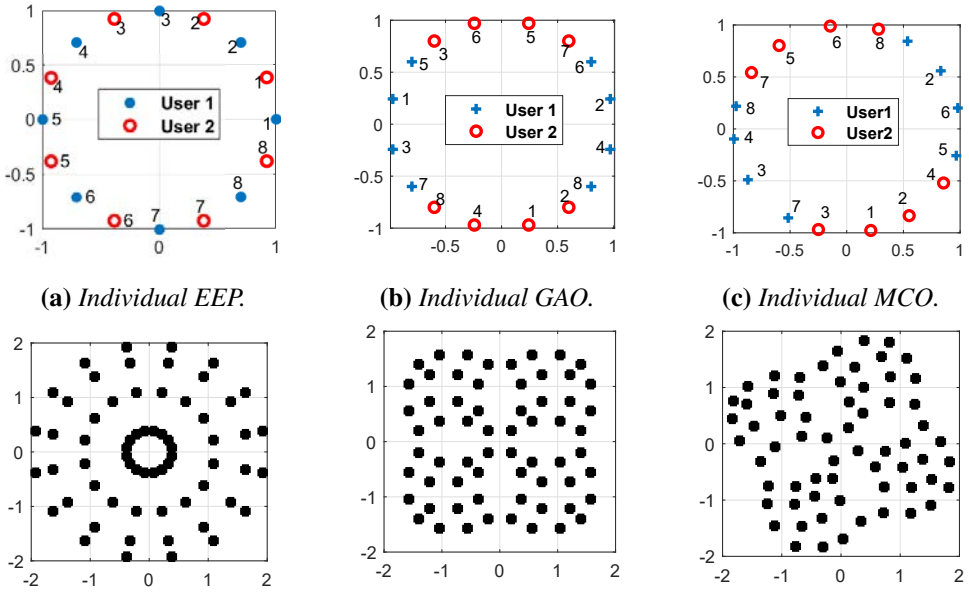

(a) *Individual EEP.* **(b)** *Individual GAO.* **(c)** *Individual MCO.*

(d) *Joint EEP.* **(e)** *Joint GAO.* **(f)** *Joint MCO.*

Figure 6.11: *Constellations for 2 users with 8 symbols per user with* $\beta_u = 1,\ \forall u$.

$N_\times$ | T	GAO (1)		GAO (2)		MCO S1		MCO S2		MCO S3		MCO S4	
U=2, M=[4 4]	$128{\cdot}10^3$	13s	$15.4{\cdot}10^3$	2.3s	$7.6{\cdot}10^{10}$	12h	$3.32{\cdot}10^{10}$	5h	$5{\cdot}10^8$	347s	-	352s
U=3, M=[4 4 4]	$1152{\cdot}10^3$	116s	$5.8{\cdot}10^3$	573s	$2.51{\cdot}10^{11}$	39h	$1.1{\cdot}10^{11}$	17h	$2{\cdot}10^9$	1231s	-	1302s
U=2, M=[8 8]	$1659{\cdot}10^3$	167s	$8.2{\cdot}10^9$	1.1h	$2.83{\cdot}10^{11}$	44h	$1.24{\cdot}10^{11}$	19h	$2.2{\cdot}10^9$	5003s	-	1315s
U=3, M=[2 2 4]	$155{\cdot}10^3$	16s	$2.56{\cdot}10^3$	0.7s	$9.2{\cdot}10^{10}$	14h	$4{\cdot}10^{10}$	6.2h	$8{\cdot}10^8$	367s	-	371s

Table 6.3: *Number of products* ($N_\times$) *and execution time* (T) *for different scenarios.*

around 10k operations per second and MCO around 150k operations per second per processor (as per Matlab matrix multiplication).

6.6.4 Non-coherent versus Coherent Scheme Performance

In this subsection, we are going to check how well the proposed NC constellations behave with respect to the coherent scheme. For this, we consider a multipath time-varying channel and an implementation with OFDM modulation according to the 5G new radio numerology. To obtain the results, the coherence time is calculated as $T_c = 0.15 f_D^{-1}$ [57], where f_D is the maximum Doppler frequency. To implement time correlation effects we use the autocorrelation model of (2) in [76]. We also consider that the duration of an OFDM symbol is the inverse of the separation between subcarriers $T_s = 1/\Delta_f$. We can obtain the ratio of coherence time to

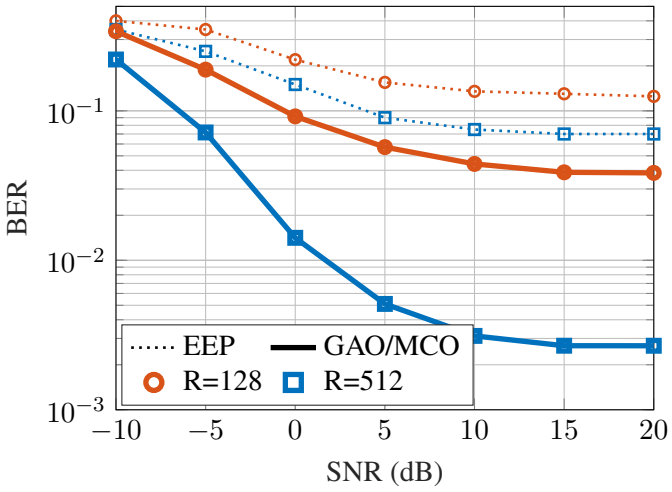

Figure 6.12: *BER vs ρ for 2 users and 8 symbols per User, for $R = 256$ and $R = 1024$. MCO obtained for R =300 and ρ=0dB.*

the OFDM symbol duration as $N_{CT} = T_c/T_s$, which is given in Table 6.4 for 5G scenarios with very high mobility, such as high speed trains, at 500 km/h (maximum speed for 5G). Only the values that are compatible with the allowed combinations of carrier frequency (f_c) and subcarrier spacing (Δ_f) in the 5G standard are shown; otherwise they are marked with "-" in the table. The coherent scheme uses channel estimation based on zero-forcing with pilot symbol assisted modulation (PSAM), as done in [11].

N_{CT}	Δ_f= 15	Δ_f= 30	Δ_f= 60	Δ_f= 120	Δ_f= 240
f_c = 0.7	7	15	29	-	-
f_c = 3.6	1.4	2.8	5.6	-	-
f_c = 27	-	-	-	1.5	3
f_c = 54	-	-	-	-	1.5

Table 6.4: *Ratio of T_c and OFDM T_s (N_{CT}), for $v = 500$ km/h for different carrier frequencies f_c in GHz and carrier spacing Δ_f in KHz.*

The results are shown in Fig. 6.16 for different N_{CT} values and multipath channels with a delay spread ($\sigma_\tau < 1\mu$s), so the minimum coherence bandwidth is $B_c \approx 1/(5\sigma_\tau) = 200$ kHz. Performing the differential encoding of the NC scheme over the frequency domain [59] and following the 5G standard [77], 4 out of 14 OFDM symbols correspond to reference signals for each slot. The SNR (ρ) for the coherent scheme has been penalized as $10\rho/14$ due to the channel estimation overhead. For high ρ, the NC outperforms the coherent scheme except for

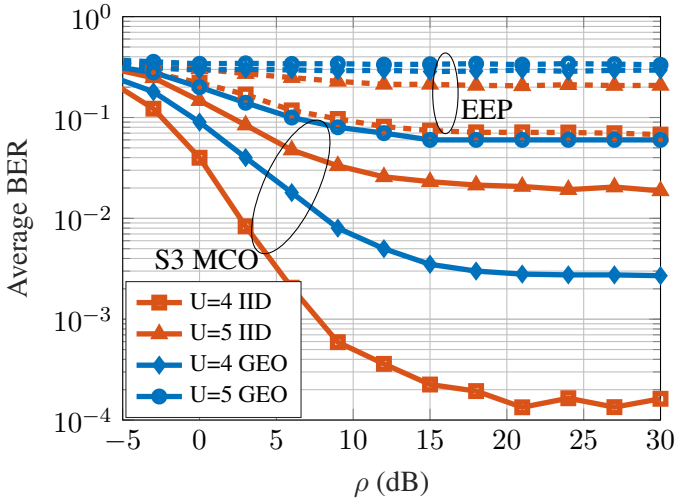

Figure 6.13: *BER vs. ρ for 4 and 5 users and 2 symbols per user with $\beta_u = 1$, for $R = 400$, for an IID and a GEO 3GPP channel. Continuous line (S3 MCO) and dashed (EEP).*

$N_{CT} \geq 10$. For $N_{CT} \leq 5$, the NC outperforms the coherent scheme for all ρ values. Also, the NC outperforms the coherent counterpart in the low ρ regime even for large N_{CT}.

6.7 Concluding Remarks of the constellation design for multi-user NC massive SIMO

In this chapter, we have proposed new constellations using a novel technique based on evolutionary computation (EC) for the NC massive SIMO in multi-user UL scenarios. The proposed constellations outperform the state-of-the-art solutions.

We have shown that a classical analytical approach is intractable and proposed two different approaches for solving this problem, referred to as GAO and MCO. The former obtains the individual constellation and the bit mapping policy for each UE by solving two different optimization problems with a constrained complexity and considering assumptions about the PDF of the received joint-symbols. The latter determines the constellations and the bit mapping policies in a single optimization problem by evaluating the system BER using a Monte-Carlo simulation. The numerical results have verified our analysis of the distribution of the received joint-symbols, and shown that both GAO and MCO significantly outperform the existing constellations, while MCO outperforms GAO in most scenarios. We have also presented the time complexity and number of operations for each scenario, confirming the validity of our com-

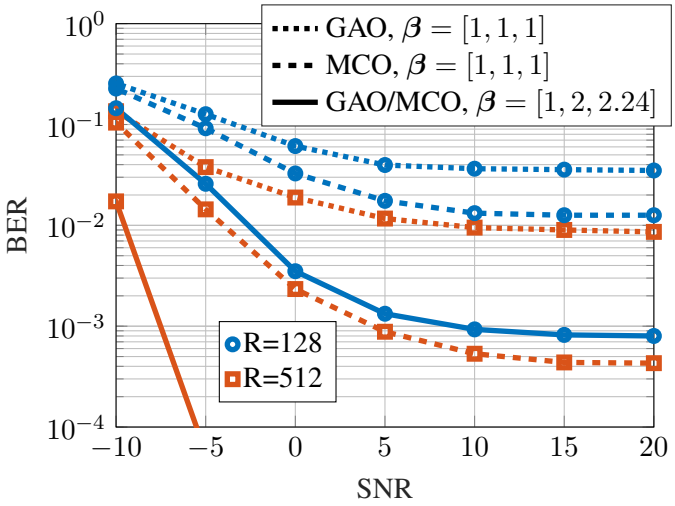

Figure 6.14: *BER vs SNR for 3 users and M=[2 2 4], for $R = 128$ and $R = 512$. MCO obtained for $R = 300$ and SNR=-3dB.*

plexity analysis.

Since these design techniques are envisaged to be executed offline, a BS could, in real time, perform user selection and power allocation strategies to select the best configuration for a particular scenario. The designs are valid for a wide range of parameters, and the selected constellations can be maintained for as long as the user distribution does not change.

This work contributes to the improvement of the performance of NC schemes combined with large number of antennas, with an offline design of the constellations. It has shown the viability of the proposed constellations to multiplex a moderate number of users with moderately large constellation sizes in the same time-frequency resources. This is a significant improvement with respect to previous NC constellations in the literature and paves the way to achieving even better multiplexing capabilities, particularly in scenarios where NC schemes are known to outperform coherent communications.

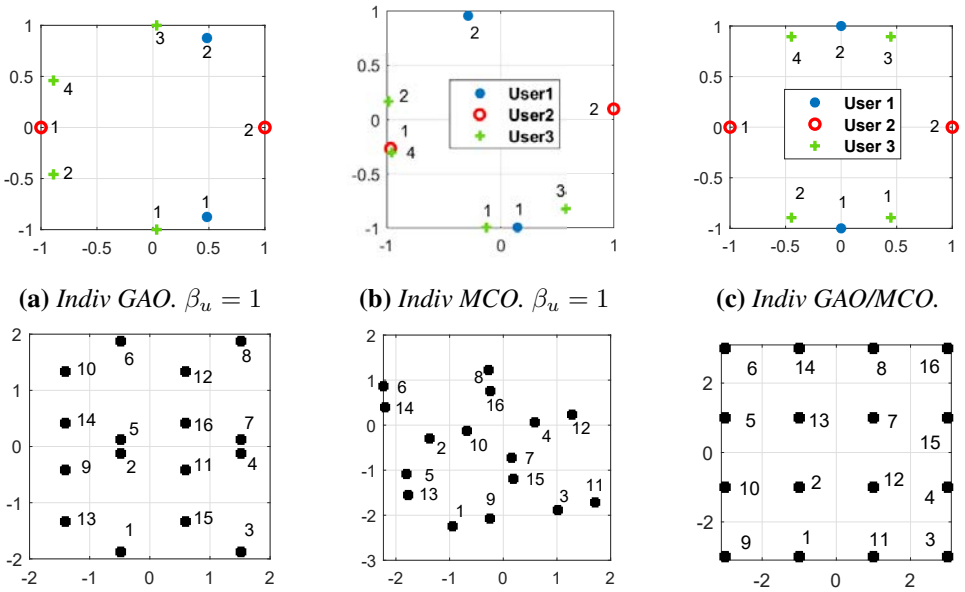

(a) *Indiv GAO.* $\beta_u = 1$ **(b)** *Indiv MCO.* $\beta_u = 1$ **(c)** *Indiv GAO/MCO.*

(d) *Joint GAO.* $\beta_u = 1$ **(e)** *Joint MCO.* $\beta_u = 1$ **(f)** *Joint GAO/MCO.*

Figure 6.15: *Constellations for 3 users with* $M = [2, 2, 4]$. *The results in the right are obtained with* $\boldsymbol{\beta} = [1, 2, 2.4]$

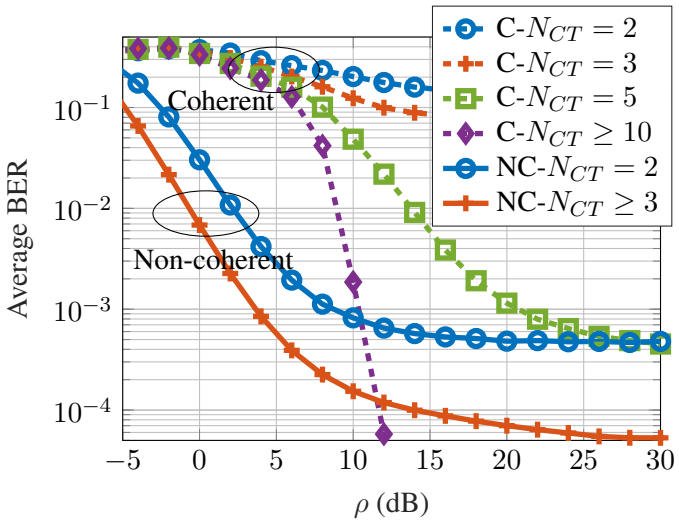

Figure 6.16: *Non-coherent (*$M_u = [4\ 4]$ *and* $\beta_u = [1\ 1]$ *from Table 6.5) vs. coherent scheme (2 users with regular QPSK) for R=128, for different* N_{CT}.

U	**M**	β_u	**Φ**				
2	2 2	1 1	0 3.14	1.57 4.71			
	2 4	1 1	5.87 2.71	1.89 0.87 4.31 5.53			
	2 4	1.3 1	3.69 0.41	1.53 4.63 2.88 5.98			
	2 4	1 1.95	2.3 5.84	2.49 0.97 4.49 5.61			
	2 8	1 1	5.87 4.37	3.53 0.82 4.76 2.14 1.49 0.2 5.67 5.20			
	2 8	1 1.5	3.11 0.58	0.44 3.8 3.06 4.6 1.07 1.87 6.14 5.16			
	2 8	1 1.8	3 0.11	2.8 0.92 4.41 1.58 5 3.35 5.9 0.16			
	2 16	1 1	1.08 4.42	2.55 0.1 0.9 3.6 1.91 4.94 1.22 5.56 2.79 0.47 3.01 3.32 2.17 5.21 1.53 5.95			
	4 4	1 1	0.98 4.11 1.88 5.03	0.33 5.68 2.65 3.51			
	4 4	1 2	0 3.14 1.57 4.71	0 3.14 1.57 4.71			
	4 8	1 1	2 1.08 4.64 3.82	3.4 2.91 1.69 2.01 5.41 2.58 0.2 5.99			
	4 8	2 1	1.94 0.23 3.47 5.03	4 3.26 4.73 5.27 1.75 2.64 0.29 6.07			
	4 16	1 1	3.85 3.23 0.22 0.87	1.53 1.33 1.88 1.15 2.85 5.61 5.21 5.42 2.28 0.15 2.14 4.28 2.51 6 4.95			
	4 16	1 1.4	2.52 4.56 5.5 1.48	0.5 6.2 3.46 3.77 1.5 0.7 3.3 0.85 5.6 4.43 3.06 0.27 1.3 5.92 4.14 2.5			
	4 16	2 1	3.05 1.5 4.64 6.05	1.04 1.37 0.7 1.08 6.07 5.8 0.18 6.06 2.52 1.9 3.05 3.6 5.04 5.44 4.36 4			
	8 8	1 1	1 0.6 3.65 3.24 6 0.2 4.17 2.92	4.93 5.3 4.46 5.74 2.21 1.72 2.57 1.29			
	8 8	1.12 1	5.5 5.75 5.2 6 3.2 2.36 1.8 2.7	1 4.55 0.68 1.5 0 5.06 4.08 3.57			
3	2 2 2	1 1 1	3.39 0.24	4.9 0.35	1.77 4.99		
	2 2 4	1 1 1	6.05 2.67	1.35 4.54	2.46 1.89 3.16 1.32		
	2 2 4	1.8 1.8 1	0.12 2.87	1.58 4.44	3.91 5.64 2.31 0.8		
	2 2 4	1 1.2 2.6	3.54 0.74	4.3 2.37	4.21 2.44 0.96 5.73		
	2 2 8	1 1 1	3.99 2.73	0.84 4.17	1.61 5.53 2.06 3.14 4.96 6 0.21 2.55		
	2 2 8	1 1.2 3.3	0.31 2.7	1.23 4.35	0.9 2.57 3.68 5.36 0.53 2.22 4.14 5.75		
	2 2 8	1.4 1.4 1	3.42 0.4	1.68 4.73	3.81 6.07 4.68 5.34 0.76 3.01 1.38 2.1		
	2 4 4	1 1 1	1.5 4.38	1.7 6.24 4.85 3.38	3.06 6.08 2.57 5.48		
	2 4 4	1.6 1.5 1	3.06 6.08	1.38 0.75 3.9 4.5	4.41 2.62 5.75 1.55		
	2 4 4	1 1 2.7	4.44 1.39	6.28 1.82 5 3.14	4.82 0.44 3.37 1.63		
	2 4 8	1 1 1	2.61 6.24	4.65 6.1 1.76 1.22	0.45 4.06 0.82 3.74 0.09 3.17 1.15 3.49		
	2 4 8	1.6 1.5 1	4.29 1.63	0.4 5.45 2.4 3.2	0.37 0.8 0.05 5.96 1.56 1.17 3.46 2.88		
	4 4 4	1 1 1	3.01 1.14 6.05 4.45	3.64 3.2 1.68 5.55	5.03 0.99 1.88 4.12		
	4 4 4	1 2.53 1	3.61 5.82 2.68 0.46	2.36 0.79 3.93 5.5	5.18 1.11 4.25 2.03		
	4 4 4	1 2 4	0 1.57 3.14 4.71	0 1.57 3.14 4.71	0 1.57 3.14 4.71		
4	2 2 2 2	1 1 1 1	5.06 3.93	5.9 0.69	1.72 4.78	0.13 3.24	
	2 2 2 2	2.1 1 2.1 1	3.87 0.55	5.38 2.2	5.29 2.32	3.85 0.6	
	2 2 2 4	1 1 1 1	5.84 2.54	0.87 4.51	4.61 2.5	3.4 1.88 4.19 0.44	
	2 2 2 4	2.4 1.4 2.4 1	2.85 5.97	3.63 0.58	4.75 1.32	6.01 4.77 1.62 3	
	2 2 2 8	1 1 1 1	5.89 1.01	2.96 5.58	4.17 1.14	4.95 5.3 0.3 0.64 1.7 3.5 2 3.95	
	2 2 4 4	1 1 1 1	0.91 1.33	3.96 4.4	3.15 0.06 2.63 5.89	5.57 2.4 0.42 3.87	
	2 2 4 4	3.3 3.1 1 2.3	4.23 1.21	2.49 5.78	5.15 3.42 0.28 1.9	1.78 0.38 5.01 3.46	
5	2 2 2 2 2	1 1 1 1 1	5.1 2.19	2.43 4.2	0.49 3.76	3.32 0.05	1.37 4.58
	2 2 2 2 2	1 1.1 1.6 3.4 2	0.58 4.53	4.65 2.55	3.65 0.33	3.3 6.26	1.9 5.2

Table 6.5: *Proposed constellations (phases in radians) for different U, M_u and β_u. Column* **Φ***, has U vectors with M_u elements each.*

Chapter 7
Conclusion and Future Research

The 1940s saw the initial conception of the cellular idea for wireless communications, and it has survived to the present day. In general, this technology has advanced in response to the need for new and improved capabilities, such as higher data rates, lower latency, and a bigger number of devices, in increasingly challenging situations. In the 5G era, the goal is to support the communication at speeds of 500km/h utilizing the least possible energy and for 6G speeds of up to 1000km/h are under discussion. In this context, future wireless generations will potentially require the need to work in further demanding scenarios, for which the avoidance in the need to utilize the CSI is very interesting.

The NC-mMIMO seems a natural choice to be able to fulfill the desired requirements of future wireless communications in scenarios with stringent conditions. The end goal is to propose a scheme which can avoid the CSI estimation that is problematic in such scenarios. This thesis addressed improvements for the single user operation of NC-mMIMO by proposing a CF approach to naturally improve its performance and by proposing a blind channel estimation with NC data to combine its use with the coherent approach. This thesis also addressed improvements for the multiuser scenario of NC-mMIMO by proposing optimal constellations for Rayleigh channels. This chapter serves as the work's epilogue, providing a summary of all contributions, conclusions, and some directions for further study.

7.1 Summary and conclusions

In Chapter 2, the path towards a pilot-less massive MIMO system that is convenient for stringent scenarios is presented. For that, the classical coherent massive MIMO-OFDM scheme is presented first, followed by the limitations imposed by the channel estimation process in scenarios with stringent propagation conditions and finalizing with a presentation of the non-coherent massive MIMO technique, explaining its history and its state-of-the-art.

Throughout Chapter 3, the system model for the entire document is presented. The propagation

channel model is explained first, where a Rician spatially, time and frequency correlated channel is described for a generic BS a, then the coherent TDD massive MIMO-OFDM is explained in which the problem of a channel estimation imperfection caused by "channel aging" and noisy estimation is detailed. Last, the system model for the non-coherent massive MIMO-OFDM is pointed out.

Chapter 4 presents a cell-free approach for the NC-mMIMO scheme, in which the reception of the NC data is performed over several APs. For this, we first analyze the distribution of the received NC symbol for Rician spatially correlated channels over several uncorrelated APs, followed by three AP selection approaches and ending with a comparison between the coherent and the non-coherent cell-free approaches. It is shown how the NC can outperform the coherent scheme for the cell-free approach and it is also shown that the NC can greatly benefit from the use of several uncorrelated APs.

A novel blind channel estimation is presented in Chapter 5, where the NC data which is detected without the need of CSI is reconstructed and utilized to estimate the channel. With this blind channel estimation two schemes are proposed. The first one is based on an UL OFDM scheme in which the classical pilot signals are substituted by NC data, with the consequent increment in the efficiency of the UL. The second one is based on performing TDD with an UL based only on NC-mMIMO and with the DL based on precoding with the channel estimated utilizing the reconstructed NC data. The DL data is differentially encoded to avoid the use of demodulation pilots. The error in the channel estimation without "channel aging" is analyzed in the first one while "channel aging" is considered in the second one. In the first one, the increment in the throughput efficiency with the proposed scheme is shown with respect to the coherent and NC schemes. In the second one, the BER performance of Monte Carlo simulation is shown for different TDD slots duration and coherence times, and it is shown that the proposed pilot-less scheme outperforms the classical pilot-based.

Lastly, Chapter 6 proposes a new design technique for the constellations in MU NC-mMIMO based on solving a numerical optimization problem by means of evolutionary computation, due to the mathematical intractability when classical design approaches are intended. With this design technique, a set of optimal constellations is provided for different number of users, constellation sizes per user and mean received power per user.

Along this thesis, the different proposals to improve both the single-user and the multi-user NC

scheme have been shown to be valid and convenient for such purpose, and demonstrated better than their coherent counterpart in fast varying and/or low SNR channels.

7.2 Future research work

In light of this thesis, the following study areas are suggested for further development:

- **Improvement of NC-CF-mSIMO for a multiuser scenario**. For the multiuser scenario, an extension of the proposed NC-CF-mSIMO scheme proposed in Section 4.3 is of interest. Utilizing a different set of suitable joint-constellations in each AP given the propagation conditions between each user and each AP, we can perform hard detection of the individual symbols of each user at each AP and combine them in the CPU to improve the detection with respect to a single-AP.

- **User Allocation Strategy for a multiuser scenario**. For the multiuser scenario, a user allocation strategy that selects the best users given different conditions of channel propagation properties and user needs is of interest for the real deployment of the multiuser NC-mMIMO. Due to the fact that it is expected that several users will enter and leave the network in real time, and their propagation conditions and communication needs will also change, mechanisms to coordinate all these users are interesting.

- **NC Constellations for Rician Channels for the multiuser scenario**. For the Rician channel, the constellation design is more complicated due to the fact that the joint-constellation in the RX side is not the sum of the individual constellations of the users affected by their mean received power. The joint-constellation is also affected by the Rician factor, and thus, other approach that may use deep learning techniques will be needed.

- **New Receivers for the NC-mMIMO**. The reception of the NC-mMIMO is based on performing a differential decoding in each antenna followed by an averaging over the antennas in the BS and there should potentially be better RXs that can increase the performance for the RX side. Some ideas are based on utilizing machine learning techniques to create deep neural networks based receivers that can outperform the state-of-the-art.

Bibliography

[1] *Study on Channel Model for Frequencies from 0.5 to 100 GHz (Release 15)*, 3GPP Std. 38.901, 2018.

[2] A. G. Armada and L. Hanzo, "A non-coherent multi-user large scale SIMO system relaying on M-ary DPSK," in *Proc. IEEE ICC*, June 2015, pp. 2517–2522.

[3] V. M. Baeza, A. G. Armada, W. Zhang, M. El-Hajjar, and L. Hanzo, "A noncoherent multiuser large-scale SIMO system relying on M-ary DPSK and BICM-ID," *IEEE Transactions on Vehicular Technology*, vol. 67, no. 2, pp. 1809–1814, Feb. 2018.

[4] D. H. Ring, "Mobile Telephony - Wide Area Coverage," Bell Laboratories Techinical Memorandum, Tech. Rep., 1947.

[5] M. Rahnema, "Overview of the GSM system and protocol architecture," *IEEE Commun. Mag.*, vol. 31, no. 4, pp. 92–100, 1993.

[6] T. Rappaport, *Wireless Communications: Principles and Practice*, 2nd ed. USA: Prentice Hall PTR, 2001.

[7] C. Johnson, *Radio Access Networks for UMTS: Principles and Practice*. Wiley Publishing, 2008.

[8] A. Ghosh, J. Zhang, J. G. Andrews, and R. Muhamed, *Fundamentals of LTE*, 1st ed. USA: Prentice Hall Press, 2010.

[9] J. G. Andrews, S. Buzzi, W. Choi, S. V. Hanly, A. Lozano, A. C. K. Soong, and J. C. Zhang, "What Will 5G Be?" *IEEE J. Sel. Areas Commun.*, vol. 32, no. 6, pp. 1065–1082, 2014.

[10] A. C. Clarke, *How the World Was One*. USA: Bantam Books, Inc., 1992.

[11] M. J. Lopez-Morales, K. Chen-Hu, and A. Garcia-Armada, "Differential Data-Aided Channel Estimation for Up-Link Massive SIMO-OFDM," *IEEE Open Journal of the Communications Society*, vol. 1, pp. 976–989, 2020.

[12] A. Immanuvel and M. Suganthi, "Performance analysis of low power channel estimator for multi user mimo-ofdm system," *Wireless Personal Communications*, vol. 107, no. 1, pp. 341–350, 2019.

[13] N. Fatema, G. Hua, Y. Xiang, D. Peng, and I. Natgunanathan, "Massive MIMO Linear Precoding: A Survey," *IEEE Systems Journal*, vol. 12, no. 4, pp. 3920–3931, 2018.

[14] J. Dulmage and M. P. Fitz, "Channel estimation, overhead, and outage for PSAM-OFDM," in *2013 International Conference on Connected Vehicles and Expo (ICCVE)*, 2013, pp. 221–226.

[15] H. Iimori, G. T. F. de Abreu, and K. Ishibashi, "Full-Duplex MIMO Systems with Hardware Limitations and Imperfect Channel Estimation," in *GLOBECOM 2020 - 2020 IEEE Global Communications Conference*, 2020, pp. 1–6.

[16] P. Xu, J. Wang, and J. Wang, "Effect of pilot contamination on channel estimation in massive MIMO systems," in *2013 International Conference on Wireless Communications and Signal Processing*, 2013, pp. 1–6.

[17] F. A. P. De Figueiredo, F. A. C. M. Cardoso, I. Moerman, and G. Fraidenraich, "Channel Estimation for Massive MIMO TDD Systems Assuming Pilot Contamination and Frequency Selective Fading," *IEEE Access*, vol. 5, pp. 17 733–17 741, 2017.

[18] L. M. Leemis and J. T. McQueston, "Univariate distribution relationships," *The American Statistician*, vol. 62, no. 1, pp. 45–53, 2008.

[19] A. Paulraj, R. Nabar, and D. Gore, *Introduction to Space-Time Wireless Communications*, 1st ed. USA: Cambridge University Press, 2008.

[20] D. Gesbert, M. Kountouris, R. W. Heath, C. Chae, and T. Salzer, "Shifting the MIMO Paradigm," *IEEE Signal Process. Mag.*, vol. 24, no. 5, pp. 36–46, 2007.

[21] T. L. Marzetta, "Noncooperative Cellular Wireless with Unlimited Numbers of Base Station Antennas," *IEEE Transactions on Wireless Communications*, vol. 9, no. 11, pp. 3590–3600, November 2010.

[22] L. Lu, G. Y. Li, A. L. Swindlehurst, A. Ashikhmin, and R. Zhang, "An Overview of Massive MIMO: Benefits and Challenges," *IEEE Journal of Selected Topics in Signal Processing*, vol. 8, no. 5, pp. 742–758, 2014.

[23] T. L. Marzetta, E. G. Larsson, H. Yang, and H. Q. Ngo, *Fundamentals of Massive MIMO*. Cambridge University Press, 2016.

[24] E. Björnson, J. Hoydis, and L. Sanguinetti, "Massive MIMO networks: Spectral, energy, and hardware efficiency," *Foundations and Trends® in Signal Processing*, vol. 11, no. 3-4, pp. 154–655, 2017. [Online]. Available: http://dx.doi.org/10.1561/2000000093

[25] A. M. Tulino and S. Verdú, "Random Matrix Theory and Wireless Communications," *Foundations and Trends® in Communications and Information Theory*, vol. 1, no. 1, pp. 1–182, 2004. [Online]. Available: http://dx.doi.org/10.1561/0100000001

[26] L. Cimini, "Analysis and Simulation of a Digital Mobile Channel Using Orthogonal Frequency Division Multiplexing," *IEEE Trans. on Comms.*, vol. 33, no. 7, pp. 665–675, 1985.

[27] T. Hwang, C. Yang, G. Wu, S. Li, and G. Ye Li, "OFDM and Its Wireless Applications: A Survey," *IEEE Trans. on Veh. Tech.*, vol. 58, no. 4, pp. 1673–1694, 2009.

[28] Z. Gao, L. Dai, Z. Wang, and S. Chen, "Spatially Common Sparsity Based Adaptive Channel Estimation and Feedback for FDD Massive MIMO," *IEEE Transactions on Signal Processing*, vol. 63, no. 23, pp. 6169–6183, 2015.

[29] Z. Tang, R. C. Cannizzaro, G. Leus, and P. Banelli, "Pilot-Assisted Time-Varying Channel Estimation for OFDM Systems," *IEEE Transactions on Signal Processing*, vol. 55, no. 5, pp. 2226–2238, 2007.

[30] H. Kim, S. Kim, H. Lee, C. Jang, Y. Choi, and J. Choi, "Massive MIMO Channel Prediction: Kalman Filtering Vs. Machine Learning," *IEEE Transactions on Communications*, vol. 69, no. 1, pp. 518–528, 2021.

[31] A. S. Al-hubaishi, N. K. Noordin, A. Sali, S. Subramaniam, and A. Mohammed Mansoor, "An efficient pilot assignment scheme for addressing pilot contamination in multi-cell massive MIMO systems," *Electronics*, vol. 8, no. 4, p. 372, 2019.

[32] J. Oetting, "A Comparison of Modulation Techniques for Digital Radio," *IEEE Transactions on Communications*, vol. 27, no. 12, pp. 1752–1762, 1979.

[33] S. Maslamani and M. Ghanbari, "Digital demodulation by a non-coherent differential PSK modem," *Electronics Letters*, vol. 26, no. 24, pp. 2028–2029, 1990.

[34] J. Henry, "DPSK Versus FSK with Frequency Uncertainty," *IEEE Transactions on Communication Technology*, vol. 18, no. 6, pp. 814–817, 1970.

[35] R. Wilson and J. Richter, "Generation and Performance of Quadraphase Welti Codes for Radar and Synchronization of Coherent and Differentially Coherent PSK," *IEEE Transactions on Communications*, vol. 27, no. 9, pp. 1296–1301, 1979.

[36] E. Geraniotis, "Performance of Noncoherent Direct-Sequence Spread-Spectrum Multiple-Access Communications," *IEEE Journal on Selected Areas in Communications*, vol. 3, no. 5, pp. 687–694, 1985.

[37] B. Hochwald and T. Marzetta, "Unitary space-time modulation for multiple-antenna communications in Rayleigh flat fading," *IEEE Transactions on Information Theory*, vol. 46, no. 2, pp. 543–564, 2000.

[38] B. Hochwald and W. Sweldens, "Differential unitary space-time modulation," *IEEE Transactions on Communications*, vol. 48, no. 12, pp. 2041–2052, 2000.

[39] T. Cui and C. Tellambura, "On Multiple Symbol Detection for Diagonal DUSTM Over Ricean Channels," *IEEE Transactions on Wireless Communications*, vol. 7, no. 4, pp. 1146–1151, 2008.

[40] R. H. Gohary and T. N. Davidson, "Noncoherent MIMO Communication: Grassmannian Constellations and Efficient Detection," *IEEE Transactions on Information Theory*, vol. 55, no. 3, pp. 1176–1205, 2009.

[41] A. Manolakos, M. Chowdhury, and A. J. Goldsmith, "CSI is not needed for optimal scaling in multiuser massive SIMO systems," in *2014 IEEE International Symposium on Information Theory*, 2014, pp. 3117–3121.

[42] M. Chowdhury, A. Manolakos, and A. J. Goldsmith, "Coherent versus noncoherent massive SIMO systems: Which has better performance?" in *2015 IEEE International Conference on Communications (ICC)*, 2015, pp. 1691–1696.

[43] ——, "Design and performance of noncoherent massive SIMO systems," in *2014 48th Annual Conference on Information Sciences and Systems (CISS)*, 2014, pp. 1–6.

[44] V. M. Baeza, A. G. Armada, W. Zhang, M. El-Hajjar, and L. Hanzo, "A Noncoherent Multiuser Large-Scale SIMO System Relying on M-Ary DPSK and BICM-ID," *IEEE Transactions on Vehicular Technology*, vol. 67, no. 2, pp. 1809–1814, 2018.

[45] E. Leung, Z. Dong, and J.-K. Zhang, "Uniquely Factorable Hexagonal Constellation Designs for Noncoherent SIMO Systems," *IEEE Transactions on Vehicular Technology*, vol. 66, no. 6, pp. 5495–5501, 2017.

[46] H. Xie, W. Xu, W. Xiang, K. Shao, and S. Xu, "Non-coherent massive SIMO systems in ISI channels: Constellation design and performance analysis," *IEEE Systems Journal*, vol. 13, no. 3, p. 2252–2263, Sept. 2019.

[47] J. Zhu, L. Xiao, P. Xiao, A. Quddus, C. He, and L. Lu, "Differential STBC-SM Scheme for Uplink Multi-User Massive MIMO Communications: System Design and Performance Analysis," *IEEE Transactions on Vehicular Technology*, vol. 70, no. 10, pp. 10 236–10 251, 2021.

[48] A. Fazeli, H. H. Nguyen, H. D. Tuan, and H. V. Poor, "Non-Coherent Multi-Level Index Modulation," *IEEE Transactions on Communications*, vol. 70, no. 4, pp. 2240–2255, 2022.

[49] K.-H. Ngo, S. Yang, M. Guillaud, and A. Decurninge, "Joint Constellation Design for Noncoherent MIMO Multiple-Access Channels," *IEEE Transactions on Information Theory*, pp. 1–1, 2022.

[50] O. Mahmoud, A. E.-S. El-Mahdy, and R. F. H. Fischer, "On Multi-User Deep-Learning-Based Non-Coherent DPSK Multiple-Symbol Differential Detection in Massive MIMO Systems," *IEEE Access*, vol. 9, pp. 148 339–148 352, 2021.

[51] Technical Specification Group, "Study on 3D channel model for LTE," 3GPP, Tech. Rep. 36.873 V12.0.0 Release 12, 2014.

[52] A. A. Polegre, R. P. Leal, J. A. G. García, and A. G. Armada, "Drive Tests-based Evaluation of Macroscopic Pathloss Models for Mobile Networks," in *Proc. 2019 European Conf. on Netw. Commun. (EuCNC)*, June 2019.

[53] L. Sanguinetti, E. Björnson, and J. Hoydis, "Toward Massive MIMO 2.0: Understanding Spatial Correlation, Interference Suppression, and Pilot Contamination," *IEEE Transactions on Communications*, vol. 68, no. 1, pp. 232–257, 2020.

[54] C. He and R. D. Gitlin, "Limiting performance of massive MIMO downlink cellular systems," in *2016 Information Theory and Applications Workshop (ITA)*, 2016, pp. 1–6.

[55] X. Zhu and J. Xue, "On the Correlation of Subcarriers in Grouped Linear Constellation Precoding OFDM Systems Over Frequency Selective Fading," in *2006 IEEE 63rd Vehicular Technology Conference*, vol. 3, 2006, pp. 1431–1435.

[56] M.-H. Hsieh and C.-H. Wei, "Channel estimation for OFDM systems based on comb-type pilot arrangement in frequency selective fading channels," *IEEE Transactions on Consumer Electronics*, vol. 44, no. 1, pp. 217–225, 1998.

[57] T. S. Rappaport *et al.*, *Wireless communications: principles and practice*. Prentice Hall PTR, 1996, vol. 2.

[58] H. Q. Ngo, E. G. Larsson, and T. L. Marzetta, "Energy and spectral efficiency of very large multiuser MIMO systems," *IEEE Communications Letters*, vol. 61, no. 4, pp. 1436–1449, April 2013.

[59] K. Chen-Hu and A. G. Armada, "Non-Coherent Multiuser Massive MIMO-OFDM with Differential Modulation," in *2019 IEEE International Conference on Communications (ICC)*, May 2019, pp. 1–6.

[60] R. Gaunt, "Variance-gamma approximation via stein's method," *Electron. J. Probab.*, vol. 19, p. 33 pp., 2014. [Online]. Available: https://doi.org/10.1214/EJP.v19-3020

[61] R. E. Gaunt, "A note on the distribution of the product of zero mean correlated normal random variables," 2018.

[62] S. Covo, A. Elalouf *et al.*, "A novel single-gamma approximation to the sum of independent gamma variables, and a generalization to infinitely divisible distributions," *Electronic Journal of Statistics*, vol. 8, no. 1, pp. 894–926, 2014.

[63] R. A. Johnson, D. W. Wichern *et al.*, *Applied multivariate statistical analysis*. Prentice hall Upper Saddle River, NJ, 2002, vol. 5, no. 8.

[64] Y. Feng, M. Wen, J. Zhang, F. Ji, and G. Ning, "Sum of arbitrarily correlated gamma random variables with unequal parameters and its application in wireless communications," in *2016 International Conference on Computing, Networking and Communications (ICNC)*, 2016, pp. 1–5.

[65] Proakis, *Digital Communications 5th Edition*. McGraw Hill, 2007.

[66] M. J. L. Morales, K. Chen-Hu, and A. G. Armada, "Effect of Spatial Correlation on the Performance of Non-coherent Massive MIMO based on DMPSK," in *2021 IEEE Global Communications Conference (GLOBECOM)*, 2021, pp. 1–6.

[67] A. A. Polegre, F. Riera-Palou, G. Femenias, and A. G. Armada, "Channel hardening in cell-free and user-centric massive mimo networks with spatially correlated ricean fading," *IEEE Access*, vol. 8, pp. 139 827–139 845, 2020.

[68] F. Xu, X. Zhu, C. C. Tan, Q. Li, G. Yan, and J. Wu, "SmartAssoc: Decentralized Access Point Selection Algorithm to Improve Throughput," *IEEE Transactions on Parallel and Distributed Systems*, vol. 24, no. 12, pp. 2482–2491, 2013.

[69] E. Björnson and L. Sanguinetti, "Making Cell-Free Massive MIMO Competitive With MMSE Processing and Centralized Implementation," *IEEE Trans. Wireless Commun.*, vol. 19, no. 1, pp. 77–90, 2020.

[70] H. Q. Ngo, A. Ashikhmin, H. Yang, E. G. Larsson, and T. L. Marzetta, "Cell-Free Massive MIMO Versus Small Cells," *IEEE Trans. Wireless Commun.*, vol. 16, no. 3, pp. 1834–1850, 2017.

[71] S. M. Kay, *Fundamentals of Statistical Signal Processing: Estimation Theory*. USA: Prentice-Hall, Inc., 1993.

[72] Ö. T. Demir, E. Björnson, and L. Sanguinetti, *Foundations of User-Centric Cell-Free Massive MIMO*. Now Publishers, 2021, vol. 14, no. 3-4. [Online]. Available: http://dx.doi.org/10.1561/2000000109

[73] K. Chen-Hu, Y. Liu, and A. G. Armada, "Non-coherent massive MIMO-OFDM for communications in high mobility scenarios," *ITU Journal on Fut. and Evolv. Tech.*, vol. 1, 2020.

[74] E. Björnson and L. Sanguinetti, "Scalable Cell-Free Massive MIMO Systems," *IEEE Trans. Commun.*, pp. 1–1, 2020.

[75] D. Mi, M. Dianati, L. Zhang, S. Muhaidat, and R. Tafazolli, "Massive mimo performance with imperfect channel reciprocity and channel estimation error," *IEEE Transactions on Communications*, vol. 65, no. 9, pp. 3734–3749, 2017.

[76] K. E. Baddour and N. C. Beaulieu, "Autoregressive modeling for fading channel simulation," *IEEE Trans. Wireless Commun.*, vol. 4, no. 4, pp. 1650–1662, July 2005.

[77] *Physical Channels and Modulation (Release 15)*, 3GPP Std. 38.211, 2018.

[78] J. L. Arbuckle, G. A. Marcoulides, and R. E. Schumacker, "Full Information Estimation in the Presence of Incomplete Data," *Advanced Structural Equation Modeling: Issues and Techniques*, vol. 243, p. 277, 1996.

[79] J. Zheng, J. Zhang, E. Björnson, and B. Ai, "Impact of Channel Aging on Cell-Free Massive MIMO Over Spatially Correlated Channels," *IEEE Transactions on Wireless Communications*, vol. 20, no. 10, pp. 6451–6466, 2021.

[80] R. Nilsson, O. Edfors, M. Sandell, and P. O. Borjesson, "An Analysis of Two-Dimensional Pilot-Symbol Assisted Modulation for OFDM," in *1997 IEEE International Conference on Personal Wireless Communications (Cat. No.97TH8338)*, Dec 1997, pp. 71–74.

[81] C. Wang, E. K. S. Au, R. D. Murch, W. H. Mow, R. S. Cheng, and V. Lau, "On the Performance of the MIMO Zero-Forcing Receiver in the Presence of Channel Estimation Error," *IEEE Transactions on Wireless Communications*, vol. 6, no. 3, pp. 805–810, 2007.

[82] Won-Gyu Song and Jong-Tae Lim, "Pilot-symbol aided Channel Estimation for OFDM with Fast Fading Channels," *IEEE Transactions on Broadcasting*, vol. 49, no. 4, pp. 398–402, 2003.

[83] S. Malkowsky, J. Vieira, L. Liu, P. Harris, K. Nieman, N. Kundargi, I. C. Wong, F. Tufvesson, V. Öwall, and O. Edfors, "The World's First Real-Time Testbed for Massive MIMO: Design, Implementation, and Validation," *IEEE Access*, vol. 5, pp. 9073–9088, 2017.

[84] G. W. Bohrnstedt and A. S. Goldberger, "On the exact covariance of products of random variables," *Journal of the American Statistical Association*, vol. 64, no. 328, pp. 1439–1442, 1969.

[85] Z. Cao, G. Wen, L. Chen, Q. Shu, and L. Chen, "Comparison of interpolation methods for pilot aided estimation in direct-detection optical ofdm system," *Microwave and Optical Technology Letters*, vol. 55, no. 11, pp. 2604–2608, 2013.

[86] J. C. Estrada-Jiménez, K. Chen-Hu, M. J. F. García, and A. García Armada, "Power allocation and capacity analysis for FBMC-OQAM with superimposed training," *IEEE Access*, vol. 7, pp. 46 968–46 976, 2019.

[87] V. M. Baeza and A. G. Armada, "Non-Coherent Massive SIMO System Based on M-DPSK for Rician Channels," *IEEE Transactions on Vehicular Technology*, vol. 68, no. 3, pp. 2413–2426, March 2019.

[88] A. Alkhateeb and R. W. Heath, "Frequency Selective Hybrid Precoding for Limited Feedback Millimeter Wave Systems," *IEEE Transactions on Communications*, vol. 64, no. 5, pp. 1801–1818, May 2016.

[89] G. Cui, X. Yu, S. Iommelli, and L. Kong, "Exact Distribution for the Product of Two Correlated Gaussian Random Variables," *IEEE Signal Process. Lett.*, vol. 23, no. 11, pp. 1662–1666, 2016.

[90] Z.-H. Yang and Y.-M. Chu, "On approximating the modified Bessel function of the second kind," *Journal of inequalities and applications*, vol. 2017, no. 1, pp. 1–8, 2017.

[91] C. Walck, "Hand-book on statistical distributions for experimentalists," *University of Stockholm*, vol. 10, Sep. 2007.

[92] N. O'Donoughue and J. M. F. Moura, "On the product of independent complex Gaussians," *IEEE Signal Process. Lett.*, vol. 60, no. 3, pp. 1050–1063, Mar. 2012.

[93] K. N. Pappi, N. D. Chatzidiamantis, and G. K. Karagiannidis, "Error performance of multidimensional lattice constellations—Part I: A parallelotope geometry based approach for the AWGN channel," *IEEE Trans. Commun.*, vol. 61, no. 3, pp. 1088–1098, Mar. 2013.

[94] A. N. Sloss and S. Gustafson, "2019 Evolutionary algorithms review," *arXiv preprint arXiv:1906.08870*, 2019.

[95] X. Qi and F. Palmieri, "Theoretical analysis of evolutionary algorithms with an infinite population size in continuous space. Part I: Basic properties of selection and mutation," *IEEE Trans. Neural Netw.*, vol. 5, no. 1, pp. 102–119, 1994.

[96] M. Srinivas and L. Patnaik, "Genetic algorithms: a survey," *Computer*, vol. 27, no. 6, pp. 17–26, 1994.

[97] M. Chowdhury, A. Manolakos, and A. J. Goldsmith, "Coherent versus noncoherent massive SIMO systems: Which has better performance?" in *Proc. IEEE ICC*, June 2015, pp. 1691–1696.

[98] Y. Gao, "Population size and sampling complexity in genetic algorithms," in *Proc. of the Bird of a Feather Workshops*, 2003, pp. 178–181.

[99] M. S. Gibbs, H. R. Maier, G. C. Dandy, and J. B. Nixon, "Minimum number of generations required for convergence of genetic algorithms," in *Proc. 2006 IEEE ICEC*, July 2006, pp. 565–572.

[100] J. Alander, "On optimal population size of genetic algorithms," in *Proc. CSSE*. IEEE Comp. Society, 1992, pp. 65–70.

[101] P. S. Oliveto, J. He, and X. Yao, "Time complexity of evolutionary algorithms for combinatorial optimization: A decade of results," *Intern. J. of Automat. and Comp.*, vol. 4, no. 3, pp. 281–293, 2007.

[102] J. Zhang, L. Zhu, Z. Xiao, X. Cao, D. O. Wu, and X. Xia, "Optimal and sub-optimal uplink NOMA: Joint user grouping, decoding order, and power control," *IEEE Wireless Commun. Lett.*, vol. 9, no. 2, pp. 254–257, Feb. 2020.